PAUL SCHERRER INSTITUT

PSI

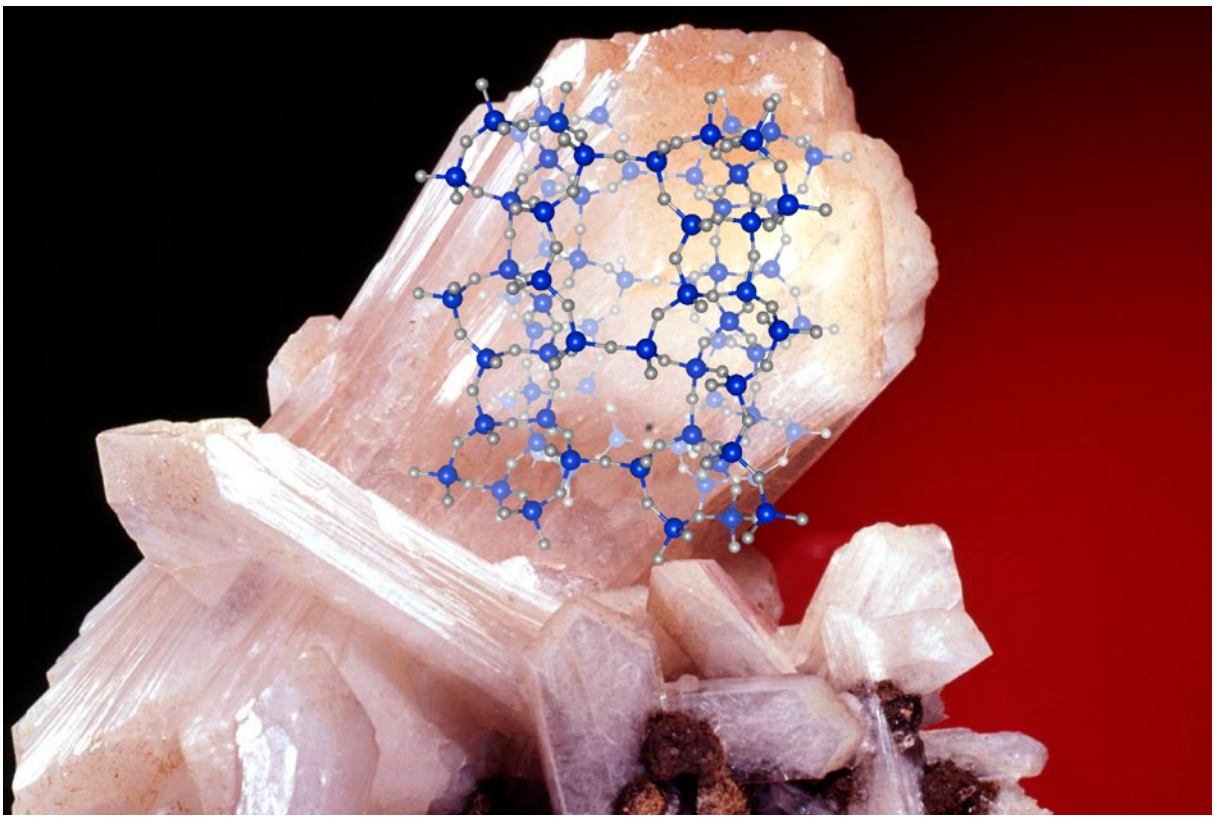

Progress Report 2022

Laboratory for Waste Management :: Nuclear Energy and Safety Department

Cover
Zeolite crystal superimposed with STI-type tetrahedral framework: Most of zeolites shrink and collapse at higher temperature due to dehydration. Pb-exchanged zeolite Stellerite (STI), has been found to show highly unusual thermal behaviour. In Pb-Stellerite, the unit cell volume and symmetry are retained at higher temperature despite dehydration due to chemical reaction within extra framework cavities (see section 6.2).

PAUL SCHERRER INSTITUT

PSI

Progress Report 2022

Laboratory for Waste Management
Nuclear Energy and Safety Department

See also our web-page
http://www.psi.ch/les/

Preface

The mission of the Laboratory for Waste Management (LES) is to carry out a comprehensive research and development (R&D) programme in support of Swiss radioactive waste disposal options. In particular, our aim is to maintain and further develop the world-leading expertise in repository geochemistry, radionuclides migration and design optimisation of engineered barrier systems based on experimental studies and numerical simulations.

The laboratory serves an important national role by supporting the Swiss Federal Government and Nagra in their tasks to safely dispose of radioactive wastes from medical, industrial and research applications as well as from nuclear power plants. The LES research activities cover fundamental aspects of repository geochemistry, radionuclide transport and retardation in geological and technical barriers. The LES' projects portfolio is a balanced combination of experimental activities conducted in dedicated laboratories for handling radioactive isotopes, field experiments and computer simulations. The work is directed towards repository implementation and the results are used by Nagra in their comprehensive performance assessments studies. The finalisation of the documentation for the general licence application and the implementation of a repository in the next decades require expertise in model-based assessments of the repository *in situ* conditions for specific repository design. The long-term strategy of LES is thus to develop experimental and modelling expertise necessary for fully coupled description of relevant repository processes in order to assist safety and economy driven design optimisation of geological disposal in Switzerland.

Together with two other laboratories in the department of Nuclear Energy and Safety, LES maintains best practices and standards in the laboratory management and data processing according to the ISO9001:2015 certified Integrated Quality Management System. The certification covers the research and scientific services for agencies in the area of nuclear waste disposal and environmental sciences.

The present report summarises the research activities and results achieved in 2022. It gives a detailed overview of research projects, personnel management, national and international collaborations, and individual contributions achieved by scientists in the four research groups at PSI and the Chair of Mineralogy at the University of Bern.

We gratefully acknowledge the support of our work by the PSI management, Nagra, and numerous research programmes within National and European Funding agencies (e.g. SNSF, Eurad), as well as national and international industrial partners.

Table of Contents

1 OVERVIEW

Churakov S.V.

1.1 Introduction

The overall progress made in the Laboratory for Waste Management (LES) from January 1st, 2022 to December 31th, 2022 is summarised in the first part of the report. The report is organised thematically according to the seven overarching research topics. These topics are multidisciplinary in nature and include contributions from different research groups at LES and the Mineralogy Group in the Institute of Geological Sciences at the University of Bern.

1.2 General

The site selection process for geological disposal of radioactive waste in Switzerland has entered its final stage. On September 12th, 2022, Nagra has announced the plans to submit the general licence application for the geological disposal of Spent Fuel/High Level Waste (SF/HLW) and Low/Intermediate Level Waste (L/ILW) in "Nördlich Lägern" region. This decision is based on decadted laboratory and field studies. In particular, a deep drilling campaign has been conducted in the period 2019-2022 with the aim to characterise the site-specific geological and hydrological conditions in potential siting regions in Switzerland. In the last year diffusion and sorption measurements on the samples extracted from the site-specific drill cores have been finalised. A complete dataset of diffusion and sorption parameters for underground rocks from relevant siting regions provide a solid scientific basis for the performance assessment calculations and the site selection decision.

The development of the scientific basis and the documentation of the arguments to justify the site selection for the general licence application to be submitted in 2024 are the main driving forces in the current research phase. The corresponding documentation will be reviewed by the Swiss regulator (ENSI) and international experts up on submission.

Following the period of very intensive site-specific explorations leading to the submission of the RBG, the implementation phase is expected to start soon after 2030 given that the approval of the proposed site is supported by the regulator and by the Swiss parliament. During the implementation phase, the underground exploration studies will be continued to confirm the findings obtained during the site exploration campaign. Further, the implementation phase foresees the optimisation of the repository design and includes a detailed specification of the materials to be used for the repository implementation. In this context, LES' national role is to maintain know-how in the field of waste disposal geo-chemistry and relevant aspects of material sciences. By the time of repository construction phase some building material currently considered as the basis for the repository design might not be available for economical or technological reasons. Accordingly, LES continues research on the main pillars of repository safety, namely the mechanistic description of radionuclide interaction with repository barriers and the processes in the repository near field. Present and future research activities focus on the behaviour of different types of spent fuel under repository conditions, the chemical evolution of the repository near field, sorption competition phenomena, the behaviour of redox-sensitive radionuclides, the role of mineral surface-induced redox reactions, and the transfer of sorption models and data from dispersed to compacted systems. In preparation of the implementation phase, LES puts strong emphasis on the further development of advanced capabilities for reactive transport simulations. These capabilities are particularly important for understanding the long-term evolution of *in situ* repository conditions and the interaction between repository barriers causing an alteration of their retention and transport properties. Such expertise is the essential basis for the optimisation of repository design.

Future research in nuclear waste disposal will strongly rely on the process-based multiscale modelling using high fidelity simulation platforms, coupling of complex physical phenomena in repository systems. Particularly challenging in this context is the parameter transfer between models at different scales and efficient process coupling in complex realistic 3D models. LES is taking a leading role in the development of so-called data driven surrogate models based on modern algorithms developed in the field of artificial intelligence and machine learning. Particularly promising are the applications of Deep Neural Networks (DNN) and surrogate models for geochemical simulations in fully coupled THMC reactive transport codes. To foster international collaboration, LES maintains a web based platform (https://www.geoml.ai) offering a python-based environment for the training of DNN in geochemical applications. These surrogate models are the basis for the development of digital twins for coupled geochemical processes. Several demonstrations of such applications are provided at (https://www.geoml.eu).

In 2019, the Joint European Research Proposal COFUND-EJP NFRP-2018-6: *"European Joint Research Programme in the management and disposal of radioactive waste Eurad"* has been approved by the European Commission. This project is a joint venture of 52 mandated research agencies, waste management organisations and technical safety organisations focusing on the most urgent research issues of nuclear waste disposal in Europe. LES participate in eight individual work packages (WPs):

FUTURE: Fundamental understanding of radionuclide retention (WP Lead and Task lead)

DONUT: Modelling of process couplings and numerical tools applied to performance assessment (Task co-Lead)

ACED: Assessment of chemical evolution of ILW and HLW disposal cells (Task Lead)

GAS: Mechanistic understanding of gas transport in clay materials (Contributor)

CORI: Cement organics radionuclide interactions (Contributor)

UMAN I+II: Uncertainty management multi-actor network (Contributor)

MAGIC: Chemo-Mechanical AGIng of Cementitious materials (Task Lead)

MODATS: Monitoring equipment and data treatment for safe repository (Contributor)

Within the EURATOM NFRP-2019-2020-10 RIA call LES participates in the project *"Pre-disposal management of radioactive waste, PREDIS"*. This 4 years EU project was approved in spring 2020 and started in September 1st, 2020. The consortium includes 47 partners from 18 Member States. In this project, LES has a leading role in the development of a model based digital twin for the evolution of cementitious waste packages during extended intermediate storage scenarios.

The reactive transport codes developed at LES are versatile and applicable in broad cross-disciplinary applications. Complementary to geochemical applications, the codes are also used in collaborative research projects including thermohydraulic applications for nuclear reactors, desalination membranes, and pharmaceutical applications. In particular, ongoing collaboration with GlaxoSmithKline Vaccines, Belgium (GSK), a science-led pharmaceutical company, focused on research, development and manufacturing of innovative pharmaceutical products has been continued. With support of Swissnuclear, further development of multiscale simulation codes for the modelling of boiling phenomena in nuclear reactors is ongoing.

Scientific exchange is an essential component of research and development programmes. Particularly important in this context is the cross dissemination of knowledge in neighbouring fields. LES actively maintains collaborations with national and international research institutes in the field of waste management and environmental research. The main multi- and bi-lateral co-operations with external institutions and universities are summarised in Table 1.1.

Participation in international research projects and independent acquisition of project funding for PhD and postdoc projects is an essential driving force for developing state-of-the-art research capabilities, knowledge transfer and education of young generation scientists. Ongoing MSc/BSc/PhD projects and postdoc fellowships approved or started in 2022 at PSI and at the University of Bern are listed below along with ongoing ones.

P. Ingold (PhD student/UBern): *"Pollutant dynamics of bottom ash landfills"*. Start date: February 2021 (Funding: Industry).

M. Mahrous (PhD student): *"Resolving dissolution-precipitation processes in porous media: Pore-scale Lattice Boltzmann modelling combined with synchrotron-based X-ray characterisation"*. Start date: March 2018 (Funding: SNSF).

S. Mingione (PhD Student/EMPA/UBern): "*Impact of process conditions on xonotlite quality and different components in xonotlite-based products on the high- T properties of these materials"*. Start date: October 2021 (Collaboration with EMPA; Funding: Industry).

J. Owusu (PhD student): "*Pore-scale simulations of gas molecules in saturated and partially saturated clays"*. Start date: November 2019 (Funding: HORIZON 2020, Eurad).

H. Peng (PhD student): *"In situ chemical tomography and modelling of reactive transport processes in porous media"*. Start date: November 2021 (Funding: PSI-Cross).

Y. Qian (PhD student): *"Adsorption of redox sensitive radionuclides on Fe-bearing clay minerals"*. Start date: November 2019 (Funding: HORIZON 2020, Eurad).

F. Saraf (PhD Student/EMPA/UBern): "*Thermoplastic shaping of ceramic materials using FDM/FFF printing*". Start date: November 2019 (Collaboration with EMPA; Funding: SNSF).

V. Stotskyi (PhD student): *"Molecular scale understanding of competitive cation adsorption on swelling clay minerals"*. Start date: May 2021 (Funding: SNSF).

X. Wei (visiting PhD Student) *"Co-migration of clay colloids and radionuclides"*. Start date: September 2022 (Funding: Sino-Swiss-NNSFC exchange programme).

D. Zerva (PhD student): *"Diffusion and retention of surface complexing radionuclides in compacted clay minerals"*. Start date: March 2020 (Funding: Horizon 2020, Eurad).

Y. Zhe (visiting PhD Student): *"Redox sensitive sorption of Cr(VI) in clay-iron systems"*. Start date: December 2021 (Funding: NNSFC exchange programme).

Dr. F. Di Lorenzo (postdoc): *"Molecular scale understanding of competitive cation adsorption on swelling clay minerals"*. Start date: June 2021 (Funding: SNSF).

G. Hu (postdoc): "*Data driven and physics based TH-model for repository near-field*". Start date: February 2022 (Funding: HORIZON 2020, Eurad).

Dr. A. Mokos (postdoc): *"Boiling crisis in nuclear reactor"*. Start date: March 2021 (Funding: Swissnuclear).

Dr. A. Rajyaguru (postdoc): *"In situ chemical tomography and modelling of reactive transport processes in porous Media"*. Start date: August 2021 (Funding: PSI-Cross).

Tab. 1.1: National and international co-operations.

Co-operations
National Nagra* (Major financial contribution, various technical working groups) Swissnuclear* (Reactor safety, material aging)
Multinational NEA Thermodynamic Database Project EURATOM HORIZON2020 (Eurad) EURATOM HORIZON2020 (PREDIS) Mont Terri Projects* (diffusion retardation, clay-cement interaction)
Universities University of Bern*, Switzerland (mineralogy, petrography, water chemistry, C-14 AMS) EPFL, Switzerland (cement systems) Université de Bourgogne, Dijon, France (molecular modelling) ETH*, Zurich, Switzerland (GEMS) Hiroshima University, Japan (clay-cement interaction) University of Luxembourg* (porous media) Sino-French Institute of Nuclear Engineering and Technology, Sun Yatsen University (diffusion) Lanzhou University, China (diffusion)
Research Centres CEA*, France (chemistry of near and far field) EMPA*, Switzerland (cement) IRE, HZDR*, Germany (XAS, TRLFS, atomistic modelling, reactive transport) INE, KIT*, Germany (near and far field; TRLFS) FZJ, Germany (sorption/diffusion of Ra, reactive transport, thermodynamics of solid solutions) SCK/CEN, Belgium (clay and cement systems) UFZ*, Germany (reactive transport, clay systems)
Industrial Partners GlaxoSmithKline* NanoCem Congineer

**formal co-operation agreements*

Several PhD students and MSc projects have been completed in 2022:

A. Bucher (BSc student/UBern): *"Atomic scale structure of magnetite water interface"* (UniBe 2021-2022).

P. Dörfer (MSc student/UBern): "*Optimisation of biomass bottom ash for use in cement production*" (UniBe 2021-2022).

N. Krattiger (MSc student/UBern): *"Comparative study of C-S-H and ASR-products in cement by GCMC modelling"* (UniBe 2021-2022).

M. Wolffers (PhD student/UBern): *"Genesis and characterisation of fly ash in Swiss waste incineration plants"*. PhD Defence date March 4th, 2022 (Funding: Industry).

The organisational chart of LES comprises four research groups located at PSI (Fig. 1.1). A fifth research group is located at the Institute of Geological Sciences (IfG) at the University of Bern. The mineralogy group at IfG is complementing the expertise in the field of mineral dissolution kinetics, structural studies of high porous materials and X-ray diffraction-based structure refinement and the geochemistry of conventional waste disposal. In particular, the mineralogy group hosts the Competence Centre for Secondary Raw Materials conducting applied research in the field of environmental geochemistry and secondary raw materials.

The LES annual report 2022 is organised in seven thematic research projects addressing specific aspects of repository geochemistry and radionuclide transport:

Chapter 2: Geochemical evolution of repository systems

Chapter 3: Development of mechanistic sorption models and experimental validation

Chapter 4: Radionuclide transport and retention in compacted clay systems at full and partial saturation

Chapter 5: Thermodynamic models and databases

Chapter 6: Fundamental aspects of mineral reactivity and structural transformations

Chapter 7: Geochemical aspects of waste materials and their disposal

The following section provides an overview of activities related to the Sectoral Plan for Deep Geological Disposal, repository near and far field, reactivity of barrier systems and code benchmarking.

1.3 Sectoral plan for deep geological disposal

The potential radiological impact of a repository is one of the main safety relevant criteria employed in the site selection process. Sorption and diffusion data are the basis for dosis calculations. The sorption databases for *in situ* repository conditions are derived using a thermodynamic approach. A new major update of LES thermodynamic database was released in 2020 in an electronic form. It is available in the GEMS geochemical solver together with detailed documentation of recommended thermodynamics parameters since 2022 (see section 5.1).

A cement sorption database been prepared for the safety assessment studies reported in the general licence application. This database was derived based on the most recent version of GEMS thermodynamic models, using PSI-TDB 2020 and imported CEMDATA18. Derivation of solubility limits using revised thermodynamic data enabled to reduce uncertainties on expected concentration of key radionuclides in the cementitious waste repository (see section 5.2).

Anhydrite ($CaSO_4$) rich rocks are present in confining units of Opalinus Clay formation. Transport properties of these rocks remain largely unknown, Experimental studies of HTO and $^{36}Cl^-$ tracer diffusion in anhydrite sample from a deep borehole at Zürich Nordost siting region are ongoing. A particular challenge for such investigations is the need to conduct experiments at elevated temperatures (50 °C) to avoid hydration reaction of anhydrite into gypsum. First experimental data provide an estimation of the tracer diffusivity and accessible porosity (see section 4.3).

1.4 Repository near field

1.4.1 Repository chemistry

The evolution of geo-chemical conditions in a cement waste repository is investigated in the framework of the EURAD WP-ACED. Cementitious waste packages often contain heterogeneous mixtures of waste materials, such as metallic and organic waste conditioned in concrete. The spatial structure of a waste package, the reactivity of the waste matrix and the interaction of the reaction products with the concrete, as well as the gas and liquid transport processes inside and outside the waste package, are likely to determine the chemical properties and performance of waste packages over time. Geochemical batch-reactor modelling, a so called mixing-tank approach, was used to assess internal processes determining chemical evolution in waste packages for various initial conditions in order to assess the importance of degradation reactions and material options under different *in situ* conditions (see section 2.2).

1.4.2 Clay systems

In the frame of the Swiss Sectoral Plan for Deep Geological Repositories (SGT), LES completed a series of cation exchange capacities (CEC) measurements on a pool of rock samples from 7 boreholes across the geological siting regions Jura Ost (JO), Nördlich Lägern (NL), and Zürich Nordost (ZNO). The samples were selected to represent different lithologies of the natural barrier system, i.e., Opalinus Clay and the upper and lower confining units. The CEC is directly correlated to the content and type of clay minerals in the rock samples, and consequently to their adsorption properties towards radionuclides. Its variability is an excellent indicator for the homogeneity of the clay mineral content along the Opalinus Clay formation as well as to the upper and lower confining units for each borehole. The fractional occupancies of exchangeable cations can act as a "fingerprint" for the *in situ* porewater compositions of the rocks (see section 3.2).

Several studies of radionuclides retention and transport in clays and argillaceous materials are performed in framework the EURAD programme WP FUTURE:

Ba and Ra uptake on montmorillonite and illite are investigated in collaboration between Forschungszentrum Jülich (FZJ) and PSI-LES. The adsorption behaviour of both elements depends on the ionic strength, which is indicative for a cation exchange mechanism (see section 3.3).

Coupled adsorption and electron transfer interface reactions governing the retention of redox-sensitive Se and Tc on Fe^{2+}/Fe^{3+} bearing clay minerals are jointly investigated by PSI and BRGM. The mineralogical characterisation of the reduced clay samples (structural Fe^{3+} reduced to Fe^{2+}) used for Tc and Se sorption experiments provide indication for surface dissolution mechanism of Fe bearing clays at different redox state. Further redox state of Se on clays with different Fe loading was identified by x-ray absorption spectroscopy (see section 3.6).

Currently used sorption models are based on the assumption that sorption is fully reversible. This assumption is not always in agreement with experimental observations. Long term investigations of Zn sorption reversibility on Illite du Puy (IdP) are ongoing. The spectroscopic characterisation of local Zn coordination at low loadings show remarkable similarities with a spectrum of Zn intrinsically present in IdP, indicating a similar structural environment. The data for the adsorption and desorption obtained for the low loaded samples are identical, indicating that the Zn surface complexes remain unchanged over the time period of 2 years after desorption (see section 3.8).

Experimental validation of the surface diffusion concept has been studied using three homoionic illite sample conditioned with Li-, Na- and Cs- electrolyte solutions at different concentrations. Use of different electrolyte enable to vary the extent of diffuse double layer and its effect on the diffusivity of the moderately sorbing tracer ($^{65}Zn^{2+}$ and $^{57}Co^{2+}$). The combination of the results from the in-diffusion experiments with transition metal cations and through-diffusion experiments with HTO suggests that the diffusivity of the moderately sorbing tracers is rather controlled by the cation distribution ratio between the mobile surface species and the species in the bulk aqueous phase than by the geometry factor (see section 4.4).

Analysis of cations, anions and water tracer diffusivities in compacted Ca^{2+}- and Na^{+}-conditioned smectites reveals that transport of Na^{+} and HTO tracers in both smectite forms is rather similar. Unexpectedly, more intriguing results were obtained for the $^{22}Na^{+}$ tracer diffusion, where a much stronger retardation effect was observed for the Ca^{2+}-conditioned clays compared to the Na^{+}-form (see section 4.5).

Experimental and theoretical studies of Ni^{2+} and Lu^{3+} uptake on synthetic saponite are conducted to obtain molecular scale understanding of competitive cation adsorption on swelling clay minerals. Mg-Saponite, employed in the study belongs to the family of trioctahedral smectites and is a common synthetic product in industrial applications. Use of synthetic clay samples allows to customise the substrate and to tune it surface properties, which is the strong advantage for the description of the sorption mechanism. Preliminary experimental sorption data for Ni^{2+} are consistent with typical behaviour of the sorption complexation of 2:1 dioctahedral smectites (see section 3.5).

Significant quantities of gas are expected to emerge in a repository, either resulting from corrosion of metallic materials or due to degradation of organic waste compounds. The gas should be able to migrate through the multi-barrier system to prevent potential pressure build up, which can lead to the loss of barrier integrity otherwise. One of the most important parameters controlling the initial gas dissipation in a disposal system of engineered barriers is the diffusive mobility of gaseous species in host rocks and buffer materials. Diffusion of gas in saturated and partially swelling clays is investigated by atomistic simulations within the EURAD WP-GAS. Combining the theoretical results and experimental observations a generic equation predicting gas diffusivity in real clay rock was formulated, which is based on readily available physical parameters of gas molecules and host rocks (see section 2.4).

A dedicated tool (UpSaGems) has been developed for uncertainty propagation and sensitivity analysis in the sorption complexation modelling. The tool provides the confidence interval for sorption model parameters taking into account all sorts of input data uncertainties used for the model calibration. The provided Sobol indices can be used for identification of model parameters responsible for the largest uncertainty at a given conditions (see section 3.4).

1.4.3 Cement systems

Calcium silicate hydrates (C-S-H) are gel-like phases providing cohesive strength of concrete. They are also responsible for the initial entrapment of radionuclides via sorption or solid solution formation mechanisms in the cementitious barriers of the radioactive waste repository. The CASH+ is formulated based on sub lattice solid solutions model and allows an incremental extension of the chemical complexity keeping the core data unchanged. The model is calibrated against various experimental data on the uptake of cations, solubility, water content, and mean silicate chain length of C-S-H phases. The fine-tuned model accurately predict cement hydration processes including cement pore solution compositions at different water to binder ratios, silica fume additives and variable temperatures conditions up to 80 ^{o}C (see section 5.3).

Alkali-silica reaction (ASR) widely occurs in concrete and it's known as "concrete cancer". ASR is one of the most important degradation mechanisms resulting in durability problems and premature loss in serviceability of massive concrete infrastructures (i.e. bridges, dams, etc.). Despite decades of analysis of ASR and its products, ASR chemistry remains poorly understood especially on the molecular scale. *Ab initio* molecular dynamics simulations were applied to reveal detailed mechanism of ASR dissolution and activation barrier controlling the ASR dissolution kinetics (see section 6.5).

1.4.4 Interface processes

Thick-wall steel casks are used to store radioactive waste in deep geological repositories and to prevent the release of radionuclides into the environment. Steel corrodes slowly under repository conditions forming mixed iron oxides, mainly magnetite (Fe_3O_4). The radionuclides, especially redox sensitive ones, are expected to interact strongly with the corrosion products and either form surface complexes or become incorporated into the crystal structures of the iron oxides. Successful theoretical modelling and interpretation of spectroscopic data require good understanding of surface speciation as function of chemical condition. The stability and speciation of magnetite surface at different pH and Eh conditions are investigated by *ab initio* quantum mechanical simulations (see section 6.4).

The thermal, hydraulic, mechanical, and chemical (THMC) evolution of the high-level waste repository nearfield is an important safety aspect. The temperature is the main parameter, which can be monitored in a pilot repository to confirm repository performance during design, construction, operation and monitoring phase. A Full-scale Emplacement experiment (FE) at the Mont Terri URL investigates different aspects of waste emplacement, backfilling and early-stage evolution of a SF / HLW repository tunnel in a clay-rich formation (Opalinus Clay), using proxy. Design and sensor data of this experiment allow to conduct the first step in the direction of a 3D digital twin of a (pilot) repository. Within the Eurad MODATS project the temperature and relative humidity evolution is being modelled taking into account a combination of physical based model for heat transport, machine learning for interpolation of early stage monitoring sensor data (temperature, humidity, …) and surrogate models for overall system evolution. Good agreement between model predictions and sensor data provide a basis for further extension of the surrogate modelling with respect to mechanical and chemical phenomena. The model can be used to optimize the repository design parameters such as the material selection and dimensionalization, waste configuration with respect to safety, performance and costs (see section 2.7).

1.5 Model development, code benchmarking, advanced analytical tools, thermodynamic databases

Reactive transport simulations are the main tool applied for the long-term performance assessment of the repository *in situ* conditions and geochemical evolution of repository near field. Coupled THMC simulations of large spatial domains performed for a long time scale are particularly challenging due to high computational resources and costs. For complex geochemical systems the performance of coupled THMC-codes is often limited by the geochemical solvers which can account for up to 90 % of the simulation time. The second challenge is related to the coupling of models at different scale and the corresponding parameter transfer.

Several projects are focused on reactive transport simulations of crystallisation processes at pore scale using most advanced modelling algorithms. In the framework of the PSI-funded CROSS project *"In situ 4D micro X-ray chemical imaging and a digital twin of miniaturized counter-diffusion experiments: co-precipitation of metals with carbonates in porous media"* numerical models are developed for real time-simulations of nucleation and grows of carbonate

minerals. The developed model is able to predict different morphology of the crystals depending on the concentration of solutes and fluid flow conditions (see section 2.3).

The application fields of artificial intelligence (AI) and machine learning methods (ML) are growing at a very fast pace. The EURAD community has recently started using ML for a) accelerating numerical simulations, b) improving the efficiency of multiscale and multiphysics couplings, c) uncertainty quantification and sensitivity analysis. Within Eurad-DONUT project a benchmark is designed to test a variety of ML techniques relevant to geochemical and reactive transport simulations in the framework of radioactive waste disposal, aiming at identifying benefits and limitations of ML (see section 2.6). In house developed modelling tools for uncertainty analysis in reactive transport simulations has been further extended using surrogate models for radionuclide transport and retention. It was shown that neural network based approach is able to provide an overall acceleration of the sensitivity analysis by three to four orders of magnitude, without significant loss in accuracy (see section 2.10).

Development of the Gibbs Energy Minimisation package GEMs has been continued. An extensive overview of the available simulation tools and features, database management, thermodynamic models and data handling routines implemented during last decade are summarised in the section 2.5.

The models and codes developed at LES are highly versatile and find further applications in different neighbouring fields. Pore Scale Lattice Boltzmann simulations are used in computational fluid dynamics applications to assess boiling flow in fuel-assembly affected by crud (see section 2.8.1), multiphase fluid flow in desalination membranes (see section 2.8.2) and pharmaceutical application (see section 2.9). Massively parallel Smooth Particle Hydrodynamics (SPH) simulations with up to 100M particles have been able to reproduce waterfall dynamics and kinematic pressure in operating hydrous power plants with high accuracy (see section 2.8.3).

1.6 Environmental impact of conventional waste disposal, secondary raw material recycling and fundamental aspects of mineral reactivity

PSI/LES and the Institute for Geological Science at the University of Bern (UBERN/IfG) have a long standing collaboration in the field of environmental mineralogy and applied geochemical engineering. The research of the Mineralogy Group at the University of Bern covers fundamental and applied aspects of mineral dissolution and precipitation, chemical factors of crystal structure stability and temperature driven phase transitions in minerals. The dedicated laboratories operated by the mineralogy group are equipped with powder and single crystal diffractometers for structural studies of minerals, and with an atomic force microscope for *in situ* characterisation of mineral surfaces. The experimental studies are widely supported by modelling activities.

The Competence Centre for Secondary Raw Materials (CCSRM, Project Leader Dr. U. Eggenberger) is embedded in the Mineralogy group and conducts applied research in the field of environmental geochemistry and secondary raw materials. The core competences of the CCSRM cover the topics of circular economy and disposal quality of conventional non-radioactive waste materials. Geochemical aspects and challenges related to the *in situ* conditions in conventional and radioactive waste disposal rely on common scientific backgrounds and modelling tools. Shared expert knowledge provides the fruitful basis for collaboration and mutual synergies between LES/PSI and CCSRM/UBERN. Recently, CCSRM has established a collaboration project with the Wyss Academy for Nature (www.wyssacademy.unibe.ch) on the topic of circular economy.

Fly ash from municipal waste incineration plants (MSWI) consists of boiler and electrostatic precipitator ash and shows elevated concentrations of heavy metals (e.g. Zn, Cu, Cd, Pb). In the context of optimizing the heavy metal recovery during the acid leaching of MSWI fly ash, a detailed knowledge about the geochemical properties and especially about the binding forms of the heavy metals is of great importance. A thermodynamic model was developed and successfully applied to simulate the sublimation process and flue gas evolution in the cooling path of the high temperature incineration plant. A good agreement was obtained between the predicted mineral stability and the mineralogical characterisation of fly ash (see section 7.3).

Quartz sand is commonly used as heat carrier in fluidised bed incinerators. Replacement of the primary quartz sand by secondary industrial residues such as bottom ash would not only reduce the use of expensive primary resource but also find a reuse of abundant secondary materials. In cooperation with Bertsch-energy and the TU Vienna (BEST group), experimental investigations of alternative materials were conducted in a bench-scale fluidised bed reactor to monitor the stability of the incineration process with a new bed material. Various ashes types generated during the incineration process were tested at the Holcim laboratories for its suitability as cement production additives (see section 7.4).

Swiss waste disposal ordinance defines an aftercare period of 50 years for the monitoring of the landfill sites. The time horizon of landfill aftercare reflects only a small part of its life cycle and is not based on scientific studies. Therefore, reliable predictions for long term behaviour of Type D landfills are challenging. To close the knowledge gap, the dynamics of pollutants leaching from landfills is investigated by monitoring the discharge water fluxes and chemistry in connection with precipitation and drainage events. The collected monitoring data provide a basis for development of a hydro-geochemical model of landfill sites evolution (see section 7.2).

Heavy-metal-exchanged zeolites are attractive materials that find applications in several research fields, from environmental remediation to catalysis. Pb-exchanged zeolites have received special attention because of their importance in environmental pollution related problems (i.e. removal of Pb from wastewater and food) and their use in industrial processes. The crystal structure of a natural zeolite, stellerite, fully exchanged with Pb, was investigated by Single Crystal X-ray Diffraction, Molecular Dynamics simulations and X-ray Absorption Spectroscopy to determine eventual structural changes induced by the lead uptake and determine the lead speciation. The study reveals rather unusual thermal behaviour of Pb stellerite, which is explained by the formation of $(PbOH)^+$ complexes responsible for an increased thermal stability and structural reversibility of Pb - stellerite as well as potential consequences for its industrial applications (see section 6.2).

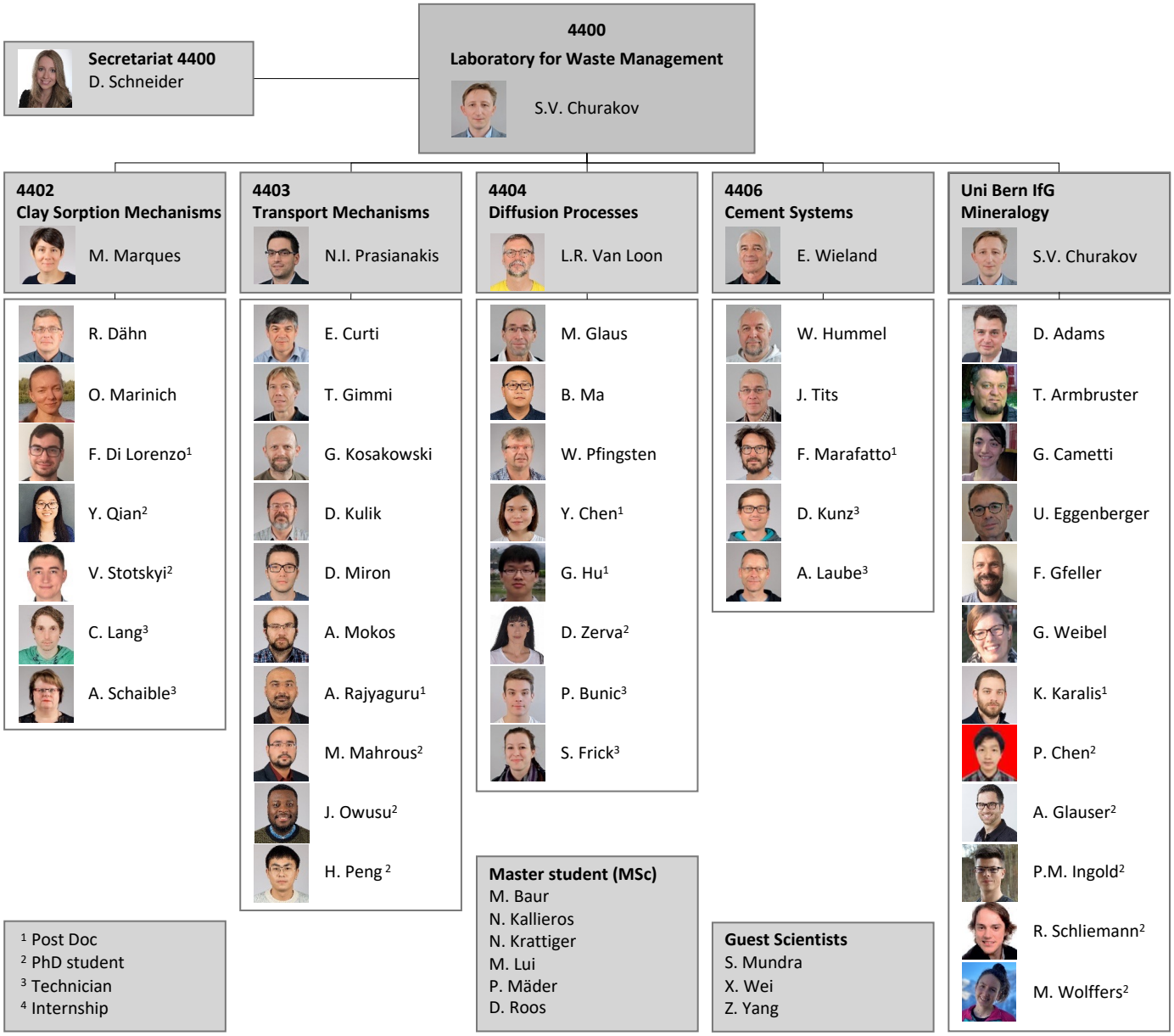

Fig. 1.1: Organisational chart of LES.

2 GEOCHEMICAL EVOLUTION OF REPOSITORY SYSTEMS

Prasianakis N.I., Churakov S.V., Curti E., Gimmi T., Pfingsten W., Kulik D.A., Miron G.D., Mokos A., Grolimund D., Rajyaguru A. (postdoc), Hu G. (postdoc), Mahrous M. (PhD student), Peng H. (PhD student), G. Goyal (internship), Kosakowski G., Cheuk Lam L. (master student)

2.1 Introduction

Cross scale THMC-numerical models and simulation tools are essential for describing the long-term evolution of the multi-barrier repository systems and geotechnical engineering. Such models are the basis for the safety assessment and cross comparison of different repository designs conducted as a part of the site selection process in the Sectoral Plan for Deep Geological Disposal (SGT) Stage 3, and the following general license application. Geotechnical engineering is a steadily growing research field aiming at optimization of the subsurface reservoirs properties, for geothermal energy production and for resource exploration.

The research activities described in this chapter cover three main topics relevant for repository near field evolution: 1) Experimental characterisation and numerical modelling of the evolution of the technical barriers and their respective interfaces e.g. cement evolution and cement-clay interaction; 2) Fundamental understanding of transport and retention of radionuclides through multiscale modelling and upscaling techniques; 3) The benchmarking of coupled codes as well as the development and coupling of state-of-the-art reactive transport codes with thermodynamic modelling tools and databases.

LES is participating in several EURAD Work Packages (WP). Within the EURAD WP GAS, molecular dynamics simulations are used to investigate the gas transport through clays. (PhD project of Jerry Owusu). Within the EURAD WP DONUT several multiscale codes and their couplings are developed. An international benchmark on Geochemistry and Machine learning has started and is led by PSI. In EURAD WP MODATS the digital twin of the Mont-Terri full scale emplacement experiment (FE) has been developed and temperature evolution predictions have been conducted. In EURAD WP ACED, the waste package geochemical evolution has been investigated including the gas release due to degradation processes.

GEM Software development is ongoing under the lead of D.A. Kulik. This year a leap towards web-based dedicated tools has been completed.

To cover the needs of industrial partners and students working in the field of cement chemistry a dedicated easy to learn user friendly web-based application CemGEMS (https://cemgems.app) has been developed within a project funded by NANOCEM. CemGEMS web application is tuned to simulate basic scenario for cement leaching, degradation, and salt attacks, and it can equally be applied in radioactive waste management studies.

The CROSS project "*In situ* 4D micro-X-ray chemical imaging and a digital twin of miniaturized counter-diffusion experiments: co-precipitation of metals with carbonates in porous media" has continued in 2022 (PhD project of Haonan Peng). The overarching research goal of the project is to elucidate the role of trace metals (Ni, Zn, Pb) in polymorph selection and growth kinetics of calcium carbonate in porous media (silica gel, mineral powders). Machine learning is a core technology for enabling the development of the digital twin technology for the crystallisation experiments. First experimental results show extremely rich physics. On the modelling side the digital twin of the experiment has been set up. 3D Lattice Boltzmann simulation simulations have allowed to evaluate the local concentrations of the involved chemical species and first crystal growth simulations have been conducted.

Several projects on multiscale multiphysics computational fluid dynamics are currently on-going, based on the advanced modelling capabilities that exist at LES. In the realms of a collaborative project with the Laboratory for scientific computing and modelling at PSI (LSM-PSI) and under the umbrella of Swissnuclear funding agency through the project "*Numerical prediction of boiling crisis considering surface characteristics*", the fundamental understanding of boiling processes from atomistic to reactor scale is pursued. By combining atomistic and pore-level simulations, it is has been possible to extract correlations between the surface roughness of ZrO_2 and the nucleation site density, a key parameter for macroscopic numerical codes. Finally, two industrial research projects with the pharmaceutical company "*GlaxoSmithKline*" have been continued in 2022.

2.2 Waste package evolution / EURAD WP ACED

The evolution of (geo)chemical conditions in a cement based deep geological repository for intermediate-level waste (ILW) is investigated in the framework of the EURAD (European Joint Programme on Radioactive Waste management) work package ACED (Assessment of Chemical Evolution of ILW and HLW Disposal Cells).

Often waste packages contain heterogeneous mixtures of waste materials, such as metallic or organic waste, conditioned in concrete. The spatial structure of a waste package, the reactivity of the waste matrix and the interaction of the reaction products with the concrete, as well as the gas and liquid transport processes inside and outside the waste package, are likely to determine the chemical properties and performance of waste packages over time. The long-term evolution of the waste packages, specifically in terms of gas production, is expected to have an impact on the geochemical evolution of disposal cells and affects the barrier function of the near field.

Geochemical batch modelling, a so called mixing-tank approach, utilizing the xGEMS python interface to the GEMS chemical solver in Jupyter notebooks was employed to assess the impact of the different degradation reactions on the evolution of the chemical conditions in waste packages for operational and decommissioning waste sorts.

The materials and inventories of the waste packages modelled in this study were retrieved from Nagra's MIRAM 14 database, which contains model wastes for the planned Swiss low- and intermediate-level waste (L/ILW) deep geological repository (Nagra, 2014). The degradation of organic materials, the corrosion of metals, the dissolution of zeolite additives, and the dissolution of siliceous aggregate (quartz used as surrogate) were considered in accordance with reaction rates reported in the literature (Kosakowski et al. 2020; Wieland et al. 2018).

The evolution of decommissioning waste is dominated by corrosion of the metallic waste, which is about 93 weight percent (wt. %) steel, 3 wt. % iron and minor amounts of aluminium, copper, zinc and brass. The anoxic corrosion of metals consumes water and releases hydrogen gas. Key factors for the control of corrosion rates are the availability of water and the pH of the pore water. The pore water pH is largely controlled by the backfill materials used to fill void spaces in waste packages. The evolution of different types of cement based backfills was investigated, namely a defined based on a CEM II/B-T without aggregates, and backfill variants based on CEM I with silica fume and clinoptinolite admixture, and carbonate or siliceous aggregates.

Fig. 2.1 demonstrates the link between temporal change of pH of the pore solution (left figure) and the mole amount of hydrogen gas produced by metal corrosion (right figure). Because of the absence of degradable organics in this waste sort, the pH is mainly controlled by the aggregate-cement reaction, i.e. the pozzolanic reaction in case of siliceous aggregates. The addition of silica fume will suppress portlandite

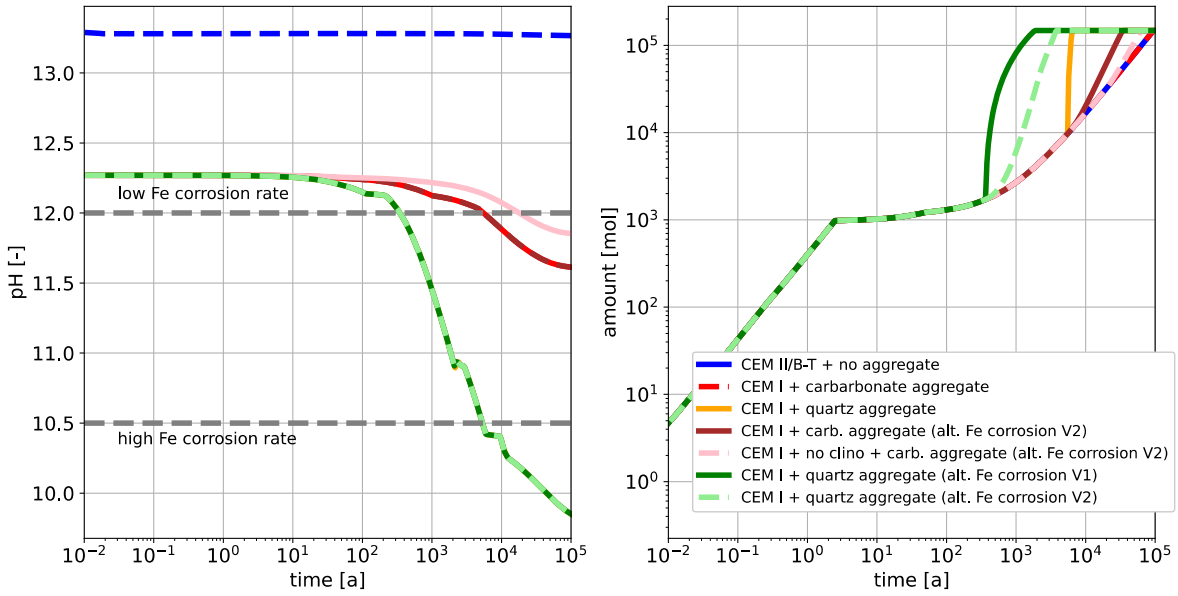

Fig. 2.1: Evolution of metallic decommissioning waste in concrete containers: pH evolution of the pore solution with time for different modelled scenarios, the gray horizontal lines signify the pH limits of different corrosion rates (left) and cumulative hydrogen gas released by metal corrosion (right). Scenarios differ in terms of cementitious infill and the rate laws used for iron corrosion. sf: silica fume, clino: clinoptilolite (modified after Kosakowski and Wieland, 2022).

formation during cement hydration and results in an initial pH below 12.6. The presented calculations assume that external water can freely enter the waste package.

The reference model for iron corrosion (Diomidis et al., 2016) is parameterised in such a way that corrosion rates above pH 10.5 are low but increase a two orders of magnitude as soon as the pH drops below 10.5. All modelled scenarios that utilise this corrosion parameterisation therefore show the same gas release until pH drops below 10.5. We show scenarios with alternative pH dependence of iron corrosion used in the ACED project. In these models the corrosion rates change linearly (V1) or non-linearily (V2) from the low rate (above pH 12.0) to the high rate below pH 10.5 (See Fig. 2.1, grey horizontal lines). Note that hydrogen production stops as soon as all metals are consumed by corrosion. The fast hydrogen production in the first three years can be attributed to corrosion of minor amounts of aluminium and zinc, which are modelled with a fast constant corrosion rate following Wieland et al. (2018).

The results of Fig. 2.1 demonstrate that gas generation in the waste packages is sensible to the composition and degradation of backfill materials and to the parameterization of steel corrosion rates at alkaline pH values.

The geochemical modelling approach enables us to assess internal processes that may controll the chemical evolution in waste packages for various initial conditions. The proposed batch modelling approach is well suited for "screening" applications with the aim of assessing the importance of degradation reactions and waste material partitioning, while it is of limited use for realistic predictions of the long-term evolution of waste forms in time and space.

2.3 Fundamental understanding of precipitation and recrystallization processes and digital twin of microfluidic experiments

In the framework of a PSI-funded CROSS project "Resolving Calcium Carbonate Polymorphs Precipitation in Porous Media: A combined modelling – experimental approach with Synchrotron-Based Tomography" micro counter diffusion (μ-CD) experiments have been carried out to study the dynamics of $CaCO_3$ precipitation and re-crystallisation over a time scale of months. The setup of the diffusion cell is shown in Fig. 2.2. It consists of two reservoirs containing 0.3 M $CaCl_2$ and Na_2CO_3 solutions connected to a 300 μm thick glass capillary filled with silica gel saturated with 0.1 M NaCl. The counter diffusion process and related precipitation/dissolution phenomena are then monitored by optical microscopy and advanced micro-XRF/XRD mapping techniques during times ranging from a few hours to several months. Of special interest are the optical microscopy observations and a preliminary interpretation in terms of non-classical nucleation theory and growth-dissolution kinetics. Quantitative schemes and equations for both nucleation and growth/dissolution are needed for the development of the Lattice-Boltzmann modelling code which is currently under development.

Fig. 2.3 shows a time series of screenshots taken by the optical microscope. Formation of three different polymorphs of $CaCO_3$ has been identified based on the precipitate morphology: (i) Sudden formation of a black precipitate, presumably amorphous calcium carbonate nanoparticles, (ii) Cauliflower-like vaterite forming at the high pH side of the capillary (right, Na_2CO_3 reservoir), (iii) formation of isometric and columnar crystals at the low pH side (left, $CaCl_2$ reservoir), presumably calcite. The former

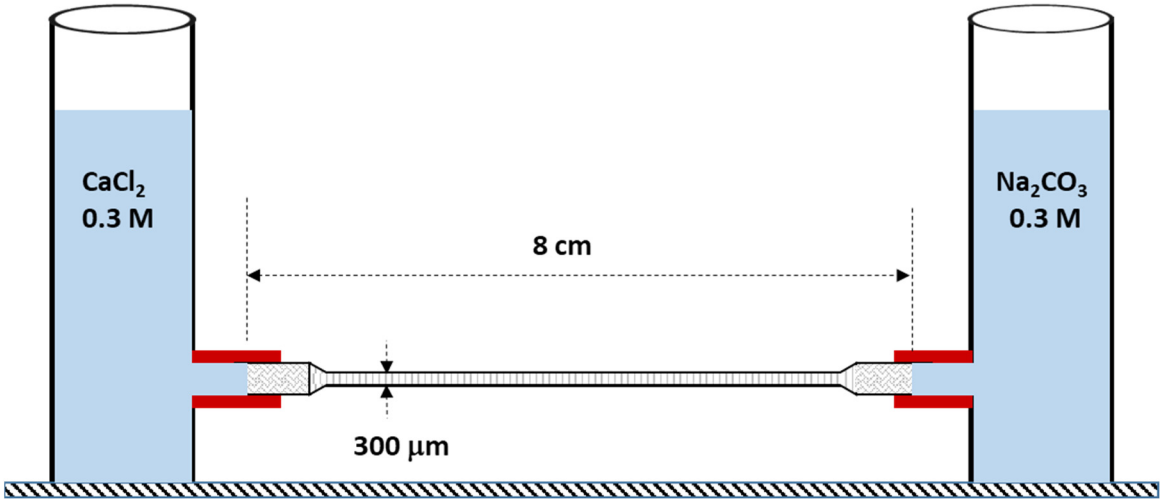

Fig. 2.2: Schematic illustration of the μ-CD experimental setup.

interpretation based purely on morphological criteria has been fully confirmed by µ-XRD data and SAXS data collected at the Swiss Light Source. With time, the prismatic-columnar calcite nucleates and grows at the left $CaCl_2$-rich side and progressively replaces vaterite at the right Na_2CO_3-rich high pH side, and finally nucleates and grows at the expense of the ACC precipitate (see arrows in Fig. 2.3).

Recently, substantial progress has been made in the understanding of $CaCO_3$ nucleation (Gebauer et al. 2014) in terms of the so-called non-classical nucleation theory, which was developped complementary to the classical nucleation theory (Kashchiev and van Rosmalen 2003). In a system simulated with the µ-CD capillary, different supersaturation conditions can onset simultaneously for different mineral phases depending on location and time.

The nano-ACC "milky zones" formed suddenly in the µ-CD experiments (black regions in Fig. 2.3) were interpreted to be the result of spinodal decomposition. Indeed, it was possible to observe formation of multiple "milky zones" along with nucleation/growth of calcite (preferentially at the low pH $CaCl_2$ side) or vaterite (only at the high pH Na_2CO_3 side). With time, vaterite re-crystallisation to thermodynamically more stable calcite occurs and new calcite crystals nucleate and grow. These processes progress at the expense of ACC, as seen from the retreating right boundary of the "milky zone". The locations of first appearance of vaterite and calcite is consistent with independent experimental data indicating that vaterite nucleation is favoured at pH > 9-10, while calcite nucleation is favoured at lower pH conditions (Avaro et al. 2020). Aragonite was detected only exceptionally and in small amounts, which is consistent with published data indicating that in Mg-free inorganic systems aragonite should precipitate only above 35 °C (Avaro et al. 2020).

The mechanistic understanding and modelling of calcium carbonate ($CaCO_3$) precipitation polymorphs (calcite, vaterite, aragonite) is very challenging due to the complexity of the involved process. Evolution of such systems is controlled by the interplay of nucleation, crystallization, precipitation kinetics, species transport, homogeneous and heterogeneous chemical reactions. During experimental investigations and in order to decipher the governing mechanisms, it is necessary to obtain a detailed description of the time evolution of the major diffusion pathways and the local conditions at the solid-fluid interfaces during the crystal growth. For this purpose, the digital twin of the counter-diffusion laboratory experiment is developed. The multi-component lattice Boltzmann method (LBM) is used as the basic framework for simulating the reactive transport processes in porous media at the pore scale. It enables to obtain information at very high spatial and temporal resolution and incorporates all necessary physical and chemical processes (Prasianakis et al. 2017). The experimental observations at the synchrotron facilities of the Swiss Light Source (SLS-PSI), in combination with numerical modelling results should allow to correlate

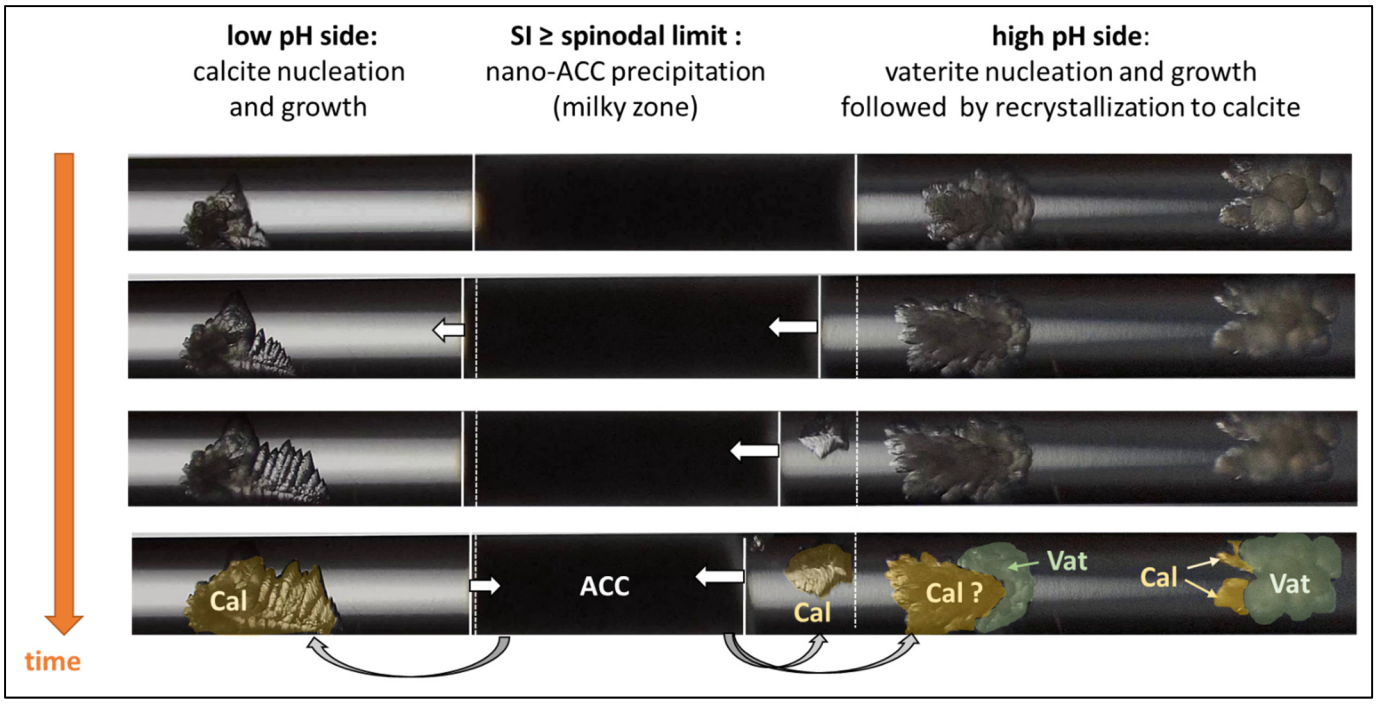

Fig. 2.3: Optical microscope images of the central portion of a µ-CD capillary filled with silica gel and connected to 0.3 M $CaCl_2$ and 0.3 M Na_2CO_3 counter-diffusing reservoir solutions for a sequence of reaction times ranging from 9.0 to 9.37 days. The length of the imaged capillary is 4 mm.

the type of polymorph precipitated with the saturation state and local composition of the aqueous solution. The preliminary model is tested by simulating the precipitation process of calcium carbonate with different Damköhler numbers, which resulted in different morphology of precipitates. In Fig. 2.4 a case of very high reactivity is shown which results in dendritic growth. Superimposing simulation results with experiments, allows, in principle, to measure numerically the local precipitation rates (via inverse modelling) in relation to the species concentrations at the crystal/fluid interface. Preliminary species concentration maps at steady state have been also numerically produced using the direct input of the experiment, for providing a first estimate of the concentration distribution around the precipitates as shown in Fig. 2.5.

These preliminary observations and simulations of nucleation and growth phenomena will serve as a basis for the full LB modelling of the reactive transport processes taking place in the capillary. To reach the state of a "digital twin", such model will require quantitative parametrization of relevant transport, reaction kinetic rates and the model parameters of non-classical nucleation theory to be obtained combining the experimental measurements and simulations.

2.4 Mechanistic understanding of gas transport processes in geological disposal of radioactive waste

Within the framework of EURAD WP GAS the mobility of gas molecules in geological disposal of radioactive waste is investigated at an atomistic scale. Phenomenological examinations of gas transport processes in clayey rocks consider four mechanisms (Marschall et al. 2005): 1) advection and diffusion of dissolved gas, 2) visco-capillary flow of gas and water, 3) dilatancy-controlled gas flow, and 4) gas transport in tensile fractures. The conducted study is focused on the diffusion of dissolved gases in saturated and partially saturated clays using molecular dynamic simulations (MD). In the past year, the mobility of dissolved gases in smectites under saturated conditions was studied (Owusu et al. 2022). It was found that pore size, type

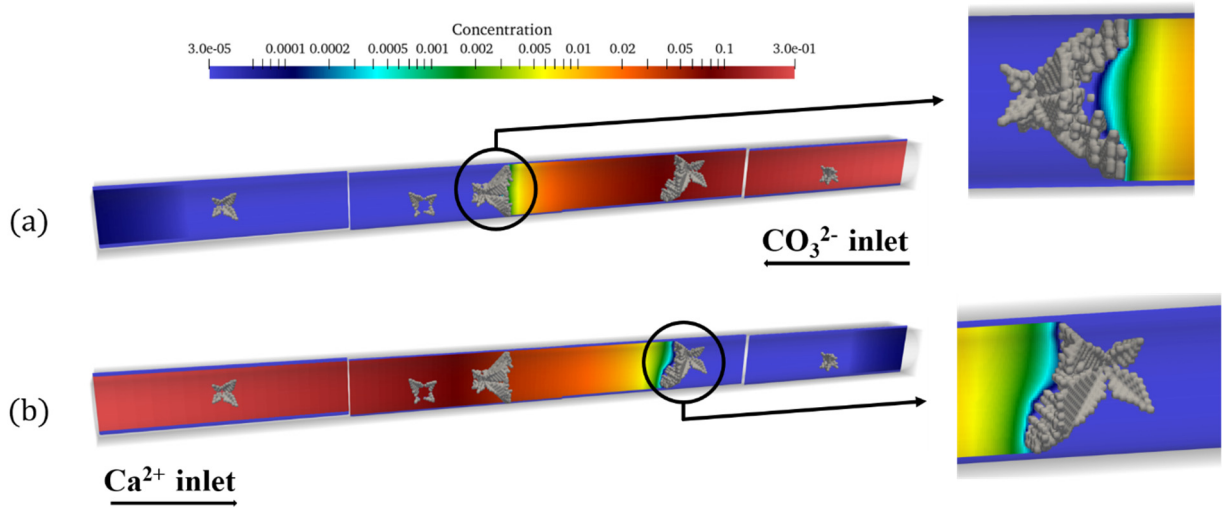

Fig. 2.4: Lattice Boltzmann simulations of heterogeneous precipitation of $CaCO_3$ in a narrow tube with Damköhler number D_a=1.0.

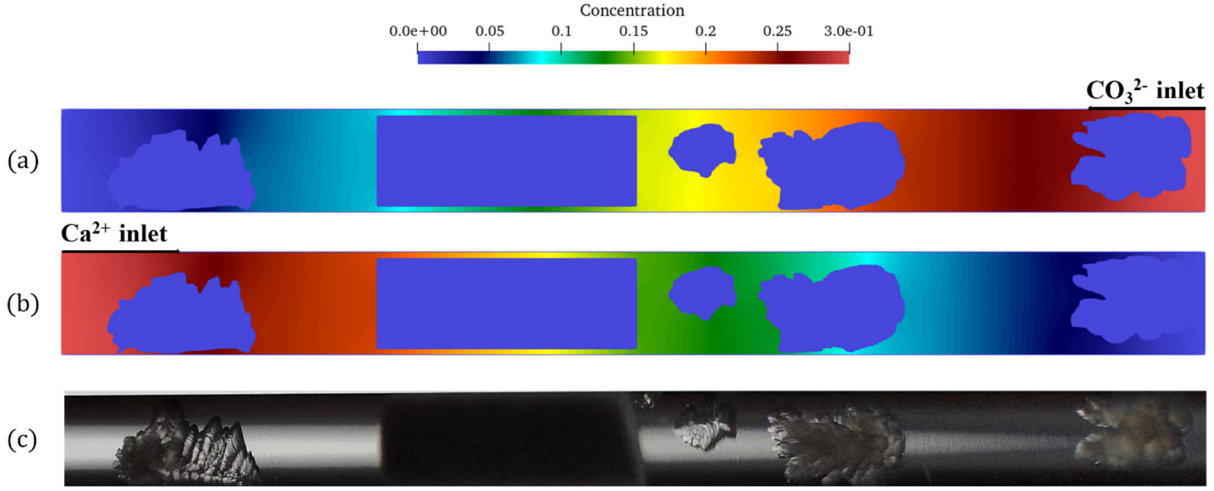

Fig. 2.5: Preliminary numerical calculation of the local concentrations within the μ-CD capillary at steady state, using directly the optical microscopy images.

of gas, temperature and surface interaction have an influence on the diffusion coefficient of gases. The simulation allowed to derive, a simple semi-empirical relationship (Fig. 2.6) relating the effective diffusivity of gases in the rocks with the diffusivity of gas molecules in bulk water, average pore size and the geometric factor of pore space (Owusu et al. 2022). These are the physical parameters readily available from previous experimental studies.

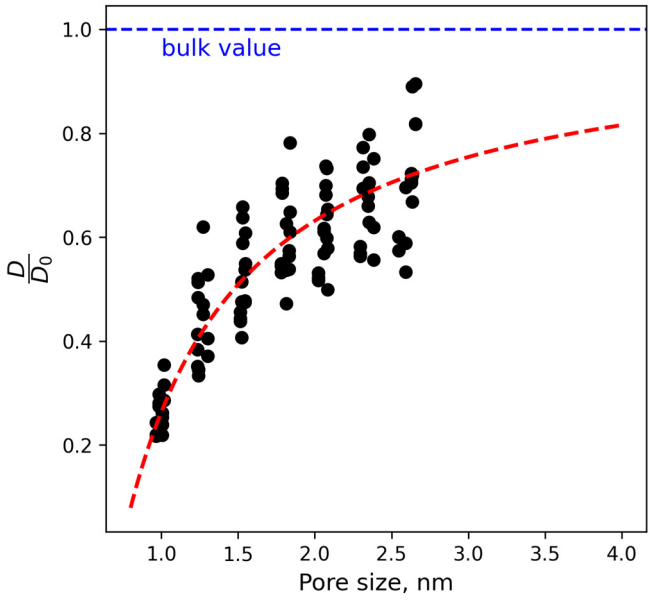

Fig. 2.6: Fit showing the relative diffusion coefficient of various non polar gases (D/D_0), in clay nanopores as a function of the pore size.

2.5 Status Update of GEMS-PSI Software

Since 2000, in collaboration with several groups in Europe and USA, LES @ PSI is developing, distributing and promoting the **G**ibbs **e**nergy **m**inimization **s**oftware (GEMS) code packages (Kulik et al. 2013; Wagner et al. 2012) and relevant chemical thermodynamic databases (TDB), see Table 2.1.

Since then, open-source GEMS codes and open-data TDBs became key scientific tools used in theoretical modelling of geochemical and reactive transport processes in geological repository systems, and in the interpretation of experimental data at LES related to nuclear engineering, degradation of construction materials (collaboration in the area of cement chemistry), hydrothermal ore geochemistry, as well as CO_2 capture, sequestration and disposal technologies (Gysi et al. 2020, Park et al. 2023).

Since 2003, Windows, MacOS and Linux installer archives for GEMS binaries and default TDBs are provided free of charge for web download from the GEMS web site at PSI (https://gems.web.psi.ch) and from other places (*Tab. 2.1, 2.2*). From 2013 on, several main codes of GEMS are available open-source from major git repository sites bitbucket.org and github.com.

The GEMS3K code library has been used by other research groups in coupled codes OpenGeoSys-GEM (Kosakowski & Watanabe 2014), CSMP++GEM (Yapparova et al. 2019), COMSOL-GEMS (Azad et al. 2016). A companion MINES TDB for applications in hydrothermal ore geochemistry (Gysi 2017), with excellent GEMS tutorials, is freely distributed from geoinfo.nmt.edu/mines-tdb by Prof. A.P. Gysi at New Mexico Bureau of Geology and Mineral Resources (USA).

Since 2003, LES@PSI, LCA@Empa and other collaborating teams held numerous workshops on training the users on the functionality of GEMS codes. Overall, our efforts have a broad impact and received a lot of recognition. To date, GEMS was downloaded ca. 10'000 times, with estimated 1'000+ active users. PSI-Nagra and Cemdata TDBs were directly used in 65+ PhD theses and (according to Google Scholar) in 1'800+ papers, in turn cited in 15'000+ publications.

With its rich GUI and built-in databases, the GEM-Selektor is a general-purpose thermodynamic modelling tool with dozens of widgets and menu options for specifying various types of phases, chemical systems and process simulations. However, for some users, this versatility is also a limitation due to ambiguous ways to achieve the same goal in the user interface, and a relatively steep learning curve.

Hence a desire to accompany an integrated "all-in-one" code package with several dedicated *services* (preferably web apps), each solving a particular data management or modelling task. This is the main idea of *ThermoEcos*, an open-source open-data "ecosystem" for integrating experimental databases(DBs) and TDBs with (geo-)chemical modeling and parameter optimization codes, and providing workflows to facilitate collaboration between scientists, industry and public.

ThermoEcos has been growing at LES during last five years, but entering in a fully operational phase is still very challenging. In ThermoEcos, databases, clients and codes fall into three main categories: (i) DBs and data access (ThermoExp, ThermoSys, ThermoHub, ThermoHubClient), (ii) Data processing and curation (ThermoFun, ThermoSol, ThermoMatch), (iii) Modeling codes (xGEMS, ThermoGEM, ThermoFit) that can use GEMS (and/or Reaktoro framework as future alternative).

A key feature of ThermoEcos is that all its dedicated *services* (web apps, local apps) will access the data JSON documents stored in ThermoHub, ThermoSys or ThermoExp online DBs. This "database-centric"

integration will allow automatic operation of both web apps and local apps.

Calculations using Pitzer aqueous electrolyte model (TSolMod, GEM-Selektor) have been extensively tested, improved and bug-fixed in the framework of Thereda-Pitzer project. This allows the use of GEM-Selektor for modelling highly saline systems. Benchmarks showed the same results as the PHREEQC code produced for the same aqueous speciation. Work is under way to be able to import data from the Thereda database (https://www.thereda.de/en), which contains an extensive set of standard state thermodynamic properties and Pitzer parameters for calculating aqueous electrolyte speciation up to high salt concentrations.

Tab. 2.1: GEMS desktop code tools and repositories (status November 1, 2022).

Name	**Functionality**	**Status, version**	**Availability, license**	**References, URL**
GEM-Selektor	Main desktop app: GUI, scripts, default TDBs, projects & help DB (builds including GEMS3K)	v.3.9.5 Win, Mac, Linux	Binaries; opensource (GPL3)	gems.web.psi.ch; bitbucket.org/gems4/gems3gui; github.com/gemshub/GEMSGUI (Kulik et al. 2004; Kulik et al. 2013; Wagner et al. 2012)
GEMS3K	GEM numerical solver & C++ API library with examples for coupled codes	v.3.9.5 Win, Mac, Linux	opensource (LGPL)	bitbucket.org/gems4/gems3gui; github.com/gemshub/GEMS3K (Kulik et al. 2013; Wagner et al. 2012)
GEMSFITS	GUI, code & DB for GEMS3K input parameter optimization and inverse modelling	v.1.3.0 Win, Linux	Binaries; opensource (LGPL)	gems.web.psi.ch; bitbucket.org/gems4/gems3gui (Miron et al. 2015)
xGEMS	GEMS3K with next-generation C++11 style API and Python API	v.1.0.4 Mac, Linux	opensource (LGPL)	bitbucket.org/gems4/xgems anaconda.org/conda-forge/xgems
GEMS-Reaktoro	Variant of GEM-Selektor for benchmarking with Reaktoro & ThermoFun	v.0.0.1 Linux	TBA (in progress)	github.com/gemshub/gemsreaktoro
UpsaGems	Uncertainty propagation and sensitivity analysis	v.0.1.0 Python	TBA (so far not public)	github.com/gemshub

Tab. 2.2: Chemical thermodynamic databases available in GEMS format (status November 1, 2022).

Name	**Applicability**	**Status, version**	**Availability**	**References, URL**
PSI-Nagra 12/07 GEMS	Waste management geological disposal incl. actinides and fission products up to 150 ºC	Open, 12/07	GEM-Selektor installers (default)	gems.web.psi.ch; psi.ch/en/les/database (Hummel et al. 2002; Thoenen et al. 2014)
SUPCRT98 GEMS	Hydrothermal systems (with/without organics), ore formation	Open, Slop98.dat (imported)	GEM-Selektor installers	gems.web.psi.ch (Dick, 2019)
Cemdata18.1	Hydrated (blended, degraded) cement systems, up to 100 ºC	Open, v.18.1	Download as GEMS plugin	empa.ch/cemdata (Lothenbach et al. 2019)
Phosphate19 Zeolite21	Data for phosphate cements and zeolitic phases, up to 100 ºC	Open, v.18.1	Download as GEMS plugin	empa.ch/web/s308/phosphate-data, empa.ch/web/s308/zeolite
MINES 19	Hydrothermal geochemical processes at < 5kbar, < 600ºC, ore formation	Open, v.19.1	Download as GEMS plugin	geoinfo.nmt.edu/mines-tdb/ (Gysi 2017)
Aq17	Hydrothermal processes, major rock-forming minerals at < 5 kbar, < 600 ºC	Open	Download as GEMS plugin	(Miron et al. 2016, 2017) researchgate.net/publication/325402295
HERACLES	Modeling of U and fission products (FP) solid gas speciation	Open	Download as GEMS plugin	psi.ch/en/heracles/ (not supported since September 2022)

GEMS3K and GEM-Selektor codes were integrated with the ThermoFun library for calculation of standard thermodynamic data for species and reactions at desired T and P (Miron et al. 2021) (https://github.com/thermohub/thermofun). This is an important improvement, especially for the standalone GEMS3K code used in several coupled reactive transport codes and in the GEMSFITS. Before the ThermoFun integration, thermodynamic data were exported from GEM-Selektor code into a lookup array (saved into many Mb large files) for a defined (regular) grid of T, P pairs covering given T and P intervals with suitable discretization. Between the grid points, the data (standard molar G^o, H^o, S^o, Cp^o, V^o, standard properties of chemical substances and properties of H_2O solvent), the 2d spline interpolation functions were automatically used to deliver the data at required T, P conditions. This kind of interpolation introduced small errors that were not uniformly distributed over the T, P grid (i.e. values in close vicinity to grid points were taken without interpolation). Instead, ThermoFun actually performs accurate calculations of standard properties of substances directly or via reactions between them, using only the standard-state data at 1 bar 25 °C, collected from any compatible TDB (online ThermoHub DB, or a GEM-Selektor project) into a local JSON document file. Hence, this improvement not only delivers accurate thermodynamic data to coupled-code calculations using GEMS3K, but also greatly reduces the size of data exchange files. ThermoFun has also been integrated with Reaktoro v.2 framework (https://reaktoro.org) in collaboration with A.M.M. Leal (ETHZ).

CemGEMS (https://cemgems.app) web based app provides thermodynamic modelling of cement hydration processes and visualization for cement chemists. The web app, online since 2020, runs the GEMS3K code (Kulik et al. 2013; Wagner et al. 2012) with a pre-configured chemical system using Cemdata18 (Lothenbach et al. 2019; https://www.empa.ch/cemdata) and PSI-Nagra GEMS chemical thermodynamic databases. Since summer 2018 until spring 2022, CemGEMS development at LES (Kulik et al. 2021) and at Congineer GmbH has been supported by Nanocem consortium (https://nanocem.org).

CemGEMS release v.0.7.0 (April 2, 2022) provided a user friendly web interface with intuitive and transparent definition or modification of processes of all types (Fig. 2.7), with a track of changes all described in tutorial web pages (https://cemgems.org) and in clips added to CemGEMS YouTube channel. The export of process simulation results/plots is made possible into graphic format files. A new "Trial mode" option without registration, providing a temporary demo user account and letting the user to test CemGEMS and decide about the conventional (permanent) registration, through which the user's profile will persist accessible from any device at any time.

CemGEMS release v.0.8.0 (pending in 2023) will provide a high-quality Python-style (Plotly) graphics with an option for plotting experimental data over the modelled curves; optional exchange of recipes and processes between registered users for education or collaboration.

Since 2 years online, CemGEMS runing 100% uptime and has attracted >490 registered users worldwide. On-going work includes: improvements and preparation of the next release v.1.0 with modified Bogue calculations, more recipe and process templates, and improved evaluation of heat effects.

2.6 Model developments in EURAD WP DONUT: GeoML Benchmark

The application fields of artificial intelligence (AI) and machine learning methods (ML) are growing at a very fast pace. The EURAD community has recently started using ML for a) accelerating numerical simulations, b) improving the efficiency of multiscale and multiphysics couplings, c) uncertainty quantification and sensitivity analysis. A number of case studies indicate that overall acceleration of geochemical and reactive transport calculations, between one to three orders of magnitude (Laloy et al. 2019, Prasianakis et al. 2020). Within EURAD WP DONUT (Development and Improvement Of Numerical methods and Tools for modelling coupled processes) a benchmark is currently designed to test a variety of ML techniques relevant to geochemical and reactive transport simulations in the framework of radioactive waste disposal, aiming at providing basic guidelines about the benefits and limitations of using ML techniques (Lead: N.I. Prasianakis).

Joint efforts of BRGM, ISTO (CNRS/INSU-BRGM), SCK-CEN, Amphos, NRG, ENRESA(UDC), UFZ, and PSI resulted in the definition of computational benchmarks relevant for the nuclear waste management. Three major geochemical solvers PHREEQC, ORCHESTRA and GEMS, are applied to model the chemical systems of interest. First results show that all three geochemical codes produce almost identical results for the systems studied. Several machine learning techniques are implemented by experts, and compared including polynomial chaos expansion, Gaussian processes, deep neural networks, tree based algorithms and distributed hash tables (Fig. 2.8).

Fig. 2.7: An example of screenshot of Process tables and plots for an example of simulating CO_2 ingress into hydrated Portland cement in CemGEMS web app v.0.7.0.

2.7 Thermal evolution and digital twins of repository systems: EURAD WP MODATS

The thermal, hydraulic mechanical, and chemical (THMC) evolution of the repository near field of high level waste and of the spent fuel is relevant to repository safety. The temperature is the main parameter, which can be monitored in a pilot repository to confirm repository performance during design, construction, operation and monitoring phase. A Full-scale Emplacement Experiment (FE) at the Mont Terri Underground Research Laboratory (URL) investigates various aspects of the construction, waste emplacement, backfilling and early-stage evolution of a SF / HLW repository tunnel in a clay-rich formation (Opalinus Clay), using proxy heaters in place of SF / HLW canisters. Design and sensor data of this experiment allow to conduct the first step in the direction of a 3D digital twin of a (pilot) repository.

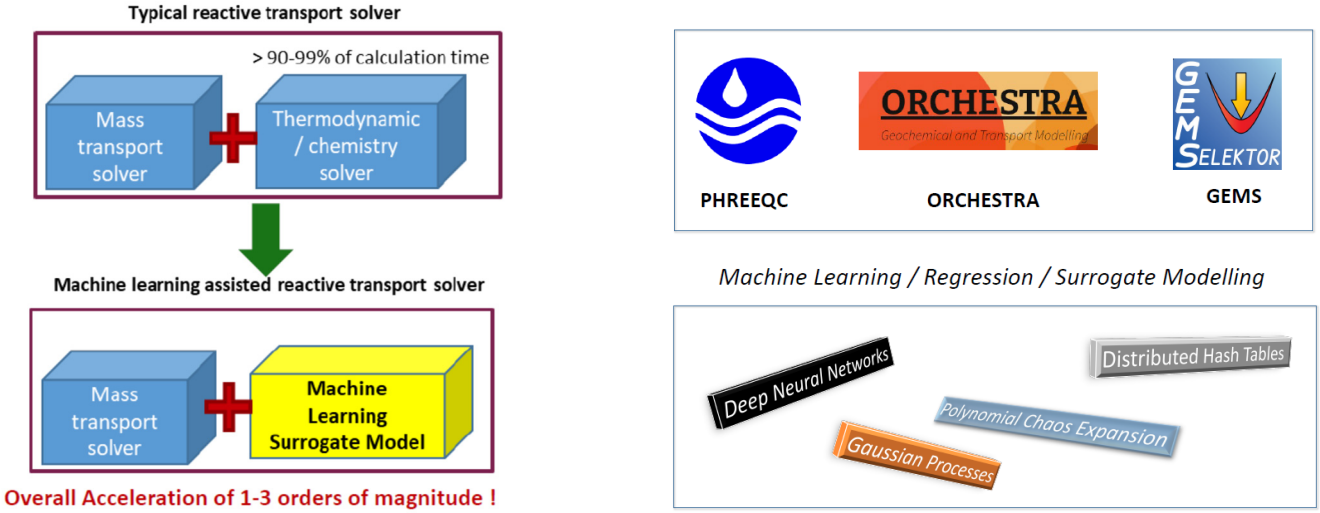

Fig. 2.8: Geochemistry and machine learning Benchmark within the EURAD WP DONUT project. Several geochemical solvers and machine learning techniques are implemented to set the ground in the growing field of accelerating reactive transport simulations.

At the moment work focuses on the prediction of the temperature evolution in the repository near-field, taking into account early stage sensor data (temperature, humidity, …) installed in the near-field of the pilot repository. Once the digital twin is built and confidence is gained, it can be extended and used to optimize the repository design parameters such the material selection and dimensionalization, waste configuration with respect to safety, performance, costs and other constraints of interest.

Within EURAD- MODATS WP sensor data from the FE experiment (Mont Terri) are used to develop a digital twin for the FE experiment. 3D parameter information, e.g. homogeneous/heterogeneous distributions for porosity, saturation degree, density, and related thermal conductivity parameters are used to setup a physical model for heat transport (Fig. 2.9). Data driven modelling is used to generate a saturation degree distribution in the whole model domain, which influences the thermal conductivity, especially that of the bentonite. Data from a set of saturation degree sensors are used (saturation degree as a function of x, y, z, time, material) to provide an interpolation for the saturation degree in the 3D model domain (Fig. 2.10). Then the physical model for heat transport is used to predict the 3D heat evolution around the three heaters (Fig. 2.11). Comparison of temperature sensor (Fig. 2.12) and physical model data allows model validation and sensitivity analysis of material properties (thermal conductivity) and related parameter uncertainty analysis. The predictions of the digital twin and the real time dependent evolution of the temperature field are in excellent agreement.

In a next step, new incoming data from the FE experiment will be used to feed the digital twin, i.e. generate surrogate model for the saturation degree, improve model physical model predictions, assess temperature sensor data with respect to sensor failures, but also to mimic FE experimental scenarios with assumptions on longer term changes of material properties around the heater in order to predict longer term evolution of the system compared to the real FE experimental duration.

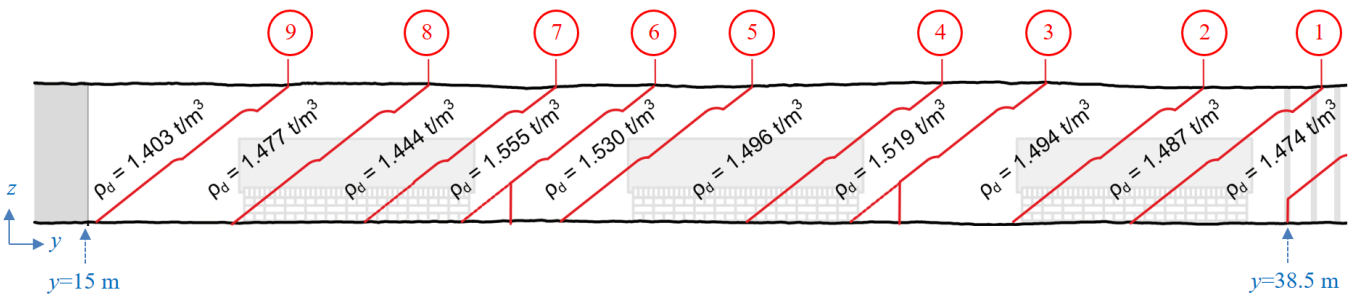

Fig. 2.9: 3-D slope scans and bulk dry densities of longitudinal section of the backfilled FE tunnel (adapted from Lanyon et al. 2020).

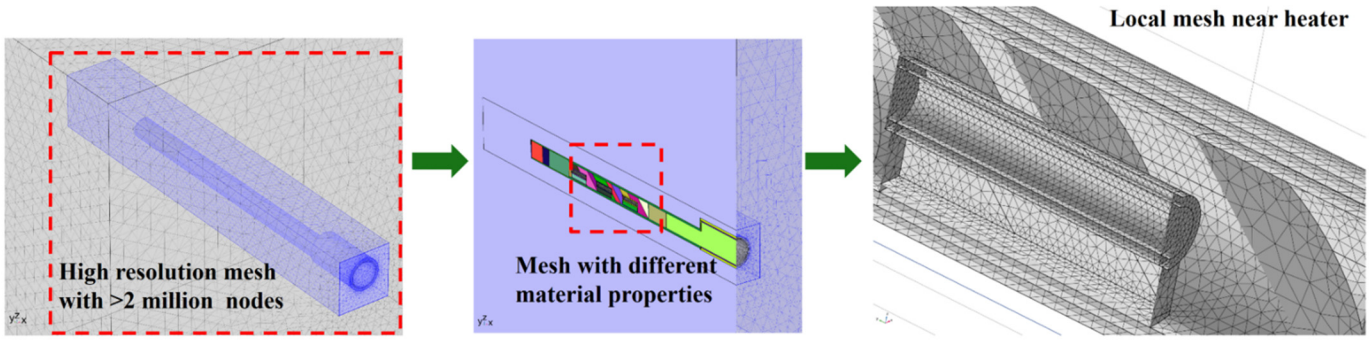

Fig. 2.10: Digital Twin of the FE-Experiment. High resolution mesh allows to integrate in the model all the important structural and material details.

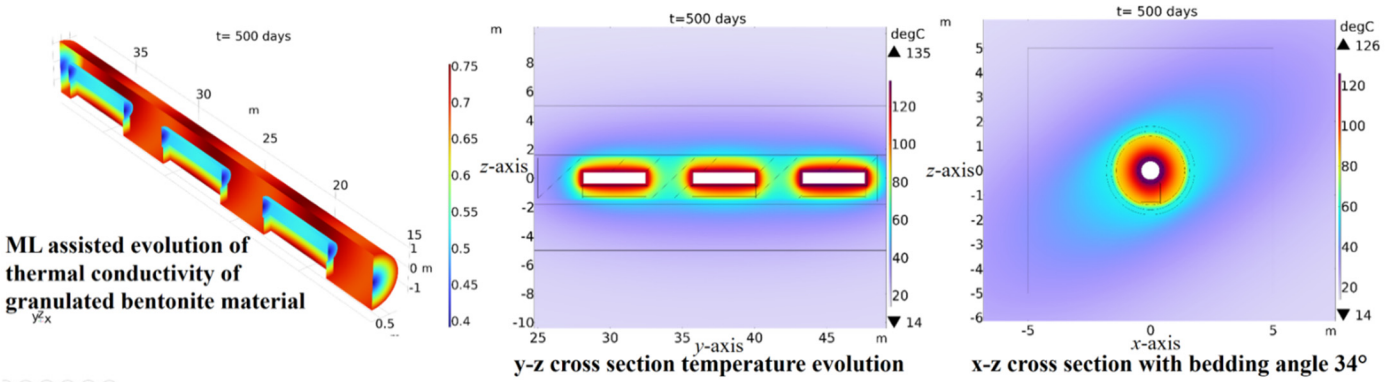

Fig. 2.11: Prediction of the FE-Experiment temperature evolution by integrating humidity sensor data via machine learning, after 584 days of operation. The simulation results of the temperature evolution are in excellent agreement with the measured sensor data.

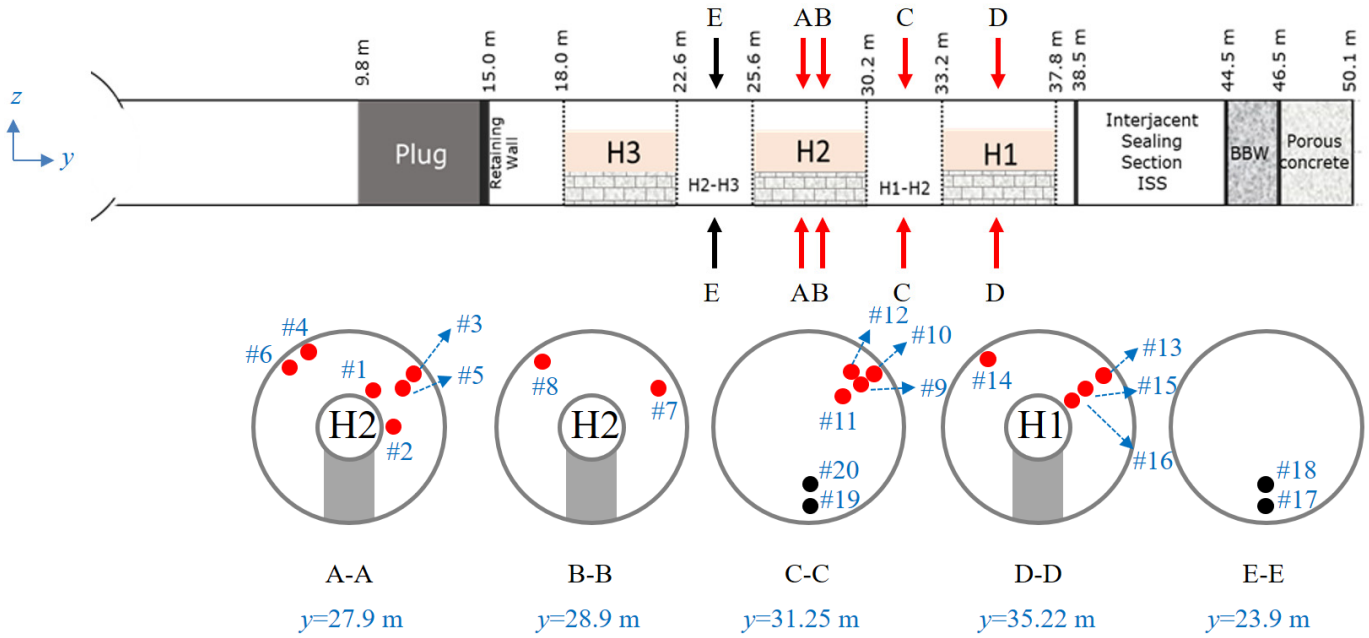

Fig. 2.12: Schematic diagram of positions of temperature/saturation degree sensors in the upper and lower half of the GBM (adapted from Nagra, 2019).

2.8 Multiphase modelling

2.8.1 Boiling flow simulation in fuel-assembly affected by crud

The project "Numerical prediction of boiling crisis considering surface characteristics" under the Swissnuclear funding agency and in collaboration with the Laboratory for Scientific Computing and Modelling at PSI (LSM-PSI) has been completed. A multiscale approach was developed to simulate two phase flow of a boiling fluid at temperature and pressure conditions corresponding to the operation of nuclear reactor. The project investigate the boiling from the atomistic and the micrometer level of description. Moreover it was possible to take into account the roughness and characteristics of the cladding surface composed by ZrO_2. The atomistic numerical simulations provids the insight into the onset of boiling and allows to measure in a detailed way the fluid-vapor-solid interaction at the boiling interface. The exact contact angles for different temperatures and surface crystallographic orientations were calculated. (Karalis et al. 2021). These results were upscaled to a 2D lattice Boltzmann (LB) solver which simulated the boiling processes by taking into account the roughness of the surfaces. After the validation phase the LB code was used to predict the nucleation site density with respect to the ZrO_2 surface characteristics. It has been the first time that the nucleation site density has been calculated applying a truly multiscale bottom-up approach without the use of empirical correlations (Fig. 2.13 (left)). The nucleation site density provided by this project is a crucial parameter which is almost impossible to be measured at reactor operating conditions, but at the same time it is a necessary parameter needed from macroscopic boiling codes such as the PSI-Boil.

A follow-up Swissnuclear project "Boiling flow simulation in fuel-assembly affected by crud" has been approved and started in 2022. The presence of a crud layer on the surface of the fuel rod is considered. Crud is a porous media and a new numerical code, using a radially averaged spectral power density algorithm coupled with a Gaussian distribution, has been developed to procedurally create a domain with the foreseen porosity and surface characteristics (Fig. 2.13 (right)). The simulations are extended to 3D, with a new thermal module added to the internal LES LB GPU code. Additional multiphase LB models are also tested for accuracy and stability. The developed model will be capable of predicting the bubble nucleation site density based on the flow regime, the surface properties and composition of the crud.

2.8.2 Pore-level simulations of realistic membranes for water desalination

The internally developed LB GPU code has been used, in collaboration with the University of Luxembourg (T. Jager and Prof. S. Leyer), to simulate a membrane water distillation process (Jäger et al. 2022). Specifically, the separation process within an air gap distillation membrane, where a hydrophobic membrane is used within an air volume separating the water feed and output, is modelled. The membrane hydrophobicity only allows vapour to pass through, trapping the salt contaminants. Four commercial membrane geometries have been considered, which were obtained through ptychographic X-ray computed tomography (Cramer et al. 2021) in the cSAXS beamline of the Swiss Light Source, PSI. The membrane material used here is Polytetrafluoroethylene (PTFE) with a pore diameter of about 200nm and the simulations were done in pore

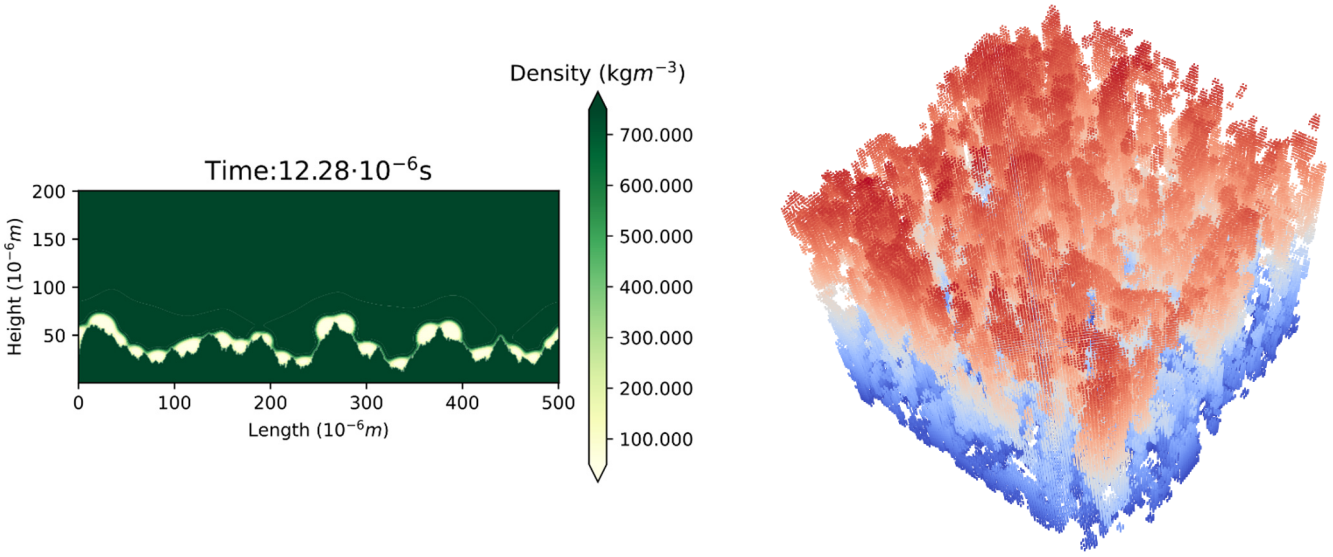

Fig. 2.13: (left) LB simulation showing the creation of vapour bubbles due to boiling, (right) algorithmically created porous media for crud simulations with 0.41 porosity.

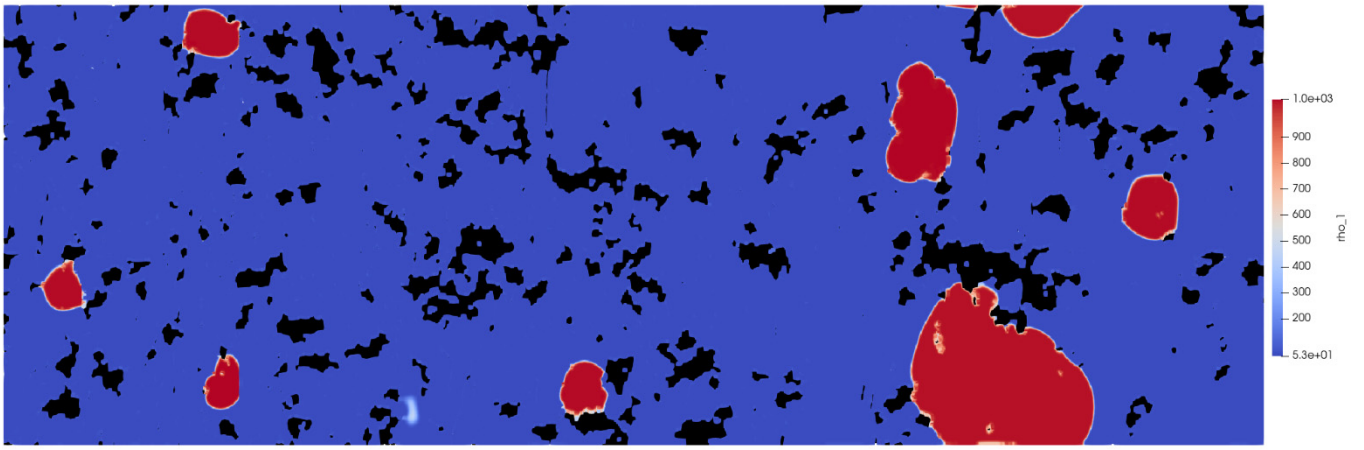

Fig. 2.14: LB simulation showing water-vapour separation at equilibrium after 1.5M steps in a hydrophobic PTFE membrane. The simulation was performed in 16 GPUs at CSCS. A 2D slice of the domain is shown here, with red representing the water volumes. 3D Realistic multiphase simulations allow to understand the heat and mass transport processes with membranes and can support their design optimization.

scale at a resolution of ~40nm. The results, with a domain initialized with a random water-vapour mixture, showed the progress of phase separation process until it reached equilibrium. Fig. 2.14 shows a slice of a membrane (FHLP1450) at equilibrium, with the liquid and vapour separated. With this methodology it has been possible to visualise the water distribution at different saturation degrees. Moreover, the water break-through pressures were predicted via 3D multiphase simulation and were found to be in agreement with the experimental values existing in the literature for similar materials. Finally, the effect of adding micro-pillars at the surface, on the wettability of the membrane has been assessed. It is now possible to investigate and design specific patterns which will control the degree of wettability. In turn, it is a promising technique to prolong the service-life of desalination membranes.

2.8.3 Smoothed particle hydrodynamics simulations

In collaboration with Electricité de France (EDF), Laboratoire d'Hydraulique Saint-Venant (LHSV) and the company Nextflow Software, the smoothed particle hydrodynamics simulations has been successfully applied to simulate waterfall occurring at a dam ogee-type spillway (Mokos et al. 2022). The multiphase air-water SPH simulations use an adaptive particle refinement technique, which enable to reproduce the experimentally measured pressure data with high accuracy. In particular, the addition of an air friction force allowed correct prediction of the falling trajectory and velocity. Further studies are conducted using new version of the open source DualSPHysics code (Domínguez et al. 2022), in collaboration with the University of Manchester and University of Vigo. The new code is capable of simulating air-water flows in an OpenMP GPU environment; this enabling to use more than 100 million particles, an order of magnitude larger than what is currently possible. Fig. 2.15 shows a 2D slice of a newly possible multiphase 3D gearbox application with 32M particles on four GPUs.

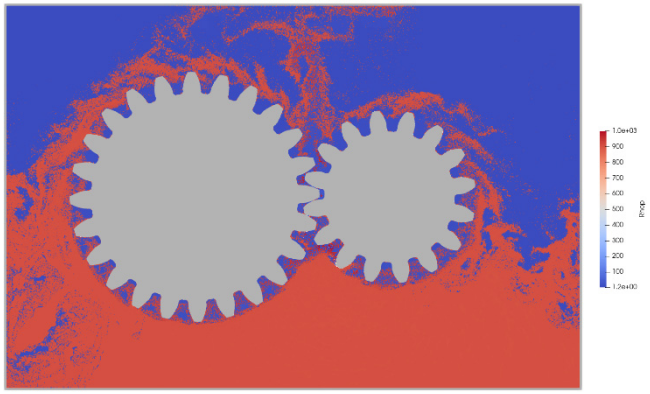

Fig. 2.15: Slice of a 3D air-oil gearbox simulation with 32M particles.

2.9 Research projects with GlaxoSmithKline Vaccines

In 2022, Work has continued on two industrial projects with the pharmaceutical company GlaxoSmithKline Vaccines, Belgium (GSK) (PI: N.I. Prasianakis). GSK is a science-led global healthcare company focused in the research, development and manufacturing of innovative pharmaceutical medicines, vaccines and consumer healthcare products. Project benefits from the in house development of advanced multiscale simulation codes and machine learning relevant to accelerated computing and data analysis.

2.10 Machine learning accelerated uncertainty and sensitivity analysis

Reactive transport simulations involve numerous dynamic physical and chemical processes, hence, for realistic applications they are inevitably time-consuming to execute. The novel idea of using machine-learning and surrogate models in accelerating reactive transport simulations was introduced in recent years. Surrogate models are also useful in sensitivity analyses (Laloy et al. 2019) and inverse modelling where large sample sizes (simulations), of the order of tens of thousands, are required and the reactive transport simulations have to be executed repeatedly for a different parameter input. Within the master thesis of Ms. L. Cheuk Lam, the machine learning accelerated uncertainty analysis of Nickel migration in Opalinus Clay has been investigated. It was shown that based on neural network approach an overall acceleration of the sensitivity analysis of three to four orders of magnitude is feasible, without significant loss in accuracy.

2.11 References

Avaro J.T., Wolf S.L.P., Hauser K., Gebauer D. (2020)
Stable Prenucleation Calcium Carbonate Clusters Define Liquid–Liquid Phase Separation. Angew. Chem. Int. Ed. 59, 6155-6159.

Azad V.J., Li C., Verba C., Ideker J.H., Isgor O.B. (2016)
A COMSOL–GEMS interface for modeling coupled reactive-transport geochemical processes. Comp. Geosci. 92, 79-89.

Cramer K., Prasianakis N.I., Niceno B., Ihli J., Holler M., Leyer S. (2021)
"Three-Dimensional Membrane Imaging with X-ray Ptychography: Determination of Membrane Transport Properties for Membrane Distillation." Transport in Porous Media 138(2), 265-284.

Dick J.M. (2019)
CHNOSZ: thermodynamic calculations and diagrams for geochemistry. Frontiers Earth Sci. 7, 180.

Diomidis N., Cloet V., Leupin O.X., Marschall P., Poller A., Stein M. (2016)
Production, consumption and transport of gases in deep geological repositories according to the Swiss disposal concept. Nagra Technical Report 16-03, Nagra, Wettingen, Switzerland.

Domínguez J. M., Fourtakas G., Altomare C., Canelas R.B., Tafuni A., García-Feal O., Martínez-Estévez I., Mokos A., Vacondio R., Crespo A.J.C., Rogers B.D., Stansby P.K., Gómez-Gesteira M. (2022)
DualSPHysics: from fluid dynamics to multiphysics problems. Computational Particle Mechanics 9(5), 867-895.

Gebauer D., Kellermeier M., Gale J.D., Lennart Bergström L., Cölfen H. (2014)
Pre-nucleation clusters as solute precursors in crystallisation. Chem. Soc. Rev. 43, 2348-2371.

Gysi A.P. (2017)
Numerical simulations of CO2 sequestration in basaltic rock formations: challenges for optimizing mineral-fluid reactions. Pure Appl. Chem. 89, 581-596.

Gysi A.P., Mei Y., Driesner T. (2020)
Advances in numerical simulations of hydrothermal ore forming processes. Geofluids, vol. 2020, Article ID 7649713, 4 pages, 2020.

Hummel W., Berner U., Curti E., Pearson F.J., Thoenen T. (2002)
Nagra/PSI Chemical Thermodynamic Data Base 01/01. Nagra NTB 02-16, Nagra, Wettingen, Switzerland.

Jäger T., Mokos A., Prasianakis N.I., Leyer S. (2022)
Pore-level Multiphase Simulations of Realistic Distillation Membranes for Water Desalination. Membranes, 12(11), 1112.

Karalis K., Zahn D., Prasianakis N.I., Niceno B., Churakov S.V. (2021)
Deciphering the molecular mechanism of water boiling at heterogeneous interfaces. Scientific reports 11(1), 1-10.

Kashchiev D., van Rosmalen G.M. (2003)
Review: nucleation in solutions revisited. Cryst. Res. Technol. 38, 555-574.

Kosakowski G., Huang Y., Wieland E. (2020)
Influence of material heterogeneities, process couplings and aggregate reactivity on the geochemical evolution of the L/ILW repository. Nagra Arbeitsberichte NAB 20-11, Nagra, Wettingen, Switzerland.

Kosakowski G., Watanabe N. (2014)
OpenGeoSys-Gem: A numerical tool for calculating geochemical and porosity changes in saturated and partially saturated media. Phys. Chem. Earth, Parts A/B/C 70–71, 138-149.

Kosakowski G., Wieland E. (2022)
Assessing the impact of chemical processes on the long-term evolution of waste packages by geochemical modelling. In: NUWCEM 2022 - International Symposium on Cement-Based Materials for Nuclear Wastes May 4-6 2022, CEA, Avignon, France.

Kulik D.A., Berner U., Curti E. (2004)
Modelling chemical equilibrium partitioning with the GEMS-PSI code. In: PSI Scientific Report 2003, Vol. IV, 109-122, Paul Scherrer Institute, Villigen, Switzerland.

Kulik D.A., Miron G.D., Lothenbach B. (2022)
A structurally-consistent CASH+ sublattice solid solution model for fully hydrated C-S-H phases: Thermodynamic basis, methods, and Ca-Si-H2O core sub-model. Cem. Conc. Res. 151, 106585.

Kulik D.A., Wagner T., Dmytrieva S.V., Kosakowski G., Hingerl F.F., Chudnenko K.V., Berner U.R. (2013)
GEM-Selektor geochemical modeling package: revised algorithm and GEMS3K numerical kernel for coupled simulation codes. Computers and Geosciences 17, 1-24.

Kulik D.A., Winnefeld F., Kulik A., Miron G.D., Lothenbach B. (2021)
CemGEMS – an easy-to-use web application for thermodynamic modeling of cementitious materials. RILEM Technical Letters 6, 36-52.

Laloy E., Jacques D. (2019)
Emulation of CPU-demanding reactive transport models: a comparison of Gaussian processes, polynomial chaos expansion, and deep neural networks. Computational Geosciences 23(5), 1193-1215.

Lothenbach B., Kulik D.A., Matschei T., Balonis M., Baquerizo L., Dilnesa B., Miron G.D., Myers R.J. (2019)
Cemdata 18: A chemical thermodynamic database for hydrated Portland cements and alkali-activated materials. Cement and Concrete Research 115, 472-506.

Marschall P., Horseman S., Gimmi T. (2005)
Characterisation of gas transport properties of the Opalinus Clay, a potential host rock formation for radioactive waste disposal. Oil Gas Sci. Technol. 2005, 60, 121−139.

Miron G.D., Kulik D.A., Dmytrieva S.V., Wagner T. (2015)
GEMSFITS: Code package for optimization of geochemical model parameters and inverse modeling. Appl. Geoch. 55, 28-45.

Miron G.D., Kulik D.A., Yan Y., Tits J., Lothenbach B. (2022)
Extensions of CASH+ thermodynamic solid solution model for the uptake of alkali metals and alkaline earth metals in C-S-H. Cem. Conc. Res. 152, 106667.

Miron G.D., Kulik D.A., Yan Y., Tits J., Lothenbach B. (2022)
Porewater compositions of Portland cement with and without silica fume calculated using the fine-tuned CASH+NK solid solution model. Materials and Structures 55, 212.

Miron G.D., Leal A.M.M., Dmytrieva S.V., Kulik D.A. (2021)
ThermoFun: C++/Python Code to Fetch Standard Thermodynamic Data from ThermoHub Database. Goldschmidt Conference 2021, Abstract 4489.

Miron G.D., Wagner T., Kulik D.A., Heinrich C.A. (2016)
Internally consistent thermodynamic data for aqueous species in the system Na-K-Al-Si-O-H-Cl. Geoch. Cosmoch. Acta 187, 41-78.

Miron G.D., Wagner T., Kulik D.A., Lothenbach B. (2017)
An internally consistent thermodynamic dataset for aqueous species in the system Ca-Mg-Na-K-Al-Si-O-H-C-Cl to 800 oC and 5 kbar. Amer. J. Sci. 317, 754-805.

Mokos A., Karalis K., Patel R.A., Churakov S.V., Prasianakis N.I. (2022)
Nano- and micro-scale simulations of atr boiling in heterogeneous surfaces. International Conference on Numerical Methods in Multiphase Flows Venice, Italy.

Mokos A., Patel R.A., Peng H., Karalis K., Churakov S.V., Prasianakis N.I. (2022)
Simulations of boiling flow on the heterogeneous surface of a nuclear reactor fuel assembly system. International Conference for Mesoscopic Methods in Engineering and Science, La Rochelle, France.

Mokos A., Violeau D., Sarret F., De Leffe M., Bercovitz Y. (2022)
"SPH modelling of the water nappe gravity fall over a dam." Journal of Hydraulic Research 60(4), 606-618.

Nagra (2014)
Modellhaftes Inventar für radioaktive Materialien MIRAM 14. Nagra Technical Report NTB 14-04, Nagra, Wettingen, Switzerland.

Owusu J.P., Karalis K., Prasianakis N.I., Churakov S.V. (2022)
Mobility of Dissolved Gases in Smectites under Saturated Conditions: Effects of Pore Size, Gas Types, Temperature, and Surface Interaction. The Journal of Physical Chemistry C, 126 (40), 17441-17455.

Park S., Lothenbach B., Jang J.G., Kim H.-Ki, Lee N. (2023)
Thermodynamic modeling and experimental study of carbonation of alkali-activated slag cements. ACS Sustainable Chemistry & Engineering, 11(10), 4049-4063.

Prasianakis N.I., Curti E., Kosakowski G., Poonoosamy J., Churakov S.V. (2017)
Deciphering pore-level precipitation mechanisms. Scientific reports 7(1), 1-9.

Prasianakis N.I., Haller R., Mahrous M., Poonoosamy J., Pfingsten W., Churakov S.V. (2020)
Neural network based process coupling and parameter upscaling in reactive transport simulations. Geochimica et Cosmochimica Acta 291, 126-143.

Thoenen T., Hummel W., Berner U., Curti E. (2014)
The PSI/Nagra Chemical Thermodynamic Database 12/07. PSI Bericht 14-04, Paul Scherrer Institut, Villigen, Switzerland.

Wagner T., Kulik D.A., Hingerl F.F., Dmytrieva S.V. (2012)
GEM-Selektor geochemical modelling package: TSolMod Library and data interface for multicomponent phase models. Canadian Mineralogist 50, 1173-1195.

Wieland E., Kosakowski G., Lothenbach B., Kulik D.A., Cloet V. (2018)
Preliminary assessment of the temporal evolution of waste packages in the near field of the L/ILW repository. Nagra Arbeitsbericht NAB 18-05, Nagra, Wettingen, Switzerland.

Yapparova A., Miron G.D., Kulik D.A., Kosakowski G., Driesner T. (2019)
An advanced reactive transport simulation scheme for hydrothermal systems modelling. Geothermics 78, 138-153.

3 DEVELOPMENT OF MECHANISTIC SORPTION MODELS AND EXPERIMENTAL VALIDATION

Marques Fernandes M., Dähn R., Miron G.D., Kulik D.A., Churakov S.V., Schaible A., Lang C., Di Lorenzo F. (postdoc), Marinich O. (scientist), Qian Y. (PhD student), Stotskyi V. (PhD student), Yang Z. (guest PhD student)

3.1 Introduction

Prediction of the retention and transport of (radio-) nuclide in argillaceous environments requires a thorough understanding of solute and solvent interaction with the most common clay minerals. Within the present project, we develop thermodynamic sorption models based on experimental data obtained over a wide range of geochemical conditions for direct use in the safety assessment of deep geological radioactive waste repositories. Further, the research is aimed at a molecular scale understanding of the different processes controlling the retardation and perform detailed characterisation of the system using by spectroscopic techniques and atomist simulations.

In the framework of the deep drilling programme carried out by Nagra, the experimental programme on core samples from the siting regions Jura Ost, Nördlich Lägern and Zürich Nordost was finalized. The sorption of Cs^{I}, Ni^{II}, Eu^{III}, Th^{IV} and U^{VI} as well as the cation exchange capacities and exchangeable cations were experimentally quantified.

The activities in the EU project FUTuRE have been continued this year. In collaboration with the Forschungszentrum Jülich (FZJ), the study on the adsorption behaviour of Ra^{II} and Ba^{II} on illite was completed. In the subtask, *Redox reactivity of radionuclides on mineral surfaces*, a PhD student has completed the Tc^{VII} sorption experiments on different reduced clay minerals (different Fe^{II}/Fe^{III} ratios) and the clay mineral characterisation by different techniques (e.g. Mossbauer spectroscopy, scanning electron microscopy (SEM), mediated electrochemical reduction/oxidation (MEO/MER), Extended X-ray absorption fine structure (EXAFS)). EXAFS measurements were performed to determine the nature of the formed Se complexs (structure and oxidation state) as a function of different geochemical parameters (e.g., clay reduction degree, metal loadings and pH). As part of the *Reversibility of Sorption subtask*, the adsorption and desorption (by varying the S/L ratio) of Zn^{II} on illite samples (different Zn loadings) that had been in equilibrium for two years were quantified and the surface complexes were studied at the molecular level by EXAFS spectroscopy.

UpSaGems (Uncertainty propagation and Sensitivity analysis for GEMS), which is a tool (currently under development) for performing error propagation and sensitivity analysis in GEMS was used to quantify the impact of uncertainties of the Mn^{II} surface species stability and aqueous speciation on calculated adsorption isotherms and edges.

Dr. Olha Marinich has joined LES within the SNSF-funded PhD and post-doc project entitled "*Molecular scale understanding of competitive cation adsorption on swelling clay minerals*" (SNF Nr. 200021-129947). In this project thermodynamic modelling calculations with the GEMS code and re-evaluation the in-house sorption data are performed for consistency with the updated TDB 2020 thermodynamic database, and to derive confidence intervals for the different constants. Further, acid-base titration experiments were performed on pure saponite and Polarized-EXAFS spectra of Lu^{III}/Ni^{II}-doped saponites were recorded to investigate the angular dependence of the coordination environment of Ni and Lu. The structural parameters will be used to constrain the DFT calculations.

Zhe Yang, a guest PhD student from China, has joined LES in December 2021. The project is focused on retention of Cr^{VI} on clay-iron systems by combining sorption experiments and EXAFS measurements.

In the frame of an international collaboration, a review paper entitled "Molecular-level understanding of metal ion retention in clay-rich materials" was finalized and published in Nature Reviews Earth & Environment (Liu et al. 2022).

3.2 Cation exchange capacities and exchangeable cations of deep drilling core samples from the siting regions Jura Ost, Nördlich Lägern and Zürich Nordost

The cation exchange capacities (CEC) and the pool of exchangeable cations of rock samples from 7 boreholes across the geological siting regions Jura Ost (JO), Nördlich Lägern (NL), and Zürich Nordost (ZNO) were experimentally determined. The samples were selected to represent the different lithologies of the natural barrier system, i.e., Opalinus Clay and the upper and lower confining units. In total 141 rock samples have been analysed.

The CEC is directly correlated to the content and type of clay minerals in the rock samples, and consequently to their adsorption properties towards radionuclides. Its

variability is an excellent indicator for the homogeneity of the clay mineral content along the Opalinus Clay formation as well as to the upper and lower confining units for each borehole. The *in situ* fractional occupancies of exchangeable cations can act as a "fingerprint" for the *in situ* formation porewater compositions.

A direct quantification of the CEC of the rock samples was obtained by using the highly selective divalent nickeltriethylenediamine (Ni-en) complex (Peigneur, 1976).

The *in situ* cation occupancies of Na, K, NH_4, Mg, Ca and Sr were determined by using the highly selective Cs^+ index cation (Baeyens & Bradbury 2004). At sufficiently high concentration, this index cation is expected to completely replace all cations present on the exchange sites of clay minerals. This approach allows the direct quantification of the CEC (consumption of the index cation) and the indirect quantification of the exchangeable cation occupancies (type and amount of cations released after correction for mineral and salt dissolution) of the rock samples. Ideally, the sum of cations (ΣCATIONS) displaced from the exchange sites should correspond to the CEC of the rock samples if all exchangeable cations are displaced and quantified.

Fig. 3.1a shows that the correlation of the CEC data obtained by the two different index cations (Cs-CEC and Ni-CEC) for all rock samples from the three regions is good. The Cs index cation, however, yields consistently higher values compared with the Ni-en

Fig. 3.1b shows the correlation between Ni-CEC and ΣCATIONS. The values obtained by these methods correlate very well, which increases the confidence in the applicability and reliability of these methods for determining cation occupancies of argillaceous rocks samples. Similar as for the Cs-CEC method, consistently higher values are obtained compared to the Ni-CEC data.

Fig. 3.2 shows the fractional occupancies (N_B values = equivalent of cation B (B = Na^+, K^+, NH_4^+, Mg^{2+}, Ca^{2+} or Sr^{2+}) adsorbed on the exchange complex divided by the equivalent of total cations (ΣCATIONS)) for the major (Na, K, Mg and Ca) and minor (NH_4 and Sr) exchangeable cations for the samples from JO, NL and ZNO, respectively.

The fractional cation occupancies (N_B values) in the Opalinus Clay samples for JO, NL and ZNO (Fig. 3.2a) are very similar. In other words, the “finger print” of the exchangeable cations of the argillaceous rock samples originating from 7 different boreholes from 3 different siting regions is almost constant. The N_B values follow the trend $N_{Na} > N_{Ca} >> N_{Mg} \sim N_K >> N_{NH4} \sim N_{Sr}$. This is not the case for the samples originating from the confining units of all 3 siting regions (see Fig. 3.2b).

For samples with extremely low clay mineral content, CEC and exchangeable cation occupancies cannot be determined reliably and hence, the methodology is not applicable.

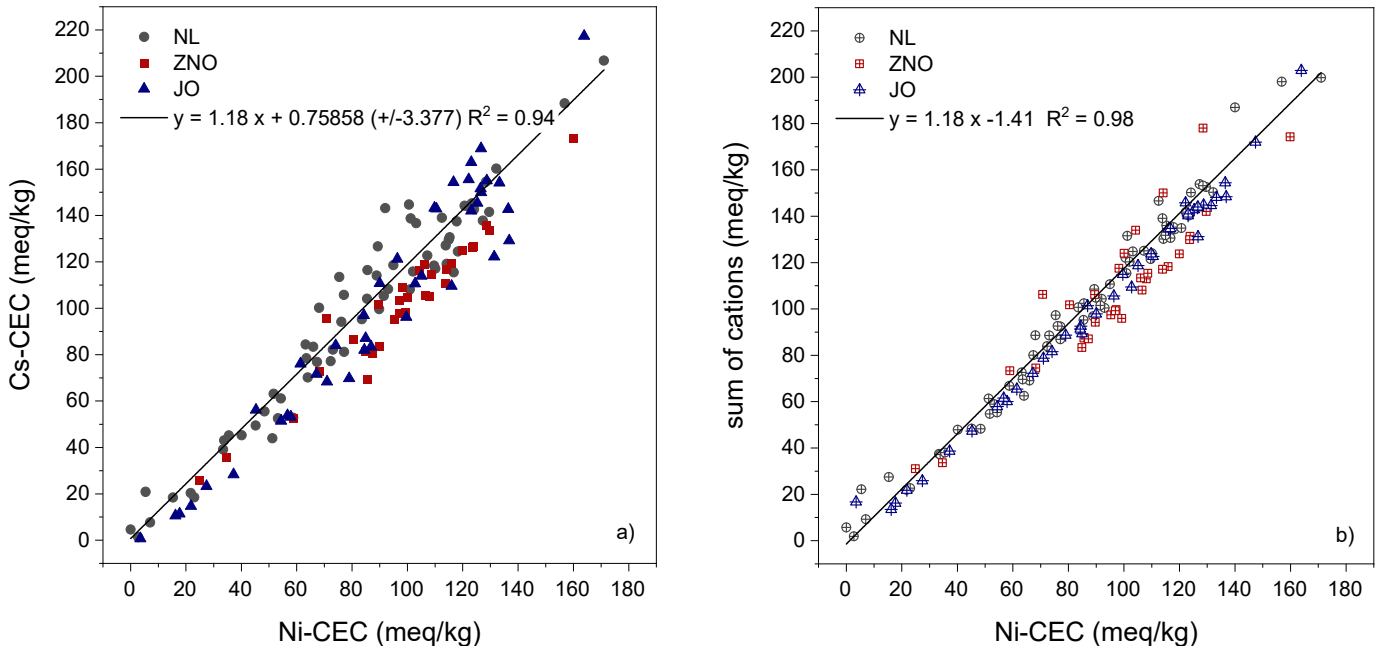

Fig. 3.1: Correlation between the Ni-CEC and (a) Cs-CEC, (b) ΣCations data determined for the drill core samples from the three siting regions.

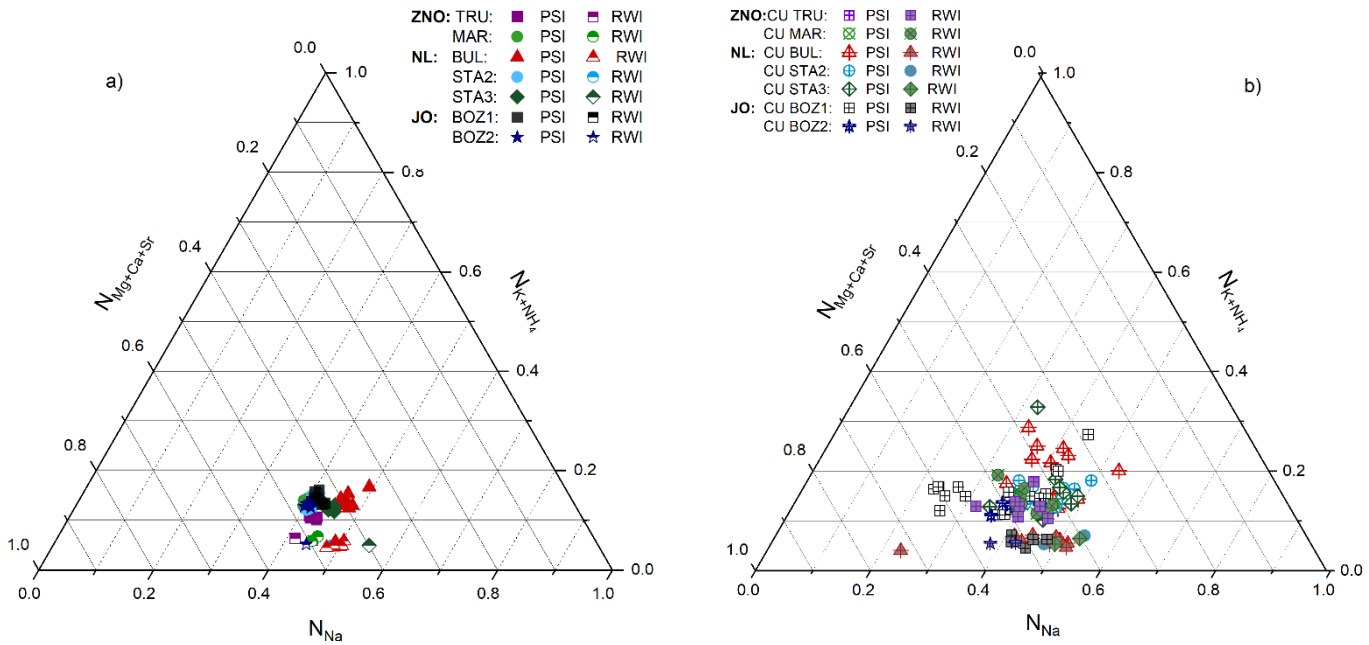

Fig. 3.2: Ternary representation of N_{Na}, $N_{Mg+Ca+Sr}$ and N_{K+NH4} determined for the samples from (a) Opalinus Clay and (b) the confining units for the samples from JO, NL and ZNO.

3.3 Ba^{II} and Ra^{II} adsorption on illite

Through collaborative project with the Forschungszentrum Jülich (FZJ) conducted within the EURAD WP-FUTuRE, the adsorption of Ba^{II} and Ra^{II} on 2:1 clay minerals is investigated. The adsorption studies on montmorillonite (SWy) were completed and published in 2021 (Klinkenberg et al. 2021). This year, the Ba and Ra adsorption measurements on illite du Puy (IdP) have started.

The adsorption of Ba and Ra at trace concentrations as a function of pH (pH edges) on homo-ionic Na-IdP at different fixe ionic strength was determined. Fig. 3.3 shows the pH dependent adsorption of Ba and Ra (plotted as log Rd values) on Na-IdP in the pH range 5 to 9.5 in 0.03 M and 0.3 M NaCl, respectively. The adsorption behaviour of both elements depends on the ionic strength, which is indicative for a cation exchange mechanism. At ionic strength of 0.3 M and pH > 8 the adsorption of Ba and Ra increases which is indicative for surface complexation. Furthermore, for both ionic strengths, the adsorption of Ra is more pronounced than for Ba (~ 0.5 log units) suggesting that Ra is more selective for the illite surface. This was observed on montmorillonite only at higher ionic strength (0.3 M).

3.4 Optimization of ClaySor model database

The PSI/Nagra chemical thermodynamic database was recently updated and released as TDB 2020 (Hummel & Thoenen 2021) for the use in safety assessments

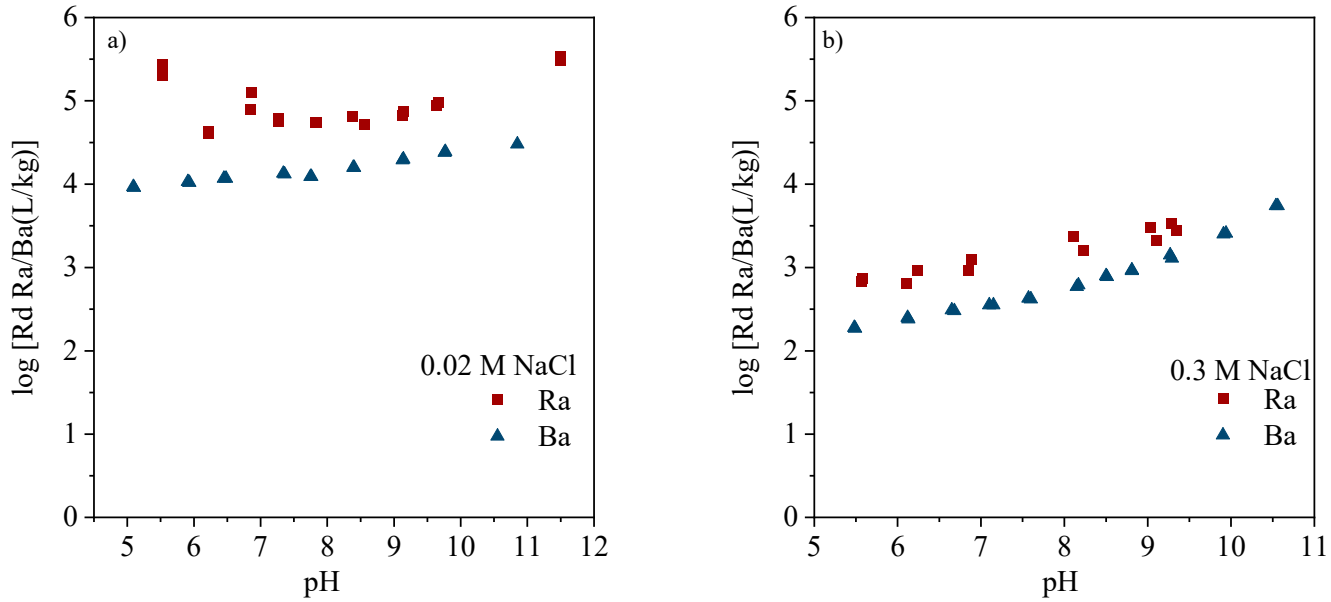

Fig. 3.3: Adsorption of trace Ba and Ra respectively as a function of pH in a) 0.02 M and b) 0.3 M NaCl on Na-IdP.

related to the general license applications (RBG). The update comprises improvement of thermodynamic constants for aqueous species and solids, filling data gaps for the relevant species, as well as changes in the speciation model (addition or removal of species) and newly selected data for solid phases. This update was done based on an extensive state-of-the-art review of the available data.

In previous versions of the ClaySor model (2SPNE SC/CE model), the stability constants of edge sorption and cation exchange species were derived using older thermodynamic data for aqueous species collected from several literature sources (Bradbury & Baeyens 2005, 2009a, b, 2017; Kulik et al. 2018). Previous ClaySor model did not include parameter uncertainty estimates.

In the revised version of ClaySor, the stability constants of adsorption species are refitted to be consistent with the updated TDB 2020 thermodynamic database, along with the derivation of parameter confidence intervals. The latter can be then used to evaluate the model uncertainty in predicting the uptake of relevant elements, which is used in repository safety assessment calculations based on a given composition of pore solution and clay rock mineralogy.

Re-parameterization of the ClaySor model was performed using the GEMSFITS parameter optimization tool (Miron et al. 2015). In particular, GEMSFITS can refine the equilibrium constants for surface complexation and ion exchange to obtain the best agreement between measured and calculated values for all used datasets. GEMSFITS provides several statistical methods to evaluate the correlation of parameters, the overall parameter sensitivity to the experimental data, and a Monte Carlo method for evaluating the parameter confidence intervals.

The parameter optimization workflow is illustrated adsorption of Mn^{II} on illite as an example. In the case of Mn, the ClaySor model includes one cation exchange and four surface complexes - two for strong- and two for weak edge sites (Table 2.1). This has been implemented in GEM-Selektor (GEMS) following the design of the 2SPNE SC/CE model (Kulik et al. 2018; Kulik et al. 2013).

The data used for the model optimisation consisted of five independent “in house” experimental datasets that comprise two pH edges in 0.1 M NaCl, and three Mn sorption isotherms (Mn concentration dependent adsorption) in 0.1 M NaCl at pH 6.0, 7.2, and 8.5. These were converted into the GEMSFITS experimental data format in preformatted excel spreadsheets, where the input and output of each experimental data point is defined in terms of GEMS equilibrium problem. The input consists of the weight of aqueous solution (kg), background electrolyte concentration, pH, and the planar (CEC) and strong and week edge sites density. The output is represented by the measured distribution coefficients Rd. All datasets were simultaneously used to get the best Gibbs energy values G^o_{298} of the 5 complexes as well as 95% confidence intervals. Measured and calculated sorption data for Mn on Illite are shown in Fig. 3.4. From the fitted G^o_{298} values with their confidence intervals and G^o_{298} values of other reactants involved in surface complexation reactions, the optimized log ${}^{SC}K$ values (at 25 °C) and their uncertainties were calculated.

During the fitting exercise, the contribution and the sensitivity of G^o_{298} of $\equiv^{W1}SOMn^+$ to the experimental data was quite low, therefore this surface complex was excluded from the model without affecting the quality of fit (Fig. 3.4b).

The UpSaGems (Uncertainty propagation and Sensitivity analysis for GEMS) has been used to perform the error propagation and sensitivity analysis for the Mn sorption on Illite model predictions (Fig. 3.5). UpSaGems is an in-house tool implemented in

Tab. 2.1: Surface complexation and cation exchange parameters for Mn^{II} on illite.

Surface complexation on strong edge sites	Site capacity	Previous values	GEMSFITS
	µmol/g clay	log ${}^{SC}K$	log ${}^{SC}K$
$\equiv^{S}SOH + Mn^{2+} \Leftrightarrow \equiv^{S}SOMn^+ + H^+$	2.0	0.90	0.84 ±0.1
$\equiv^{S}SOH + Mn^{2+} + H_2O \Leftrightarrow \equiv^{S}SOMnOH^0 + 2H^+$		-6.70	-6.45 ±0.1
Surface complexation on weak edge sites			
$\equiv^{W1}SOH + Mn^{2+} \Leftrightarrow \equiv^{W1}SOMn^+ + H^+$	40.0	-2.30	excluded
$\equiv^{W1}SOH + Mn^{2+} + H_2O \Leftrightarrow \equiv^{W1}SOMnOH^0 + 2H^+$		-9.20	-9.46 ±0.17
Cation exchange on planar sites		log K_{GT}	log K_V
$2Na\text{-}IdP + Mn^{2+} \Leftrightarrow Mn\text{-}IdP + 2Na^+$	225.0	0.70	0.16 ±0.53

$^{W1}SOMn^+$ was finally excluded from the refined model.

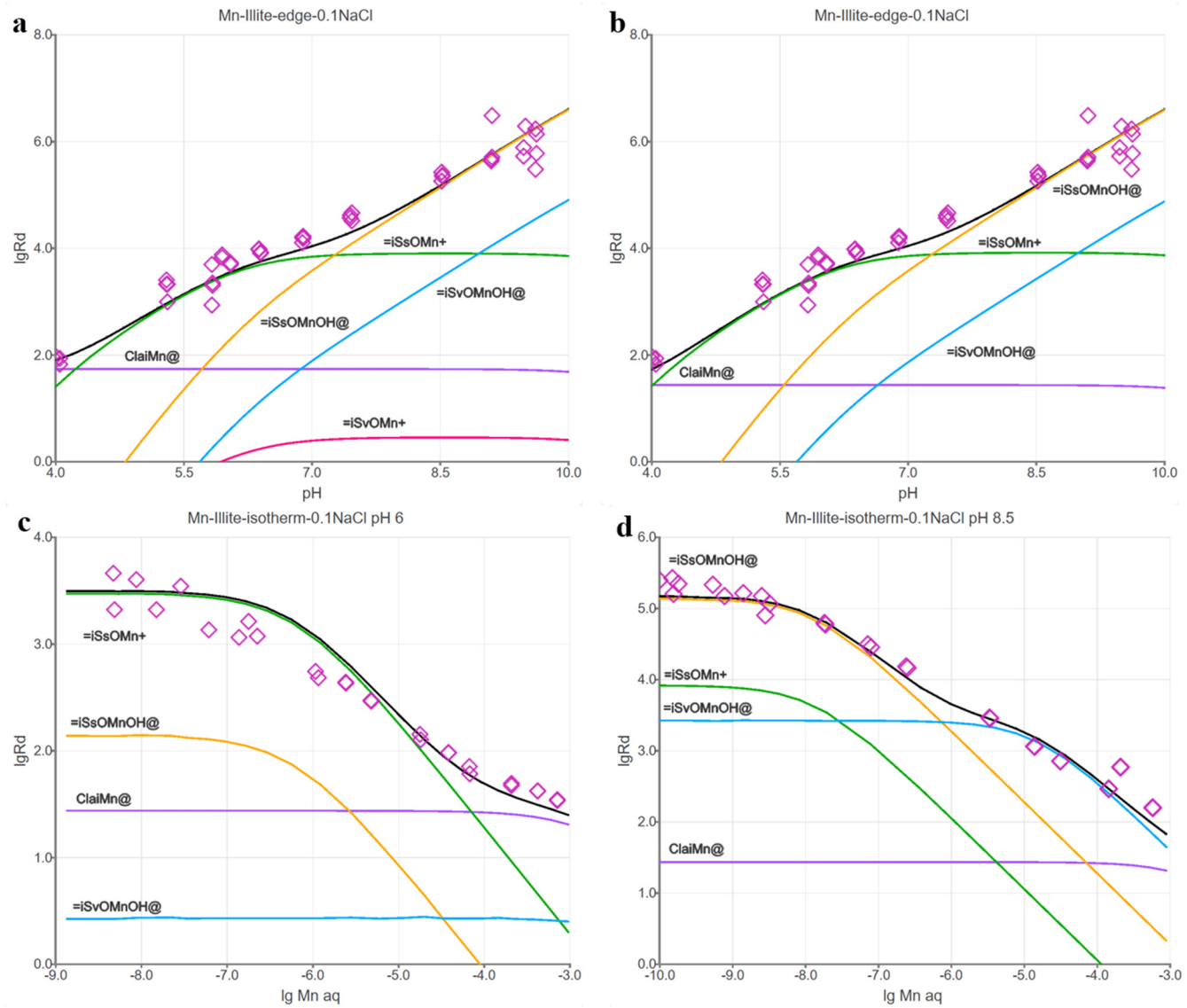

Fig. 3.4: Mn adsorption data on Illite, experimental and modeling (25 °C). a) and b) as a function of pH ($4.14 \cdot 10^{-8}$ M Mn); c) and d) as a function of Mn concentration; b) without $^{W1}SOMn^{+}$ ("$iSvOMn^{+}$") species.

Python within the JupyterLab notebook for performing error propagation and sensitivity analysis of parameters in thermodynamic models. The output of the analysis is the model standard deviation (σ), 95% confidence interval, as well as the contribution of different sorption sites to the overall variability defined as Sobol indices (Saltelli 2002). The confidence interval takes into account only the uncertainty of a surface complex derived from GEMSFITS that reflects the scatter of experimental data points; low scatter and large number of data points improve the model precision. Because the thermodynamic sorption model is directly linked to the aqueous electrolyte model, any change to G^{o}_{298} of the aqueous species will be propagated into the stability of surface complexes via stability constants of surface complexation reactions. While the values of G^{o}_{298} will change, their errors will not change since they are mainly based on the measured sorption data. Therefore, the error in calculated aqueous speciation does not have to be considered in the model confidence interval.

The model confidence interval (Fig. 3.5a) provides information on the precision of the model in predicting the uptake of a given element, accounting for the collective errors from each model parameter (i.e., G^{o}_{298} of complexes). The Sobol indices can help identify, which parameter provide the largest contribution to the model uncertainty at given conditions. In the example shown in Fig. 3.5b) these are linked to the G^{o}_{298} error and the concentration of the surface complex. The model can be improved by making more measurements for conditions where the standard deviation is high and where species with large errors display large Sobol indices.

3.5 Molecular scale understanding of competitive cation adsorption on swelling clay minerals

In the SNF project *"Molecular scale understanding of competitive cation adsorption on swelling clay minerals"* sorption experiments and spectroscopic

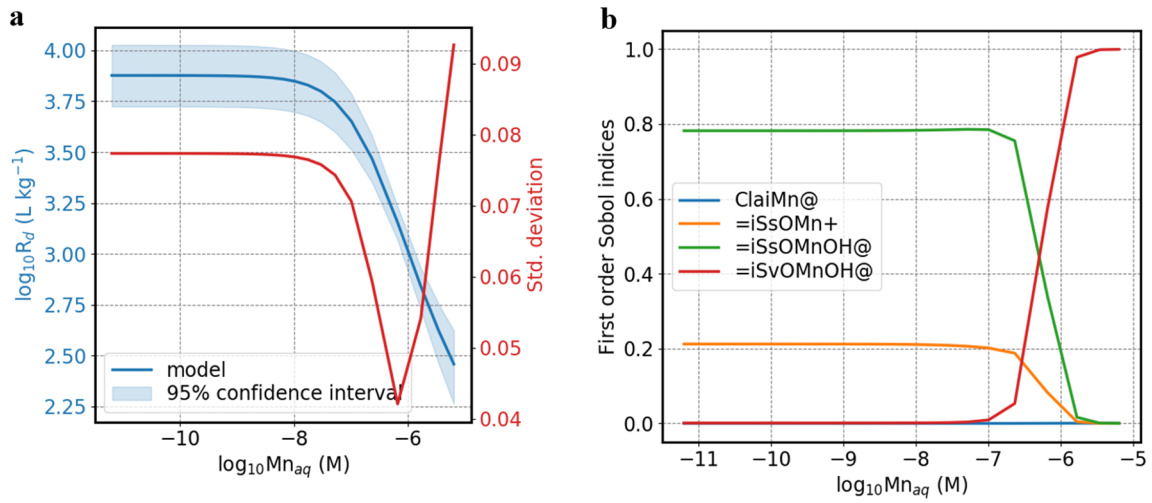

Fig. 3.5: Results of the error propagation and sensitivity analysis of Mn sorption isotherm on Illite (pH 7.5, 25 °C).

measurements have been performed to understand the uptake mechanism of the Ni^{II} and Lu^{III} on the tri-octahedral 2:1 clay saponite ($Na_{0.4}Mg_3Si_{3.6}Al_{0.4}O_{10}(OH)_2$). Saponite is a common synthetic product used in industrial applications. Synthetic saponite has a well-defined crystallographic structure and chemical composition, thus making it the ideal tri-octahedral 2:1 clay mineral for the characterisation of cation uptake mechanisms. The Ni^{2+} adsorption isotherm at pH 7 on Na-Mg-Saponite (Fig. 3.6) exhibits an overall non-linear behaviour. At low [Ni_{eql}] the adsorption is linear (Langmuir type, slope equal 1) with increasing concentrations the adsorption becomes non-linear and exhibits a Freundlich-type behaviour (slope < 1). The non-linearity of the isotherm follows the expected concentration dependency and complies with the adsorption on at least two different site types as observed in previous studies on dioctahedral phyllosilicates (Baeyens & Marques Fernandes 2018). EXAFS measurements on Zn^{II} and Fe^{II} loaded montmorillonite (a di-octahedral 2:1 clay) samples allowed to identify two structurally different crystallographic sorption sites (Dähn et al. 2011; Kéri et al. 2020; Soltermann et al. 2014; Soltermann et al. 2013). In order to verify whether similar adsorption sites exist on Na-Mg-Saponite, two Ni loaded saponite samples (S1 with 2 mmol/kg Ni and S2 with 40 mmol/kg Ni), were characterised with EXAFS. In addition to the adsorption samples, saponites with Ni incorporated into the structure (stoichiometric substitution of $Mg(NO_3)_2$ for $Ni(NO_3)_2$) were synthesised and analysed by EXAFS. Three different Ni doped saponites were investigated, D1 and D2 with Ni loadings similar to the adsorption samples and a fully Ni substituted (Mg free) referred as Na-Ni-Saponite.

The radial structure functions (RSF) of the samples D1 and D2 show similar backscattering signals up to 6 Å, indicating that the loading has no effect on the structural environment. The spectra of the pure Na-Ni-Saponite shows similarities to the two doped samples.

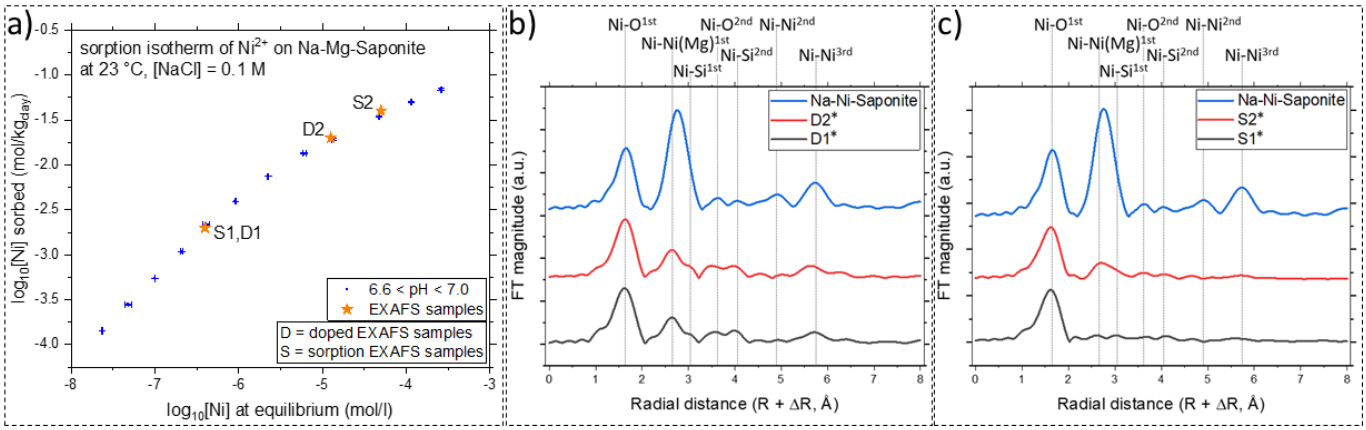

*Fig. 3.6: (a) Sorption isotherm of Ni on Na-saturated Mg-Saponite in circumneutral pH conditions; the experiments chosen for EXAFS are marked with labels and orange star-shaped symbols. Radial structure functions of b) Ni in the doped (D1 and D2) and fully-substituted saponites (Na-Ni-saponite). (c) Ni sorption samples with low (S1) and high (S2) metal loadings. *In sorption and doped samples, the atom predominantly responsible for the scattering from the octahedral sites is Mg^{2+} rather than Ni^{2+}.*

However, all backscattering amplitudes are higher in the reference compared to the doped samples. In addition the second peak in the RSF is clearly shifted to higher values in R + ΔR (Fig. 3.6b), indicating that Ni-Ni interactions play a predominant role.

The samples D1 and D2 exhibit minor Ni-Ni backscattering pairs from Ni atoms present in the octahedral sheets. In addition, Ni-Mg and Ni-Si backscattering pairs were used to fit the contributions from the second shell. The RSF's of the two sorption samples differ significantly from each other (Fig. 3.6c). Sample S2 has a backscattering contribution at ~ 2.7 Å (R + ΔR) similar to the doped samples, originating from Ni-Ni interaction and suggesting the formation of a Ni-rich phase. The precipitation of the solubility limiting phase $Ni(OH)_2$ can be excluded based on thermodynamic calculations. The spectrum of sample S1 does not exhibit this backscattering contribution, suggesting a less ordered environment or the formation of outer-sphere complexes. The formation of a surface precipitate was not observed for divalent cations (e.g., Zn or Fe) sorbing on dioctahedral clays at loadings not exceeding the edge site capacity of 40 mmol/kg at pH 7 (Dähn et al. 2011; Soltermann et al. 2014; Soltermann et al. 2013). The overlapping Ni-Ni, Ni-Mg and Ni-Si contributions making an univocal identification of the Ni complexes in high loading sorption powder samples (S2) challenging. This problem can be overcome by the polarized EXAFS measurements which have been performed. The P-EXAFS data shell provide more geometrical constrains, which will allow to identify the newly formed phase. The results of P-EXAFS are currently being interpreted for a forthcoming publication.

Molecular Dynamics simulations, based on Density Functional Theory, are used to calculate theoretical EXAFS spectra for Ni^{2+} surface complexes on the structurally different Saponite surfaces, and to predict thermodynamic of the surface complexation reactions. These modelling results are currently combined to interpret the experimental measurements and the spectroscopic data.

3.6 Redox reactivity of Tc^{VII} and Se^{IV} on iron bearing clay minerals

This year, the mineralogical characterisation of the reduced clay samples (structural Fe^{3+} reduced to Fe^{2+}) used for Tc^{VII} and Se sorption experiments were completed. The degree of clay dissolution during Citrate-Bicarbonate-Dithionite (CBD) reduction was quantified by measuring the amount of structural elements such as Fe, Si and Al released as a function of increasing dithionite concentration (Fig. 3.7). The conditions used to reduce our iron richest nontronite samples (20.5 wt% Fe total), low-red NAu and high-red NAu, are indicated by an arrow in Fig. 3.7. Under the used CBD conditions, a maximum of 3% of clay dissolves congruently. At higher dithionite concentration, the clay starts to dissolve incongruently (preferential dissolution of the Fe containing octahedral layer). Transmission electron microscope imaging (Fig. 3.8) show that the dissolution only occurs on the external basal plan without affecting the bulk clay structure (layer-to-layer distance around 11 Å).

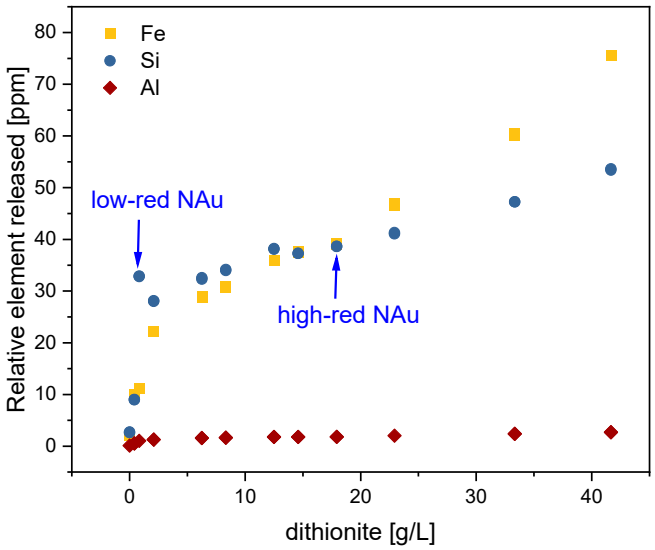

Fig. 3.7: Concentration of Fe, Si and Al relased during CBD clay reduction as a function of dithionite concentration.

Se^{IV} sorption experiments on non-reduced and reduced clays both show quantitatively similar behaviour. No increased sorption is observed on the Fe^{II} containing clays, as it is the case of Tc^{VII} for example. To determine the oxidation state and the structure of the Se surface complexes, sorption on different clays (reduced and non-reduced), at different pH values and Se loadings were investigated by X-ray absorption spectroscopy at the Rossendorf Beamline at the ESRF (Grenoble, France). X-ray absorption near edge structure **(**XANES**)** spectra indicate the reduction of Se^{IV} to Se^0 on most reduced clays (Fig. 3.9). Partial reduction is observed on both iron poor clays, red STx (fully reduced Texas montmorillonite with 0.5 wt% Fe^{II}) and red SWy (fully reduced Wyoming montmorillonite with 2.6 wt% Fe^{II}). On the low reduced iron rich nontronite (low_red NAu) (20.5 wt% Fe total, 19 wt% Fe^{II}) Se is fully reduced whereas the reduction is negligible on the high reduced nontronite (20.5 wt% Fe total, 45 wt% Fe^{II}).

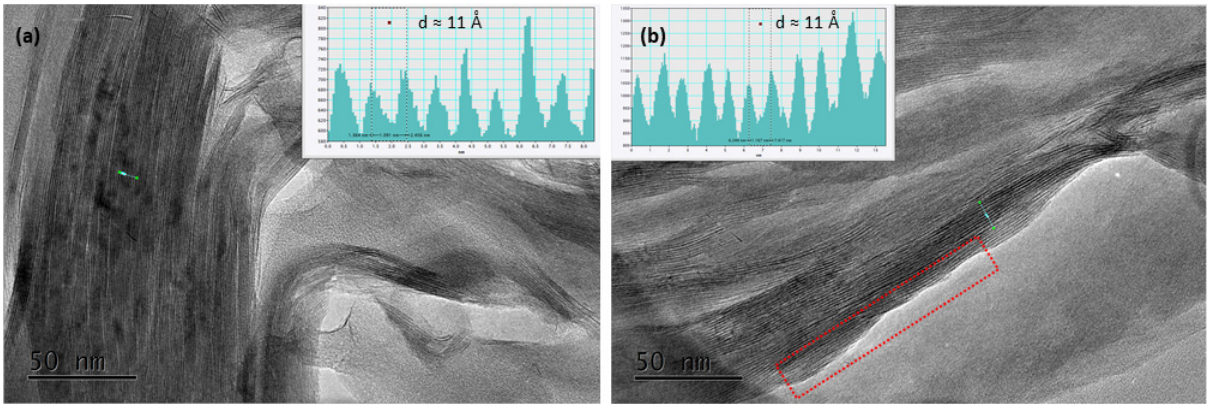

Fig. 3.8: Transmission electron microscope (TEM) pictures of nontronite sample (a) native NAu, (b) high-red NAu.

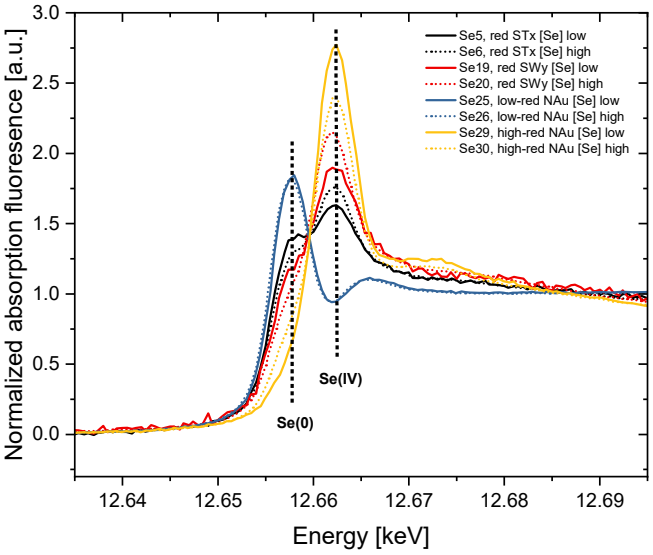

Fig. 3.9: Se K-edge XANES spectrum.

3.7 The sensitively inhibited Fe-Cr redox in quartz-montmorillonite-ferrihydrite systems

Quartz (Qtz), clays, and iron (hydr)oxides are the major inorganic minerals in soils/sediments, in which, compared to the skeleton role of Qtz, clays and iron (hydr)oxides serve as the major sink for many metals and nutrients. Thus in this study, Qtz, montmorillonite (Mt), and ferrihydrite (Fh) were chosen as mineral references to study the Fe-Cr redox behaviour in simulated soil/sediment systems (Fig. 3.10). No influence of Qtz-Mt-Fh on Fe-Cr redox is observed at pH 8. With increasing pH from 8 to 9 the redox is controlled by Fh, while remarkably affected by the association of Fh to Qtz and Mt at pH ≤ 7. However, due to the limited electron transfers (ETs) from interlayer-located Fe(II) to Cr(VI) at pH 6, the integration of Mt with Fh at first equilibrium can strengthen the inhibition of ETs further, making the proportion Cr(VI) in solids, $QCr(VI)_s$, > 11%. Unlike the strong integration in Mt-Fh, increasing pH to 7 contributes to the formation of dense and unstable Fh aggregation in Qtz-Fh, especially with Qtz/Fh ratios < 1.5. This process can generate surface-related Cr(III) hydroxides despite the main Fe-Cr co-precipitates in Qtz and Fh, which also intensifies the limitation of ETs from Fe(II) to $Cr(VI)_{ads}$. Because of the collective influences by Qtz, Mt, and Fh at pH 7, the $QCr(VI)_s$ is highest with (Mt+Fh)/Qu ratio of 4, which is highly ascribable to the "sandwich"-shaped configuration of Qtz-Mt-Fh integrations. As the major components of soils/sediments, the solid-related interactions among quartz, clays, and iron (hydr)oxides are common and significant (Dong et al. 2012; Liao et al. 2019; Peretyazhko et al. 2012), while their influences on Fe-Cr redox are not clearly described. Our study confirms the sensitive Fe-Cr redox in Qu-Mt-Fh, which is determined by many factors, e.g., the type of $Fe(II)_{ads}$, the sorption of Cr(VI), the Fe(II)-driven recrystallization of Fh, the pH, the integration of different minerals and their contents/compositions. This study can offer significant implications for the fate of redox-sensitive contaminations, particularly oxyanions (e.g., CrO_4^{2-} and AsO_4^{3-}) in the subsurface environments, where despite the sufficient amount of electron donors, the redox might be inhibited due to the solid-related interactions.

3.8 Eurad project FUTURE - Reversibility of sorption

The sorption of radionuclides on clay minerals in engineered and geological barrier systems is a main pillar in the safety case for deep geological disposal of radioactive waste. The currently used sorption models are based on the assumption that sorption is fully reversible. Therefore, investigations on the reversibility of Zn on Idp were carried out in the subtask 2.3 of the Eurad WP-FUTURE.

Zn adsorption on Na-IdP was studied at three loadings (2 mmol/kg, 24 mmol/kg, 67 mmol/kg) in 0.1 M NaCl background electrolyte at pH 7 at a S/L ratio of 1.4 g/l and a reaction time of 2 years.

The desorption samples were prepared in 0.1 M NaCl background electrolyte at pH and a S/L ratio of 14.2 g/l. After a reaction time of 7 days the samples were diluted

by a factor of 10 in 0.1 M NaCl, containing no Zn, to reach a S:L ratio of 1.4 g/L. After two years of reaction time both the adsorption and desorption samples were centrifuged and the wet clay pastes were filled into Plexiglas sample holders. The EXAFS measurements were performed at the beamline ID20 of the Diamond Light Source.

ICP-OES measurements of the supernatants indicate that the Zn loading of the adsorption samples amounted to 2 mmol/kg, 23 mmol/kg, and 65 mmol/kg, respectively. The desorption samples had a loading of 2 mmol/kg, 19 mmol/kg, 29 mmol/kg, respectively. Therefore, based on ICP-OES measurement it could be expected that at low and medium loadings reversibility is not playing a predominant role. However, at high loadings the amount of Zn present in the samples decreased from 65 mmol/kg to 29 mmol/kg, which differs significant even when errors in the ICP analysis are taken into account.

The EXAFS data at low loadings show remarkably similarities with a spectrum of Zn intrinsically present in IdP (Fig. 3.11), indicating a similar structural environment, e.g. that Zn is located in the continuity of octahedral sheets. The data for the adsorption and desorption data for the low loaded samples are identical indicating the Zn surface complexes remain unchanged during desorption experiment conducted over the time period of 2 years. The fact that there is no difference in the wet chemistry observed in the medium loaded Zn samples is reflected by the unchanged EXAFS spectra (Fig. 3.11). The only difference which can be observed between spectra of the adsorption and desorption samples is occurring at high loadings, e.g. at 65 mmol/ and 29 mmol/kg, respectively. The changes in the spectra indicate that desorption affects samples with a high loading. It should be noted that in none of the samples Zn-Zn backscattering pairs could be observed, indicating that even at high loadings precipitation of new phases did not occur. EXAFS data analysis indicates that the changes in the structural parameters are only minor and are essentially within the error margins ($CN_{Zn\text{-}O}$ 5.6(7), $R_{Zn\text{-}O}$ 2.07(1) Å; $CN_{Zn\text{-}Al}$ 1.5(6), $R_{Zn\text{-}Al}$ 3.03(2) Å; $CN_{Zn\text{-}Si}$ 3.0(7), $R_{Zn\text{-}Si}$ 3.28(2)) for the adsorption; $CN_{Zn\text{-}O}$ 5.8(9), $R_{Zn\text{-}O}$ 2.07(1) Å; $CN_{Zn\text{-}Al}$ 1.6(7), $R_{Zn\text{-}Al}$ 3.03(2) Å; $CN_{Zn\text{-}Si}$ 3.0(8), $R_{Zn\text{-}Si}$ 3.25(2)) for the desorption). It can therefore be concluded that sorbed species at the Idp are very stable over the employed reaction time.

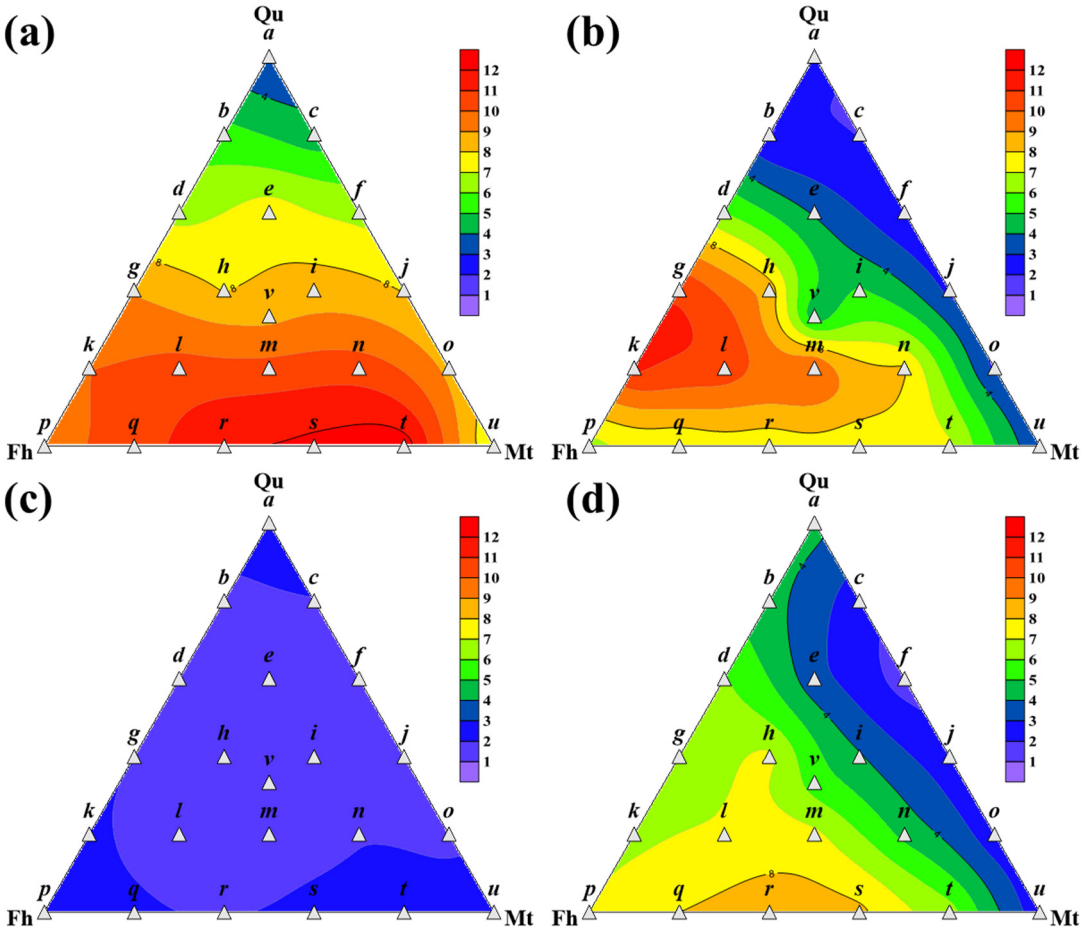

Fig. 3.10: The $QCr(VI)_s$ at pHs of 6 (a), 7 (b), 8 (c), and 9 (d) in Qtz-Mt-Fh.

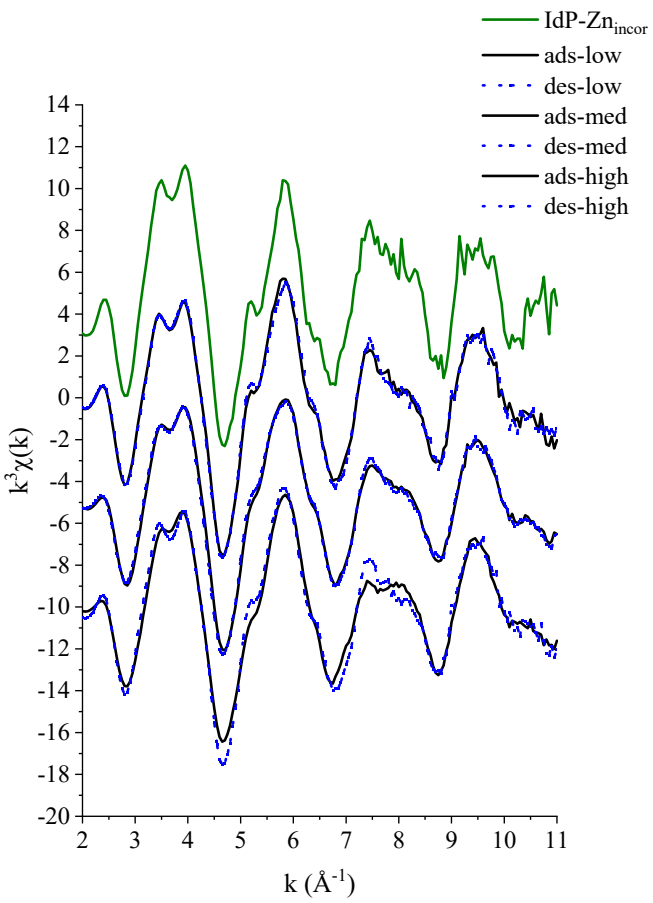

Fig. 3.11: EXAFS spectra of Zn in pure Idp and in adsorption and desorption Idp samples at three different loadings after two years of reaction time.

3.9 References

Baeyens B., Bradbury M.H. (1995a)
A quantitative mechanistic description of Ni, Zn and Ca sorption on Na-montmorillonite. Part I: Physico-chemical characterization and titration measurements. PSI Bericht Nr. 95-10, Würenlingen and Villigen.

Baeyens B., Bradbury M.H. (1995b)
A quantitative mechanistic description of Ni, Zn and Ca sorption on Na-montmorillonite. Part II: Sorption measurements. PSI Bericht Nr. 95-10, Würenlingen and Villigen.

Baeyens B., Bradbury M.H. (2004)
Cation exchange capacity measurements of illite using the sodium and cesium isotope dilution technique: Effects of the index-cation, electrolyte concentration and competition: Modeling. Clays and Clay Minerals 52, 421-431.

Baeyens B., Marques Fernandes M. (2018)
5 - Adsorption of heavy metals including radionuclides. In Developments in Clay Science (eds. R. Schoonheydt, C. T. Johnston and F. Bergaya). Elsevier 9, 125-172.

Bradbury M.H., Baeyens B. (2005)
Experimental and Modelling Investigations on Na-Illite: Acid-Base Behaviour and the Sorption of Strontium, Nickel, Europium and Uranyl. PSI Bericht Nr. 05-02, Paul Scherrer Institut, Villigen, Switzerland.

Bradbury M.H., Baeyens B. (2009a)
Sorption modelling on illite Part I: Titration measurements and the sorption of Ni, Co, Eu and Sn. Geochimica Et Cosmochimica Acta 73, 990-1003.

Bradbury M.H., Baeyens B. (2009b)
Sorption modelling on illite. Part II: Actinide sorption and linear free energy relationships. Geochimica Et Cosmochimica Acta 73, 1004-1013.

Bradbury M.H., Baeyens B. (2017)
The development of a thermodynamic sorption data base for illite and the application to argillaceous rocks. PSI Bericht Nr. 17-06, Paul Scherrer Institut, Villigen PSI and NTB 17-14, Nagra, Wettingen, Switzerland.

Dähn R., Baeyens B., Bradbury M.H. (2011)
Investigation of the different binding edge sites for Zn on montmorillonite using P-EXAFS – the strong/weak site concept in the 2SPNE SC/CE sorption model. Geochimica et Cosmochimica Acta 75, 5154-5168.

Dong W., Tokunaga T.K., Davis J.A., Wan J. (2012)
Uranium(VI) Adsorption and Surface Complexation Modeling onto Background Sediments from the F-Area Savannah River Site. Environmental Science & Technology 46, 1565-1571.

Hummel W., Thoenen T. (2021)
The PSI Chemical Thermodynamic Database 2020, in: N.-V. Nagra Technical Report, Switzerland. (Ed.).

Kéri A., Dähn R., Marques Fernandes M., Scheinost A.C., Krack M., Churakov S.V. (2020)
Iron Adsorption on Clays Inferred from Atomistic Simulations and X-ray Absorption Spectroscopy. Environ. Sci. Technol. 54, 11886-11893.

Klinkenberg M., Brandt F., Baeyens B., Bosbach D., Fernandes M.M. (2021)
Adsorption of barium and radium on montmorillonite: A comparative experimental and modelling study. Applied Geochemistry 135, 105117.

Kulik D.A., Marques Fernandes M., Baeyens B. (2018)
The 2SPNE SC/CE sorption model in GEM-Selektor v.3.4 code package (ClaySor): Implementation, tests, and user guide. Nagra Arbeitsbericht NAB 18-27, Nagra, Wettingen, Switzerland.

Kulik D.A., Wagner T., Dmytrieva S.V., Kosakowski G., Hingerl F.F., Chudnenko K.V., Berner U.R. (2013)
GEM-Selektor geochemical modeling package: revised algorithm and GEMS3K numerical kernel for coupled simulation codes. Computational Geosciences 17, 1-24.

Liao W., Ye Z., Yuan S., Cai Q., Tong M., Qian A., Cheng D. (2019)
Effect of Coexisting Fe(III) (oxyhydr)oxides on Cr(VI) Reduction by Fe(II)-Bearing Clay Minerals. Environ. Sci. Technol. 53, 13767-13775.

Liu X., Tournassat C., Grangeon S., Kalinichev A.G., Takahashi Y., Marques Fernandes M. (2022)
Molecular-level understanding of metal ion retention in clay-rich materials. Nature Reviews Earth & Environment 3, 461-476.

Marques Fernandes M., Baeyens B. (2019)
Cation exchange and surface complexation of lead on montmorillonite and illite including competitive adsorption effects. Applied Geochemistry 100, 190-202.

Miron G.D., Kulik D.A., Dmytrieva S.V., Wagner T. (2015)
GEMSFITS: Code package for optimization of geochemical model parameters and inverse modeling. Applied Geochemistry 55, 28-45.

Peigneur P. (1976)
Stability and adsorption affinity of some transition metal-amine complexes in aluminosilicates. Ph.D Thesis, Univ. Leuven, Belgium.

Peretyazhko T.S., Zachara J.M., Kukkadapu R.K., Heald S.M., Kutnyakov I.V., Resch C.T., Arey B.W., Wang C.M., Kovarik L., Phillips J.L. and Moore D.A. (2012)
Pertechnetate (TcO4−) reduction by reactive ferrous iron forms in naturally anoxic, redox transition zone sediments from the Hanford Site, USA. Geochimica et Cosmochimica Acta 92, 48-66.

Saltelli A. (2002)
Sensitivity analysis for importance assessment. Risk Anal 22, 579-590.

Soltermann D., Marques Fernandes M., Baeyens B., Miehé-Brendlé J., Dähn R. (2014)
Competitive Fe(II)–Zn(II) Uptake on a Synthetic Montmorillonite. Environmental Science & Technology 48, 190-198.

Soltermann D., Marques Fernandes M., Baeyens B., Dahn R., Miehe-Brendle J., Wehrli B., Bradbury M.H. (2013)
Fe(II) Sorption on a Synthetic Montmorillonite. A Combined Macroscopic and Spectroscopic Study. Environmental Science & Technology 47, 6978-6986.

4 RADIONUCLIDE TRANSPORT AND RETENTION IN COMPACTED CLAY SYSTEMS AT FULL AND PARTIAL SATURATION

Glaus M.A., Van Loon L.R., Ma B., Pfingsten W., Baeyens B., Marques Fernandes M., Churakov S.V., Frick S., Bunic P., Zerva D. (PhD student), Hu G. (postdoc), Kuster D. (Department Hot Laboratory), Spahr A. (Department Hot Laboratory)

4.1 Introduction

The retention of radionuclides by clay minerals in engineered and geological barrier systems is a key process responsible for the radiological safety of a deep geological repository. Reliable sorption data (R_d values) and a mechanistic understanding of sorption and transport processes are thus mandatory for a proper evaluation of the barrier safety function. Sorption studies are mainly performed in batch systems using dispersed clays with a low solid to liquid ratio. In such an experimental setup the composition of the solution can be well controlled (e.g. pH, Eh, concentrations of anions and cations, organic and inorganic ligands) and/or varied in order to study their effect on the sorption. Undisturbed clay rocks, however, are very dense and are characterised by a high solid-to-liquid ratio. It is still an unanswered question, whether the data and models derived from dilute dispersed systems can be transferred to the natural consolidated rocks and compacted clays. The aim of this project is to resolve conceptual difficulties in applying the existing sorption models to diffusion in compacted argillaceous rocks.

A second focus of the project deals with the question whether adsorbed ions should be treated as immobile or only partially immobile. These two conceptual model assumptions have fundamental implications for the transport behaviour of ions in compacted systems. In the case of a full immobilisation, a pore diffusion model can describe transport whereas in the case of partial immobilisation surface diffusion models have to be applied.

4.2 Diffusion of moderately/strongly radionuclides in clay rocks

The potential for upscaling of diffusion results gained from compacted illite as a model system to Opalinus Clay has been recently demonstrated for the case of the diffusion of Co^{2+} (Glaus et al. 2021). An extension of such experiments using Opalinus Clay samples from the deep borehole drilling campaign of Nagra is foreseen to be accomplished during the work carried out for the general license application. For an unequivocal interpretation of such experiments, control of the mechanical integrity of the Opalinus Clay samples and their embedding in a polymeric resin is necessary. Extended tests for the mechanical preparation and microscopic characterisation of such samples were undertaken in collaboration with staff from the Department Hot Laboratory (AHL). Fig. 4.1 shows mechanical preparations of cylindrical clay rock samples from the machining to the embedding in epoxy resin and the processing on the lathe for obtaining the final dimensions. Contrary to the previous sample preparation method using a hollow driller, the new approach allows for a sample preparation with bedding orientation in direction of the cylindrical axis or perpendicular to it. Furthermore it was possible to produce specimens with varying thicknesses of the resin embedding in order to investigate the mechanical behaviour of the clay rock samples during the saturation with artificial pore water (APW). Fig. 4.2 shows the cross section of the open surface of an Opalinus Clay foreseen to be in contact with tracered APW. The left- and right-hand plot compares the sample after mechanical preparation and after exposure to APW. While the geometry of clay cylinder and resin embedding was concentrically circular (left-hand plot), it is obvious that the circular dimensions of the Opalinus Clay sample are distorted with stronger expansion in the direction perpendicular to the bedding (characterised by the calcareous inclusions) than parallel to it. However, a general expansion of such samples by at least 0.1 mm can be recognised. Thereby the porosity of the samples increase significantly.

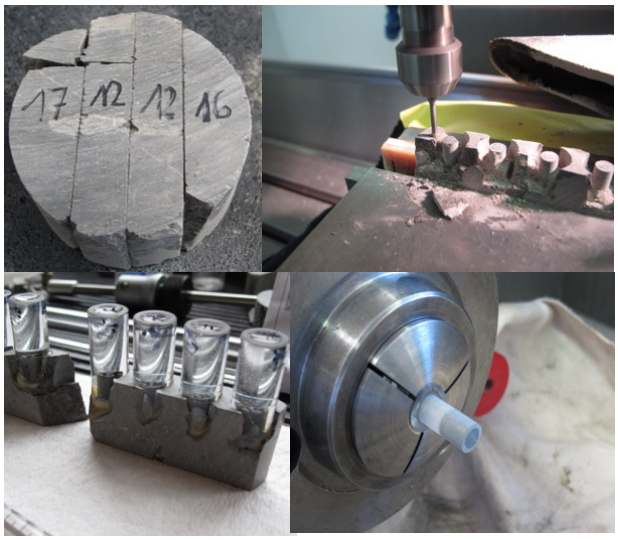

Fig. 4.1: Mechanical preparation (left to right and top to down) of cylindrical Opalinus Clay sample embedded in epoxy resin for diffusion experiments with strongly sorbing tracers.

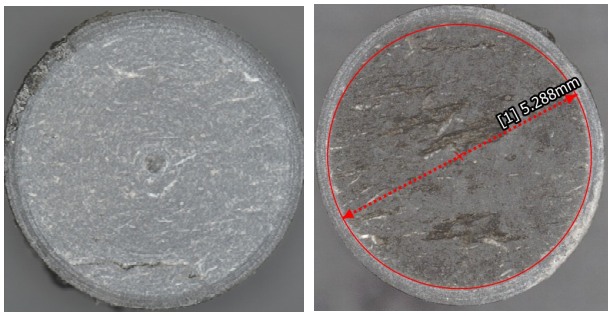

Fig. 4.2: Comparison of the geometry of an epoxy resin embedded sample of Opalinus Clay after preparation (left-hand plot) and after saturation with APW for ~30 days (right-hand plot). The red circle in the latter plot is only shown to illustrate the anisotropic expansion of the clay rock sample which was stronger in the direction perpendicular to the clay bedding than parallel. The dimensions shown do not have an immediate meaning.

This observation by microscopy is in good agreement with the results of diffusion of HTO in which porosities of up to ~30 % (instead of values of ~7–15 %) were measured. Despite these alterations, such samples can be used for measuring the diffusion properties of strongly sorbing tracers. Appropriate values for the total porosity and geometry factors – as obtained by a previous measurement of HTO diffusion on the same samples – have to be taken into account for the interpretation of the results.

4.3 Diffusion measurements on Gipskeuper samples from Nagra deep bore holes

In order to evaluate tracer profiles of Cl^- and $H_2{}^{18}O$ in deep boreholes in the Zürich Nordost region, diffusion properties of anhydrite ($CaSO_4$) have to be known. To this end, diffusion of HTO and $^{36}Cl^-$ in an anhydrite sample from a deep borehole in Marthalen 1-1 (Zürich Nordost) was measured in the laboratory. The measurement was performed at 50 °C to avoid hydration of the sample and conversion of anhydrite to gypsum. An artificial NaCl solution saturated w.r.t gypsum was used (NaCl = 0.2 M; $CaSO_4$ = 23 mM) in order to prevent dissolution of anhydrite. A breakthrough of HTO was observed after ~10 days whereas a break-through of $^{36}Cl^-$ could be measured after ~30 days. At day 180 of the diffusion experiment, first estimates of the effective diffusion coefficient and accessible porosity were done.

For HTO the effective diffusion coefficient $D_e = (1.01 \pm 0.20)\times10^{-13}$ $m^2\ s^{-1}$ and the accessible porosity is 0.026. In the case of ^{36}Cl the $D_e = (1.40 \pm 0.30)\times10^{-15}$ $m^2\ s^{-1}$ and the accessible porosity is 0.0001.

4.4 Eurad project FUTURE: Subtask mobility

Profile analysis of in-diffusion experiments with $^{57}Co^{2+}$ were carried out for Li^+-, Na^+- and Cs^+- homoionic forms of illite compacted at a bulk-dry density of ~1500 $kg\cdot m^{-3}$ varying ionic strength of the background electrolyte concentrations between 0.03 and 0.5 M at pH ~5.5. The first results reveal the effect of the cationic loading on tracer diffusivity (Fig. 4.3). According to the surface diffusion concept, the effective diffusivity of the diffuse layer species in Li^+-illite is larger than in the respective Cs^+-illite. In the latter case, the negative surface charge is more strongly shielded by the increased formation of immobile surface complexes and the concentration of diffuse-layer species is thereby reduced. Experiments with $^{65}Zn^{2+}$ are currently on-going. They comprised additionally a lower electrolyte concentration (0.01 M) and K^+-illite was included in order to complete the variation of the alkali cations. In these experiments, similar trends on the tracer reservoir depletion during the in-diffusion were observed as for the experiments with $^{57}Co^{2+}$.

HTO through diffusion experiments with these 4 homoionic forms of illite show that the cationic loading has only a minor effect on the effective diffusivity of HTO and thus on the pertinent geometry factors valid for these clay variants. However, this is not the case for the anion exclusion phenomena: Experiments studying the anion exclusion effects of Li and Cs illite have shown a significant difference in anion accessible porosity between these 2 forms of illite.

Combing the information from in-diffusion experiments with transition metal cations and through-diffusion experiments with HTO, we may conclude that

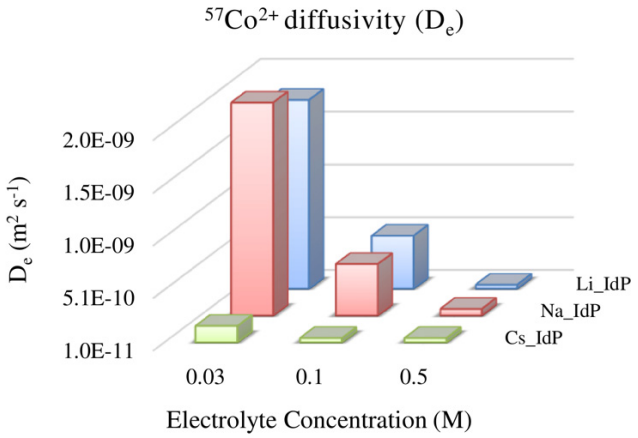

Fig. 4.3: D_e values for $^{57}Co^{2+}$ in illites compacted at a bulk-dry density of ~1500 kg m^{-3} as a function of the type of cation at the planar surfaces and of ionic strength. pH in the contacting solution was around ~5.5.

the diffusivity of the former tracers is rather controlled by the distribution ratio between the mobile surface species and the species in the bulk aqueous phase than by the geometry factor.

4.5 Diffusion of HTO, $^{22}Na^{+}$ and $^{36}Cl^{-}$ in compacted Ca^{2+}- and Na^{+}-conditioned smectites

To compare and determine the diffusion behaviour of a few representative key species in smectite-type clays under different electrolyte environments, through-diffusion experiments of HTO, $^{22}Na^{+}$ and $^{36}Cl^{-}$ in both Ca^{2+}-conditioned and Na^{+}-conditioned clays were conducted using the stainless steel through-diffusion cells. Three types of montmorillonite (Mt) rich clays were investigated, including Volclay bentonite (containing 64%-71% Mt) (Van Loon et al. 2007), GMZ bentonite (containing 72%-75% Mt) (Wu et al. 2018), and Milos montmorillonite (nearly pure Mt) (Dähn et al. 2011). Accessory and secondary phases include quartz, feldspar, calcite, albite, etc. The background electrolytes of 0.25 M $CaCl_2$ and 0.5 M NaCl were used for Ca^{2+}-conditioned and Na^{+}-conditioned clays, respectively. The same amounts of radiotracer was introduced in each the clay systems studied.

The results for HTO diffusion do not show any significant difference between the Ca^{2+}- and Na^{+}-forms of each type of clay, indicating that the accessible porosity for neutral species is the same in the Ca- and the Na-forms. The steady-state flux (in Bq cm^{-2} d^{-1}) measured in different clays decreased in the order of GMZ (~27) > Volclay (~25) > Milos (~15).

Regarding $^{36}Cl^{-}$ diffusion results, the flux curves between the Ca^{2+}- and Na^{+}-forms of Volclay and GMZ are quite similar in terms of the breakthrough time and the steady-state flux. In contrast, Milos Mt shows rather different flux curves between Ca^{2+}- and Na^{+} forms, with the Ca^{2+} form having 2-3 times longer time for reaching the steady flux state compared to Na^{+}-form. Besides, the steady flux of Ca-Milos (1.3 Bq cm^{-2} d^{-1}) was ~2 times lower than that of Na-Milos (2.6 Bq cm^{-2} d^{-1}). As shown in Fig. 4.4a, the steady flux of the three types of clays was in the order of GMZ > Volclay > Milos. All these results indicate that anion-exclusion effects are also pronounced in the Ca^{2+}-forms of the smectites.

Unexpectedly, more intriguing results were obtained in the $^{22}Na^{+}$ diffusion study through the Ca^{2+}-conditioned clays, where a much stronger retardation effect was observed compared to the Na^{+}-conditioned clays. As illustrated in Fig. 4.4b, the flux of $^{22}Na^{+}$ at the zero-concentration boundary was quite low for all the three clays and was in the order of Ca-Volclay > Ca-GMZ > Ca-Milos, with the flux in Ca-Milos staying at zero even after 48 days. The retardation process hidden behind the extraordinary data remains unknown. A change in the selectivity for the exchange between sodium and calcium is only one possible explanation. Precipitation of sodium seems less likely. Further experiments, e.g., profile analysis and diffusion/sorption experiments at different compaction density, need to be conducted to better understand the roles of the accessible porosity and the potential sorption sites of the Ca^{2+}-based clays controlling the diffusive transport of $^{22}Na^{+}$.

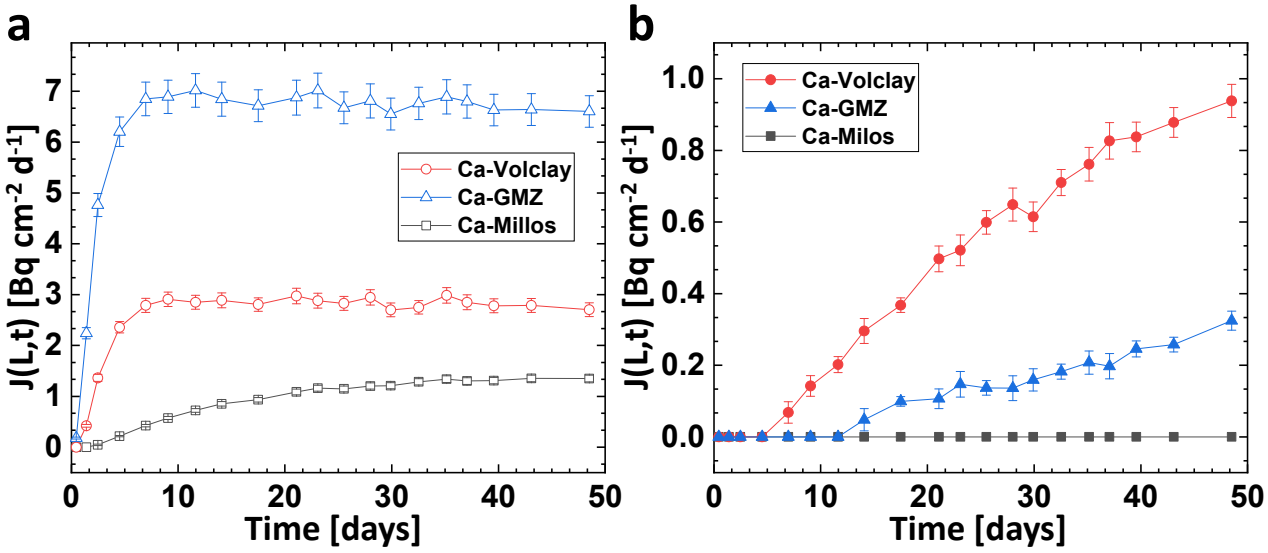

Fig. 4.4: Flux at the zero-concentration boundary of $^{36}Cl^{-}$ (a) and $^{22}Na^{+}$ (b) through-diffusion in three types of Ca^{2+}-conditioned clays (including Volclay bentonite, GMZ bentonite, and Milos montmorillonite) at ρ_{bd} = 1600 kg m^{-3} and 0.25 M $CaCl_2$ external salt concentration.

4.6 References

Dähn R., Baeyens B., Bradbury M.H. (2011)
Investigation of the different binding edge sites for Zn on montmorillonite using P-EXAFS – The strong/weak site concept in the 2SPNE SC/CE sorption model. Geochimica et Cosmochimica Acta, 75, 5154-5168.

Glaus M.A., Frick S., Van Loon L.R. (2021)
Competitive effects of cations on the diffusion properties of strongly sorbing trace cations in compacted illite and Opalinus Clay. ACS Earth and Space Chemistry, 5, 2621–2625.

Van Loon L.R., Glaus M.A., Müller W. (2007)
Anion exclusion effects in compacted bentonites: Towards a better understanding of anion diffusion. Applied Geochemistry, 22, 2536-2552.

Wu T., Wang Z., Tong Y., Wang Y., Van Loon L.R. (2018)
Investigation of Re(VII) diffusion in bentonite by through-diffusion and modeling techniques. Applied Clay Science, 166, 223-229.

5 THERMODYNAMIC MODELS AND DATABASES

Hummel W., Kulik D.A., Miron G.D.

5.1 Introduction

The aim of this project is to further develop and improve thermodynamic models and databases used for the reactive transport simulations, the derivation of model parameters for safety assessment studies and the preparation of various technical reports describing the repository evolution for the general license applications (RBG). Among others, the solubility and sorption databases and synthesis reports are an important part of the documentation for RBG.

The latest comprehensive update of PSI Chemical Thermodynamic Database took place in 2020 (TDB 2020, Hummel & Thoenen 2022). These carefully selected unified thermodynamic data provide the basis for pore water definitions, for the solubility limits calculations, the development of the sorption databases and simulation of the repository *in situ* conditions. The consistent and consequent use of TDB 2020 throughout all types of thermodynamic calculations is of crucial importance.

To support the thermodynamic calculations and to maintain the thermodynamic databases, the GEM Software (GEMS) code collection, https://gems.web.psi.ch/, has been developed at PSI/LES since 2000 by a community team lead by D.A. Kulik.

A cement sorption database (SDB 2023, Tits, in prep.) is under development and has to be ready for the next safety assessment study related to RBG for the planned repository for low- and intermediate-level (L/ILW) waste repository in Switzerland. Solubility calculations of 27 radionuclides for use in the development of SDB 2023 were performed with the most recent version of GEMS, using TDB 2020 imported by G.D. Miron into GEMS format and combined with the CEMDATA18 TDB adjusted to TDB 2020 (Lothenbach et al. 2019) https://www.empa.ch/web/s308/cemdata.

A new flexible and extendable calcium aluminium silicate hydrate (CASH+) sublattice solid solution model describing accurately the stability, solubility, density, water content and mean silicate chain length of CASH phases – the main product of cement hydration, has been updated and made available for the GEMs users.

5.2 Solubility of radionuclides in a concrete environment

For SDB 2023, solubilities of Ca, Al, Si, $^{14}CO_3^{2-}$ and Ni are required to assess isotopic exchange processes. Solubility limits for Ac, Ag, Am, Cm, Cs, Eu, Hg, Ho, Nb, Np, Pa, Pb, Po, Pu, Ra, Sn, Sr, Th, Ti, U, Zr are needed in connection with an assessment of sorption competition. Sorption competition with Fe(II, III) is taken into account for those cationic, dose-relevant radionuclides that are preferentially taken up by C-S-H phases in all stages of the cement degradation. A graphical summary of all elements considered here is given in Fig. 5.1.

Solubility limits for the mentioned 27 elements have been calculated in concrete porewater representing stage II of the degradation of container concrete at pH 12.8 under suboxic (Eh = -376 mV) and anoxic (Eh = -609 mV) conditions using TDB 2020 (Hummel et al. 2022).

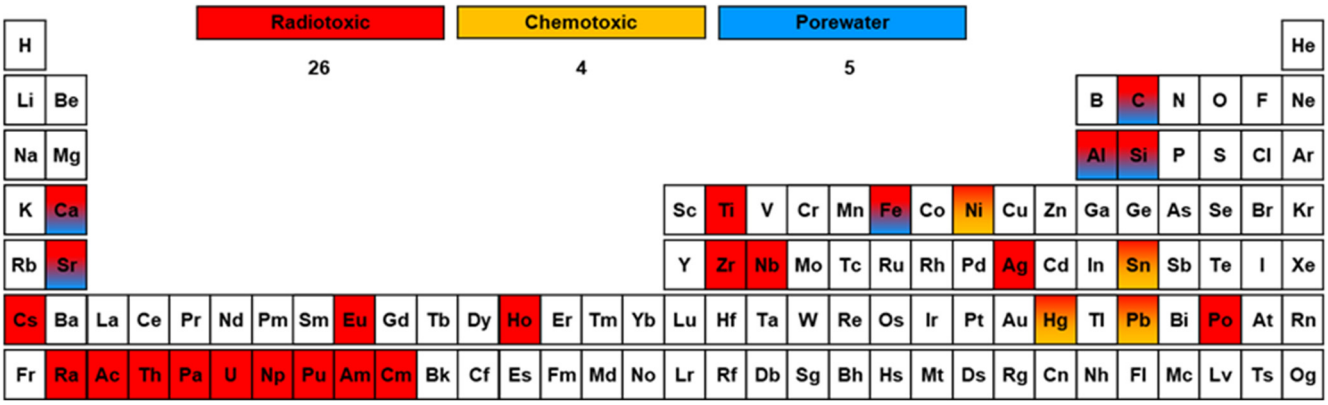

Fig. 5.1: Chemical elements for which the solubility limits were calculated. Some elements shown in different colours are chemotoxic and have radioactive isotopes occurring in the list of dose-relevant nuclides for radioactive waste disposal. Likewise, elements can be constituents of ground- and pore-waters and also occur in the list of dose-relevant radionuclides.

TDB 2020 contains thermodynamic data for all radionuclides considered in this solubility modelling study and thus, no additional thermodynamic data were needed from other sources.

The present study (Hummel et al. 2022) basically is an update of the solubility limits derived by Berner (2014), apart from the new elements Al, Hg, Si and Ti.

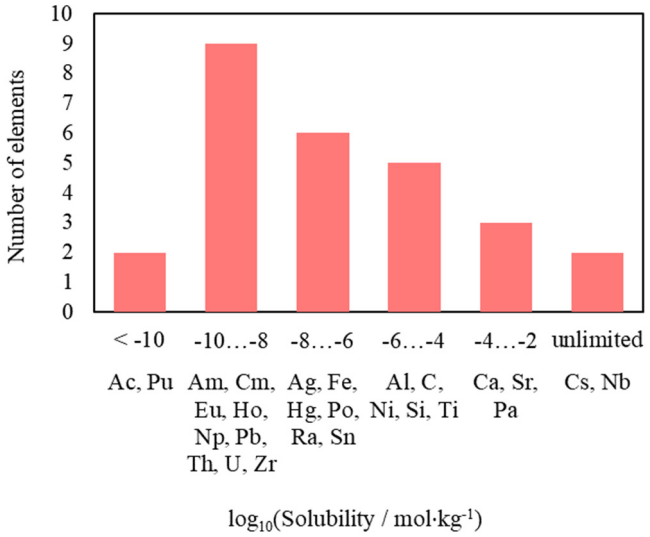

Fig. 5.2: Distribution of solubility limits for radionuclides under anoxic conditions. The concentrations of Al, C, Ca, Fe, Si and Sr are determined by the definition of the porewater. The distribution of solubility limits under suboxic conditions is the same as for anoxic conditions with two exceptions, Pb and U, which show orders of magnitude higher solubilities under suboxic conditions.

As can be seen in Fig. 5.2, 17 out of these 27 elements exhibit maximum solubilities below the micromolar range, i.e., < 10^{-6} mol/kg H_2O.

Looking closely at the 10 elements, which maximum solubilities are predicted to be above the micromolar range, we see that the concentrations of Al, C, Ca, Si and Sr are determined by the definition of the porewater itself.

Two elements are listed with “unlimited” solubility (Fig. 5.2). However, only one of them, namely Cs, is chemically “unlimited”, i.e., its concentration in the porewater is only limited by the Cs inventory in the waste and the availability of natural Cs.

Nb is formally “unlimited” because of the complete lack of thermodynamic data for a solubility limiting solid phase at pH 12.8, although experimental data indicate that the Nb concentration under the chosen condition is < 10^{-8} mol/kg H_2O.

The calculated high concentration limit of Pa > 10^{-4} mol/kg H_2O might be an overestimation due to the lack of thermodynamic data for Pa(IV) which is expected to be the dominating redox state of Pa under anoxic conditions.

The calculated maximum solubility of Ti > 10^{-5} mol/kg H_2O could also be an overestimation due to the lack of thermodynamic data for the potentially dispersed solid phases $CaTiO_3$ (perovskite) or $CaTiSiO_5$ (titanite) in the cementitious system.

The results obtained in this modelling study (Hummel et al. 2022) are compared with those obtained by Berner (2014) in Fig. 5.3.

Note that the length of the bars in Fig. 5.3 cannot be compared directly, as Berner (2014) discussed his chemical systems in some detail while in the present study solely uncertainties in thermodynamic data were used to calculate upper and lower limits.

Furthermore, the chemical system used in the modelling study of Berner (2014) with Eh = -498 mV is in between the suboxic conditions (-376 mV) and anoxic conditions (-609 mV) studied here, but somewhat closer to the anoxic conditions.

Most elements shown in Fig. 5.3 are barely redox sensitive and thus, mainly the results obtained in the anoxic system are compared with the data of Berner (2014). Exceptions are Pb and U, where results for suboxic conditions are shown in Fig. 5.3, which are in excellent agreement with Berner (2014), while the results for Pb and U under anoxic conditions are more than 6 and 3 orders of magnitude lower, respectively.

Generally, Fig. 5.3 shows good agreement between the data provided by Berner (2014) and the new results. However, a few special cases might be worthwhile mentioning.

The database used by Berner (2014) did not contain any thermodynamic data for Ac. Hence, Berner (2014) used his results for Eu(III) as an estimate for Ac(III). Such an estimation was conservative, as the thermodynamic Ac data now reviewed and included in TDB 2020 lead to an Ac solubility, which is more than 4 orders of magnitude lower than the estimate.

The large ambiguity in the thermodynamic data of Ag, discussed by Berner (2014) and shown in Fig. 5.3 as a bar extending over 9 orders of magnitude, has now been resolved thanks to an extensive review of Ag data for TDB 2020.

The review efforts concerning the rare earth elements Eu and Ho in TDB 2020 finally resulted in lower solubilities than previously calculated by Berner (2014).

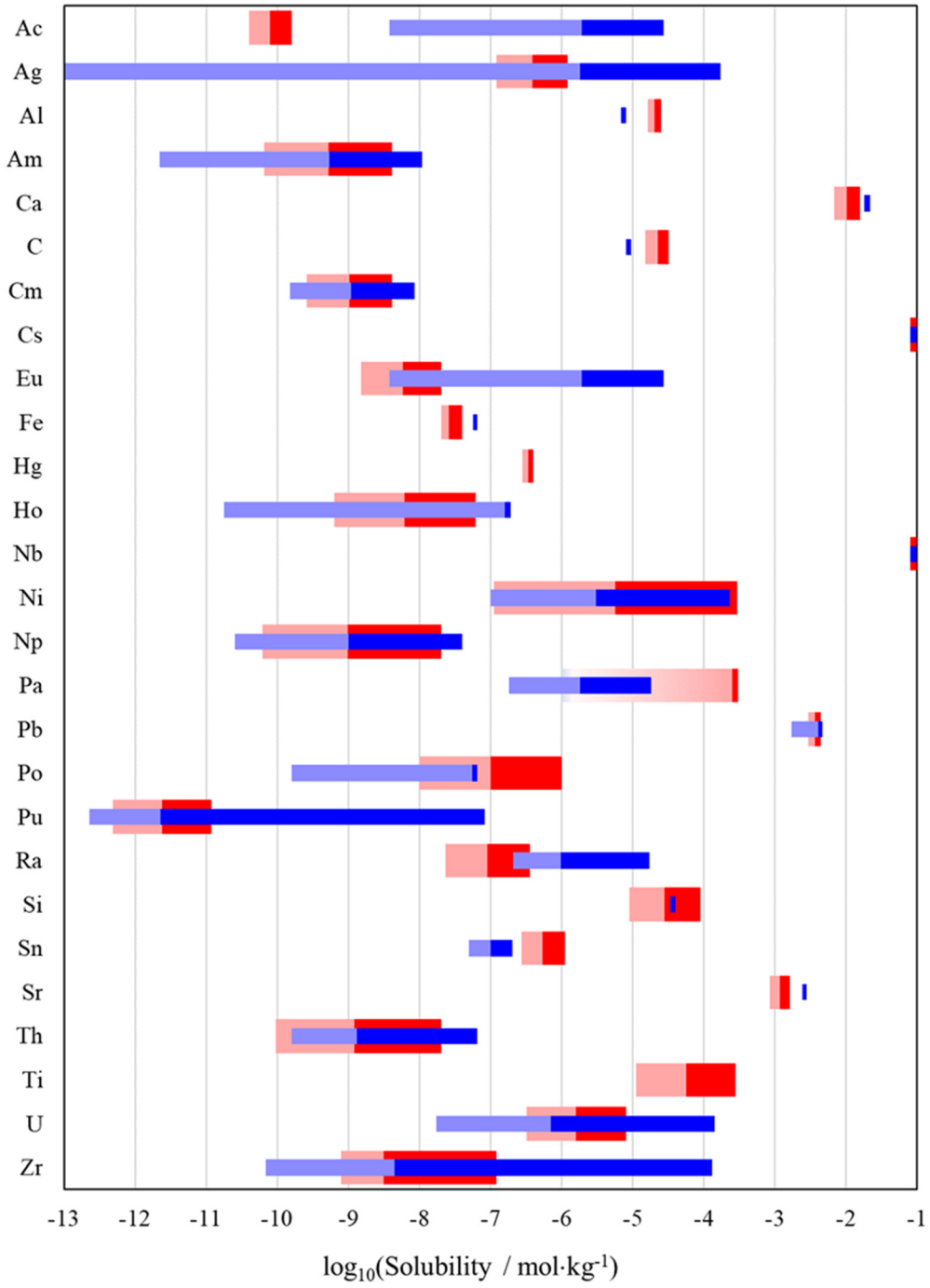

Fig. 5.3: Comparison of updated solubility limits with those reported by Berner (2014). The results of the present modelling study are shown as red bars and those of Berner (2014) as blue bars. The length of a bar represents the range between lower and upper limiting values. The "interface" between the light and dark colours indicates the recommended value. The red bars represent results for anoxic conditions, except for Pb and U results for suboxic conditions. "Unlimited" solubilities are arbitrarily shown as small bars at log_{10}(Solubility) = -1. See text for details.

The database used by Berner (2014) did not contain any thermodynamic data for Po. Hence, Berner (2014) used his results for Th(IV) as an estimate for Po(IV), declaring the upper limiting value for Th(IV) as the recommended value for Po(IV). This estimate by Berner (2014) is remarkably close to the new calculated value based on an extensive review of Po data in TDB 2020 (Fig. 5.3)

No progress has been made concerning Pa. Just an upper limit can be given for its solubility and the lack of data is symbolised in Fig. 5.3 by a fading bar towards lower values.

Last but not least, Berner (2014) did not consider Hg and Ti, so no comparison is possible for these elements.

5.3 Am improved CASH+ solid solution model

C-S-H gel-like phases are the most important binding phases in cement. They determine the most relevant properties and the durability of hydrated cement pastes and concretes. They are also responsible for the initial entrapment of radionuclides via sorption or solid solution formation mechanisms in the cementitious barriers of the radioactive waste repository. In addition to the low crystallinity, their composition can show significant variations.

The newly developed CASH+ solid solution model (Kulik et al. 2022; Miron et al. 2022b) can accurately calculate the solubility, water content, and elemental uptake in C-S-H. The model is calibrated against various experimental data on the uptake of cations, solubility, water content, and mean silicate chain length of C-S-H phases. These experiments are conducted at very low solid to liquid ratios as opposed to the high ratios found in hydrated cement mixtures. Therefore, an accurate and mechanistic thermodynamic model is essential for the transferability of data between the experimental and real conditions.

The alkali binding by the abundant C-S-H controls the distribution of alkali metals between solids and aqueous solution, and thus influences the pore solution composition in Portland and blended cements. In this study, the CASH+ model has been systematically tested against the pore solution data (Vollpracht et al. 2015) from hydrated Portland cement (PC) and cement blended with silica fume (PC + SF).

As a result, the G^{o}_{298} values of two CASH+ model endmembers, TCKh and TCNh (both relevant at high Ca/Si mole ratios), had to be adjusted with +7.0 and +5.0 kJ·mol^{-1}, respectively, yielding an improved agreement with the measured pore solution data (Miron et al. 2022a).

The fine-tuned model can be used to simulate cement hydration processes (Fig. 5.4), where it predicts cement pore solution compositions with an improved balance of alkali metals, in a good agreement with the measured data for systems at different water to binder ratios, silica fume additions, and temperatures up to 80 °C.

5.4 References

Berner U. (2014)
Solubility of Radionuclides in a Concrete Environment for Provisional Safety Analyses for SGT-E2. Nagra Technical Report NTB 14-07, 81 pp., Wettingen, Switzerland.

Hummel W., Kulik D.A., Miron G.D. (2022)
Solubility of radionuclides and influence of EDTA for use in the development of the cement sorption database (SDB 2022). Nagra Work Report NAB 22-38, 56 pp., Wettingen, Switzerland.

Hummel W., Thoenen T. (2022)
The PSI Chemical Thermodynamic Database 2020. Nagra Technical Report NTB 21-03, 1334 pp., Wettingen, Switzerland.

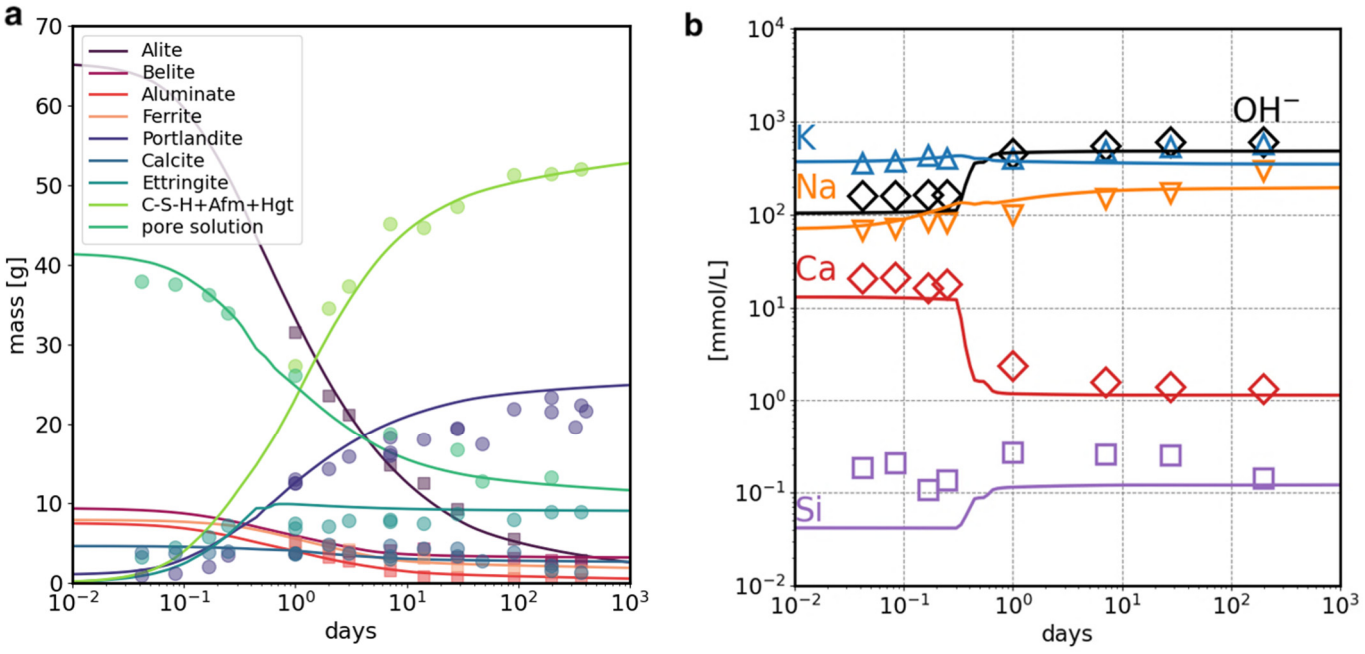

Fig. 5.4: Hydration of Portland cement modelled using the CASH+ model. Calculated (lines) and measured (symbols) (Lothenbach et al. 2008) (a) evolution of masses of phases and (b) pore solution composition. GEM-Selektor calculations using Cemdata18 (Lothenbach et al. 2019) and in-house PSI-Nagra thermodynamic databases. Modified from Miron et al. (2022a).

Kulik D.A., Miron G.D., Lothenbach B. (2022)
A structurally-consistent CASH+ sublattice solid solution model for fully hydrated C-S-H phases: Thermodynamic basis, methods, and Ca-Si-H_2O core sub-model. Cem. Concr. Res. 151, 106585.

Lothenbach B., Le Saout G., Gallucci E., Scrivener K. (2008)
Influence of limestone on the hydration of Portland cements. Cem. Concr. Res. 38, 848–860.

Lothenbach B., Kulik D.A., Matschei T., Balonis M., Baquerizo L., Dilnesa B.Z., Miron G.D., Myers R. (2019)
Cemdata18: A chemical thermodynamic database for hydrated Portland cements and alkali-activated materials. Cement and Concrete Research 115, 472-506.

Miron G.D., Kulik D.A., Lothenbach B. (2022a)
Porewater compositions of Portland cement with and without silica fume calculated using the fine-tuned CASH+NK solid solution model. Mater. Struct. 55, 212.

Miron G.D., Kulik D.A., Yan Y., Tits J., Lothenbach B. (2022b)
Extensions of CASH+ thermodynamic solid solution model for the uptake of alkali metals and alkaline earth metals in C-S-H. Cem. Concr. Res. 152, 106667.

Vollpracht A., Lothenbach B., Snellings R., Haufe J. (2015)
The pore solution of blended cements: a review. Mater. Struct. 49, 3341–3367.

6 FUNDAMENTAL ASPECTS OF MINERAL REACTIVITY AND STRUCTURAL TRANSFORMATIONS

Churakov S.V., Cametti G., Katheras A.S. (PhD student), Karalis K. (postdoc), Krattiger N. (MSc student), Bucher A. (BSc student)

6.1 Introduction

PSI/LES and the Institute for Geological Science at the University of Bern (UBERN/IfG) collaborate in the field of mineralogy, crystallography and environmental geochemistry. The research field of the Mineralogy group at the University of Bern covers fundamental aspects of mineral dissolution and precipitation mechanisms, chemical aspects of crystal structure stability and temperature driven phase transitions in minerals. The dedicated laboratories operated by the group are equipped with powder and single-crystal diffractometers for structural studies of minerals and an atomic force microscopy laboratory for *in situ* characterisation of mineral surfaces. The experimental studies are widely supported by modelling activities. In particular, we develop and apply numerical methods for investigations of reaction mechanisms and theoretical predictions of mineral thermodynamics. Main research activities are focused on the characterisation of mineral structure transformations in natural and synthetic zeolite materials as result of dehydration and cation exchange processes. These structural characterisation studies are conducted combining single crystal X-ray diffraction experiments, spectroscopic measurements, and molecular simulations. *Ab initio* molecular dynamics simulations are further used to elucidate the mechanism of mineral surface interactions at an atomic-scale. Dedicated laboratory nucleation and re-crystallisation experiments, surface characterisations and geochemical modelling are applied to develop sustainable strategies for heavy metal extraction from contaminated water via carbonates precipitation.

Combined investigations of structural transformation in zeolite with particular focus on extra framework cation are continued. A very peculiar behaviour of Pb-exchanges zeolites was observed in which volumetric expansion of the structure taking place concurrently with the dehydration process.

In the framework of an interactional project on retention of radionuclides by minerals, the surface stability and the speciation of magnetite is investigated. The obtained surface stability phase diagrams are the basis for further investigations of radionuclides absorption on magnetite surface.

In collaboration with Holcim foundation, the reactivity of ASR is investigated by *ab initio* molecular dynamics.

6.2 Anomalous thermal behaviour of Pb-exchanged zeolites

Zeolites with STI framework type are abundant medium-pore-size microporous material represented in nature by Ca- and Na- endmembers. The extra framework cations, Na and Ca, can be easily exchanged with other cations modifying the structural behaviour and stability of the framework. The structural investigations of a Pb-exchanged zeolite ($Pb_{13.4}(OH)_{10}Al_{17.4}Si_{54.6}O_{144}\times 38H_2O$) with **STI** framework type (see front cover), revealed a highly unusual volume increase of the crystallographic cell taking place under continuous heating and dehydration (Cametti et al. 2022). Understanding the fundamental mechanisms leading to such a peculiar behaviour is essential for technological applications and interpretation of chemical bonding in zeolites. The dehydration was tracked *in situ* from 25 to 450 °C by single crystal X-ray diffraction, infrared and X-ray absorption spectroscopy. Further interpretation of the experimental observations was supported by *ab initio* molecular dynamics simulations. Initially, Pb-STI unit-cell volume contracts (ΔV = -3.5%) from 25 to 100°C. This agrees with the trend observed in **STI** zeolites. Surprisingly, at 125°C, the framework expanded (ΔV = +2%), adopting a configuration, which resembles that of the room temperature structure (Fig. 6.1). Upon heating, the structure loses H_2O but no de-hydroxylation occurred. The key mechanism leading to the sudden volume increase was found to be the formation of $Pb_x(OH)_y$ clusters, which prevent the shrinking of the channels, rupture of the tetrahedral bonds and occlusion of the pores. This zeolite has therefore an increased thermal stability with respect to other **STI** metal-exchanged zeolites. These results suggest that the incorporation of Pb in form of $(PbOH)^+$ species into zeolites can increase the thermal stability and widen the range of temperatures for which the structural changes are reversible, with important consequences on its applications.

6.3 Phase transitions in Pb-phosphate minerals

Minerals of apatite group are the most abundant rock-forming phosphates and the main host of phosphorous in crustal rocks. The chemical formula of apatite group minerals can be generalised as $A_5(TO_4)_3X$, where A = large cations, T = metals or metalloids, and X = anions. The presence of Pb^{2+} in the A site is of interest for both catalytic and environmental applications. Among them,

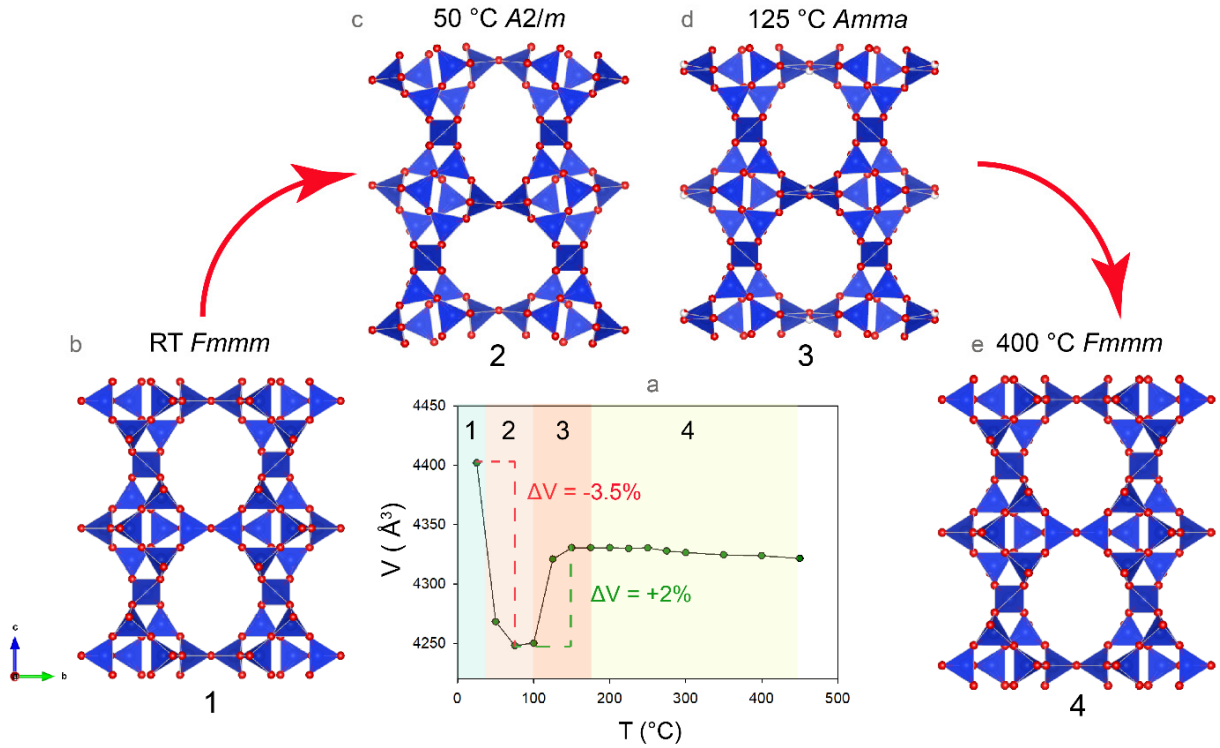

Fig. 6.1: ***(a)*** *Evolution of the unit-cell volume of Pb-STI as a function of temperature obtained by SC-XRD.* ***(b-e)*** *Corresponding structural changes in* ***STI*** *framework of Pb-stellerite observed in situ at different temperatures.*

Pb-apatites are used as metal scavengers in treatment of water and contaminated soils, and for the immobilization of radioactive iodine (Wang 2015; Cao et al. 2017). In this study, the crystal structure of mimetite $Pb_5(AsO_4)_3Cl$ has been investigated *in situ* at 123, 173, 273, 288, 353, and 393K by single-crystal X-ray diffraction. A careful inspection of the diffraction pattern and subsequent structure refinements indicated that mimetite transforms from the monoclinic to the hexagonal polymorph with increasing temperature. At 123 K a monoclinic superstructure, mimetite-2M, with cell parameters a = 20.4487(9), b = 7.4362(2), c = 20.4513(9) Å, β = 119.953(6)° ,V = 2694.5(2) Å^3, and space group $P2_1$ was observed. From 173 to 353 K, the reflections of the supercell were evident only along one direction of the corresponding hexagonal apatite-cell, and the structure transforms to the polymorph mimetite-M, with space group $P2_1/b$ and cell parameters a = 10.2378(3), b = 20.4573(7), c = 7.4457(2) Å, β = 120.039(5)°, V = 1349.96 (9) Å^3. Only at higher temperature, i.e. 393 K, mimetite adopts the hexagonal space group $P6_3/m$ characteristic of apatite structure-types. The role of the electron lone-pairs of Pb atoms in the phase transition was investigated through the analysis of the electron localization function (ELF) calculated based on the DFT-geometry optimized structures of the three polymorphs (Fig. 6.2). The changes in spatial distribution of the 6s^2 electron density during the phase transitions were explored by means of the Wannier Function Centres (WFCs), derived from *ab initio* molecular dynamics trajectories. In the high-temperature hexagonal structure, the 6s^2 electrons are spherically symmetric relative to the position of Pb atoms. At low temperature, the maximum of 6s^2 electron density is displaced relative to the position of Pb atom contributing to the polar interaction in the monoclinic polymorphs (Cametti et al. 2022).

6.4 Magnetite surfaces stability and speciation

Magnetite (Fe_3O_4) is mixed iron oxide, commonly found as the main corrosion product of steel waste casks in deep geological repositories. It can act as matrix for sorption or incorporation of dissolved radionuclide ions and, hence, contribute to the retention of these hazardous ions. The ability of magnetite surface to participate in geochemical reaction depend on the surface structure and speciation as function of temperature and redox conditions. There are investigated *ab inito* simulations.

Based on observation that natural magnetite crystals occurring in pre-dominantly octahedral shape, the (111) surface is investigated using CP2K (Kühne et al. 2020). Although six different layers with the resulting surface are possible being either oxygen or iron terminated (see Noh et al. 2015), bare iron at the surface seems unlikely in subsurface geological conditions. Consequently, only the oxygen-terminated surface configuration were analysed. Each of the four surfaces is referred to by the structure of outmost iron layer as octahedral - oct or tetrahedral – tet. The

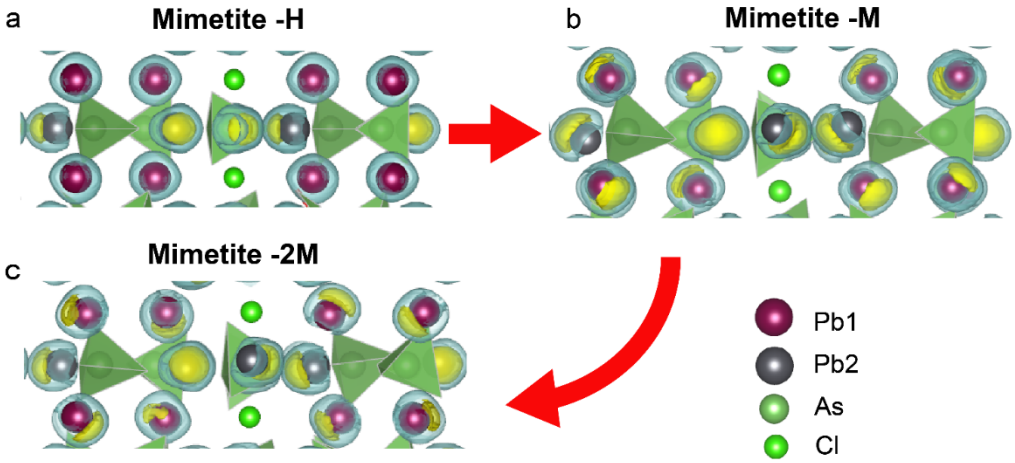

Fig. 6.2: Fragment of the DFT-optimized structures of mimetite-2M, -M, and –H (projection along the [110]$_{hex}$, c_{hex}-axis vertical). ELF isosurfaces are reported in yellow and light blue for ELF = 0.96 and ELF = 0.90, respectively. As tetrahedra are shown in light green, Cl atoms in green. Dark-grey and purple spheres represent Pb atoms residing at Pb2 and Pb1 crystallographic sites, respectively.

systems were prepared as slabs with two surfaces of the same kind separated by bulk-like structural domain.

Classical molecular dynamic (MD) simulations were applied to investigate the mobility of water and monovalent ions (Na^+ and Cl^-) near the surfaces with different terminations (Table 7.1). As the tet1-surface has rough structure (Fig. 6.3), the water molecules interact more strongly with the tet1-surface, resulting in a lower diffusion coefficient (Tab. 6.1). However, under the presence of 0.5 M NaCl, the diffusion coefficient is increased as the ions compensate for a part of the surface electrostatic forces increasing the water mobility.

To analyse the surface speciation under possible repository conditions, a surface stability diagrams were calculated. The most relevant parameter is the surface energy γ which depending also on the chemical potential μ of the system compounds; magnetite, oxygen and water (eq. 6.1), the surface area A and the number N of involved compounds. For the mobile species, μ can be expressed as function of water and oxygen fugacity (partial pressure) as shown in eq. 6.2. The energy of the possible surfaces terminations can, hence, be compared and the lowest is expected to be stable over a range of water and oxygen fugacity (Fig. 6.2). The oct1- and tet2-surfaces were found to be the most stable in water saturated conditions expected in the repository. These results are the basis for further investigation of the interaction of radionuclide ions with magnetite surfaces.

$$\gamma = \frac{1}{2A}\left(G_{slab} - N_{Fe_3O_4}\mu_{Fe_3O_4} - N_{O_2}\mu_{O_2} - N_{H_2O}\mu_{H_2O}\right) \quad (6.1)$$

$$\mu_{mobile} = E_{DFT} + E_{ZPE} + \Delta G_{0K\rightarrow T} + k_B T \ln\left(\frac{p}{p^0}\right) \quad (6.2)$$

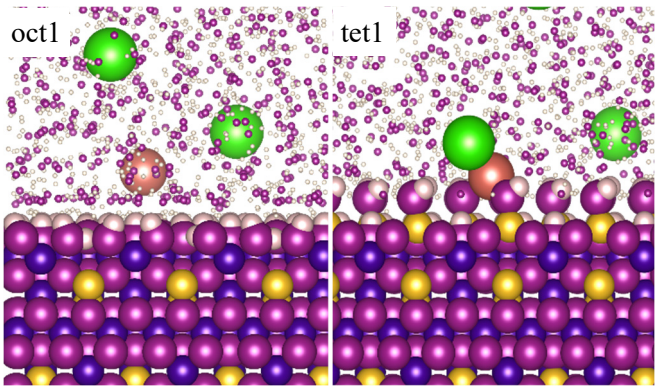

Fig. 6.3: Side view of an octahedrally (oct) and tetrahedrally (tet) terminated magnetite (111) surface with water and NaCl (orange and green spheres) in *MD simulation.*

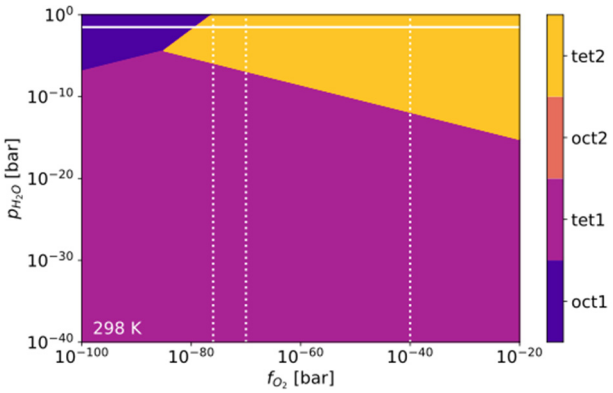

Fig. 6.4: Surface stability analysis of chosen magnetite (111) terminations over an expected range of water and oxygen fugacity. The dotted lines represent the mineral redox buffers of iron minerals under different oxygen fugacity, the solid line is the water saturation pressure at 298 K.

Tab. 6.1: Ratio of diffusion coefficients of water molecules measured above the oct1/tet1 surface and balk water diffusion coefficient (H_2O) obtained by classical MD simulations. Further, the ratios of systems including dissolved NaCl are listed. The surface layers correspond to the water structuring near the surface at 0-3, 3-6, and 6-9 Angstrom distance, respectively.

Surface layer	oct1 : H_2O	tet1 : H_2O	oct1 – NaCl : H_2O	tet1 – NaCl : H_2O
0-3 Å	0.34	0.15	0.49	0.21
3-6 Å	0.73	0.47	0.74	0.80
6-9 Å	0.77	0.69	0.87	0.93

6.5 Dissolution mechanism of ASR products

Alkali-silica reaction (ASR) widely occurs in concrete and it's known as "concrete cancer". ASR is one of the most important degradation mechanisms resulting in durability problems and premature loss in serviceability of massive concrete infrastructures (i.e. bridges, dams, etc.). Despite decades of analysis of ASR and its products, ASR chemistry remains poorly understood especially at the molecular scale. This study aims at the understanding of the ASR mechanism, which is critical and essential to predict and prevent the deleterious ASR expansion behaviour and develop effective mitigation measures.

The atomistic mechanism of shlykovite surface, having a similar structure with crystalline ASR, is investigated by applying large-scale *ab initio* molecular dynamics simulations using CP2K code. Since the dissolution of ions from mineral surfaces is a rare event with a high free energy barrier (larger than the thermal fluctuations) the Meta Dynamics (method was utilized. In this approach, the reaction progress is monitored by a set of collective variables (CVs) which accurately describe the change between reactants and products. From the analysis of the MetaD simulations, the dissolution mechanisms of K, Si and Ca were identified, as well as the activation energies for these rare events. The simulations predict that the release and incorporation of K ions in the structure has a very low activation energy whereas the dissolution mechanism of Si tetrahedral is comparable with the mechanism observed in the studies of clay minerals (Schliemann and Churakov (2021)).

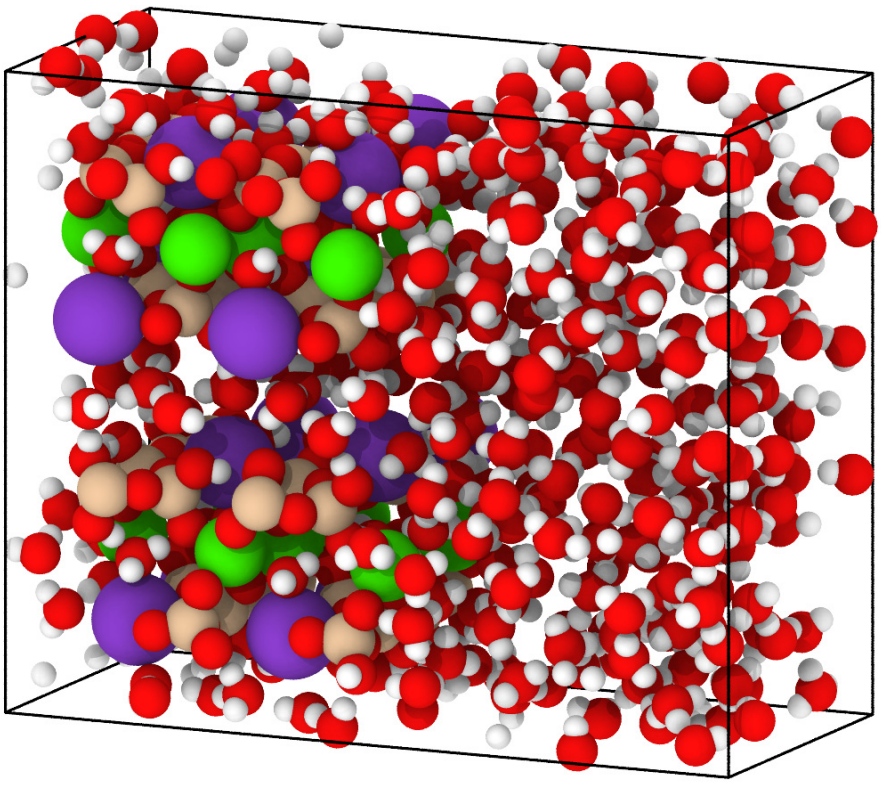

Fig. 6.5: Schematic view of the system setup for large scale simulations of ASR dissolution. Green, violet and beige spheres are Ca, K and Si atoms respectively. Oxygen and hydrogen is show with red and white colours.

6.6 References

Cao C., Chong S., Thirion L., Mauro J.C., McCloy J.S., Goel A. (2017)
Wet chemical synthesis of apatite-based waste forms-A novel room temperature method for the immobilization of radioactive iodine. Journal of Materials Chemistry A, 5, 14331.

Kühne T.D., Iannuzzi M., Ben M.D., Rybkin V.V., Seewald P., Stein F., Laino T., Khaliullin R.Z., Schütt O., Schiffmann F., Golze D., Wilhelm J., Chulkov S., Bani-Hashemian M.H., Weber V., Borštnik U., Taillefumier M., Jakobovits A.S., Lazzaro A., Pabst H., Müller T., Schade R., Guidon M., Andermatt S., Holmberg N., Schenter G.K., Hehn A., Bussy A., Belleflamme F., Tabacchi G., Glöß A., Lass M., Bethune I., Mundy C.J., Plessl C., Watkins M., VandeVondele J., Krack M., Hutter J. (2020)
CP2K: An Electronic Structure and Molecular Dynamics Software Package - Quickstep: Efficient and Accurate Electronic Structure Calculations. The Journal of Chemical Physics 152, 194103.

Noh J., Osman O.I., Aziz S.G., Winget P., Brédas J.-L. (2015)
Magnetite Fe3O4 (111) Surfaces: Impact of Defects on Structure, Stability, and Electronic Properties. Chemistry of Materials 27 (17), 5856–5867.

Schliemann R., Churakov S.V. (2021)
Atomic scale mechanism of clay minerals dissolution revealed by ab initio simulations. Geochimica Et Cosmochimica Acta 293, 438-460.

Thompson A.P., Aktulga H.M., Berger R., Bolintineanu D.S., Brown W.M., Crozier P.S., in 't Veld P.J., Kohlmeyer A., Moore S.G., Nguyen T.D., Shan R., Stevens M.J., Tranchida J., Trott C., Plimpton S.J. (2022)
LAMMPS - a flexible simulation tool for particle-based materials modeling at the atomic, meso, and continuum scales. Computer Physics Communications, 271, 108171.

Wang J. (2015)
Incorporation of iodine into apatite structure: a crystal chemistry approach using Artificial Neural Network. Frontiers in Earth Science 3, 1-11.

7 GEOCHEMICAL ASPECTS OF WASTE MATERIALS AND THEIR DISPOSAL

Churakov S.V., Eggenberger U., Weibel G., Wolffers M., Ingold P. (PhD student), Dörfler P. (MSc student)

7.1 Introduction

The Competence Center for Secondary Raw Materials (Fachstelle Sekundärrohstoffe (FSSR)) at the Institute of Geological Sciences conducts applied research in the field of environmental geochemistry and secondary raw materials. The core competencies of the FSSR include the topics of recycling management and disposal quality of conventional non-radioactive waste. The sustainable implementation of recycling technologies is waste type specific and requires detailed knowledge of material composition, long-term behaviour and process couplings controlling material degradation. To close material cycles and conserve primary raw material reserves, new approaches and processes are needed to use secondary raw materials on a larger scale and in new areas.

In Switzerland, an annual quantity of approximately 800'000t of bottom ash and 80'000t of fly ash arise from Municipal Solid Waste Incineration (MSWI fly ash), whereby these solid residues are deposited at landfills in Switzerland as they do not meet yet the quality criteria for recycling as a result of high metal contents. Under the latest Swiss Waste Ordinance (Swiss Confederation, 2016), the requirements for residues have been tightened and metal recovery must be implemented by 2026 for MSW fly ash, e.g. by acid leaching (e.g. FLUWA process (Bühler & Schlumberger 2010)). The recovery and recycling of these heavy metals represent a valuable contribution to the sustainable closure of material cycles, as the metals from primary raw material mining can be partially replaced. However, for metal recycling from municipal solid waste incineration residues, detailed knowledge of the formation and composition of the incineration residues (slag, fly ash) is essential to maximise the metal recovery. In addition to metal recovery, the behaviour of residues in landfills is a key component of our research. Furthermore, studies are also being carried out to assess the potential to reuse the residues in the materials cycle, for example for the ash from wood incineration. The ashes from wood energy utilization represent a promising waste stream for use in the cement industry. While the filter ashes from waste wood incineration are subject to a heavy metal recovery regulations from 11.2025 on, the grate and bed ashes are deposited in landfills consideration of recycling opportunities. Due to their geochemical properties, grate and bed ashes in particular, could be considered as a promising secondary raw material for active components in clinker production. The recycling of wood ash fractions in the cement industry combines the circular economy approach in two ways: the amount of necessary primary resources can be reduced and landfill space can be saved. The partial replacement of raw materials with secondary ones in clinker production also brings a major environmental thanks to reduction of CO_2 emissions.

7.2 MSWI bottom ash: Effects of heavy rain fall on pollutant mobilization in bottom ash landfill leachate

The residues after the incineration are treated for metal recovery and deposited at around 30 landfill sites of Type D (BAFU, 2016). These residues are deposited as a permeable system on the surface. Therefore, rainwater infiltrates into the landfill and interacts with the deposited bottom ash. Consequently, polluted leachate is generated, which is collected and discharged into the sewerage system. For discharge, the concentrations of several heavy metals must be below the regulatory limits (BAFU, 2021).

Previous studies of bottom ash leachate suggest that the composition of discharged waters from landfill sites are strongly affected by the volume and dynamics of precipitation events. During rain events, pH and concentrations of matrix elements (Na, Cl, K, Mg, Ca and SO_4) and various heavy metals (Mo, V, Mn and Zn) decrease due to dilution by preferential flow of rainwater into the drainage leachate. On the other hand, Al, Cu, Sb and Cr increase in concentration with increased discharge (Johnson et al. 1999). Thermodynamic calculations indicate that whilst mineral dissolution/precipitation reactions may control the concentrations of various components, sorption and complexation reactions may influence heavy metal concentrations as well.

In February 2022, 24 leachate samples were taken during a heavy rain event (Fig. 7.1). In addition, leachate was samples before the precipitation event in order to determine the initial leachate composition. During the event, electrical conductivity of the leachate decreased from 22.1 mS/cm to 12.7 mS/cm. while the discharge increased from 18.4 L/min to 53.7 L/min. Matrix element concentrations (Na, Ca, K, Cl, SO_4 and NO_3) showed a decrease during the event (Fig. 7.2), which is consistent with the observations of Johnson et al. (1999). The heavy metals however, showed variable concentration curves. While Cr, Cu, Mo and Sb showed

decreasing concentrations, increasing concentrations were found for Al and V (Fig. 7.3). In the case of Cu, Sb and V, opposite concentration trends were thus observed compared to Johnson et al. (1999). The pH value of the leachate showed an increase during the precipitation event.

It is assumed that observed chemical and hydraulic evolution of the landfill are mainly controlled by permeability and the reactivity of the materials in the system. The reduction of highly soluble elements such as Na, K, Cl and SO_4 during the precipitation events is explained by dilution effects. Preferential flow paths, which are activated during heavy precipitation event, lead to increased fluxes and thus shorter interaction times with the solid matrix. On the basis of the geochemical behaviour. The heavy metals can be divided into two different groups. Cr, Cu, Mo and Sb behave similar to the matrix elements (e.g. dilution), while Al and V show increasing concentrations during the precipitation event.

These observation can be explained by flushing micropores filled with saturated pore water solution in which the leachate has a long interaction time. In batch experiments, certain heavy metals reach very high concentration values, while others show no significant concentration differences compared to the initial leachate. In addition, the pH rises to strongly basic values in solutions with long interaction times, which explains the pH increase during the precipitation events.

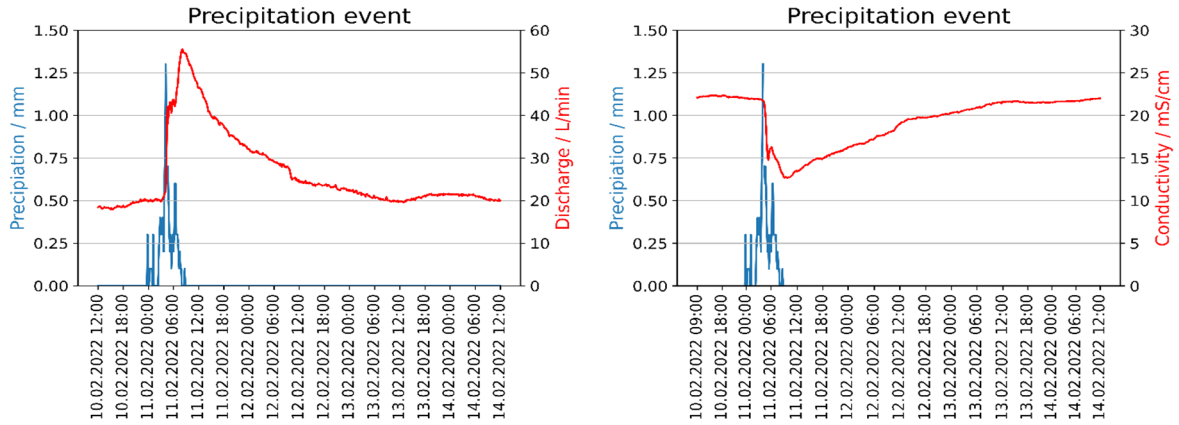

Fig. 7.1: Leachate discharge and electrical conductivity during the investigated precipitation event.

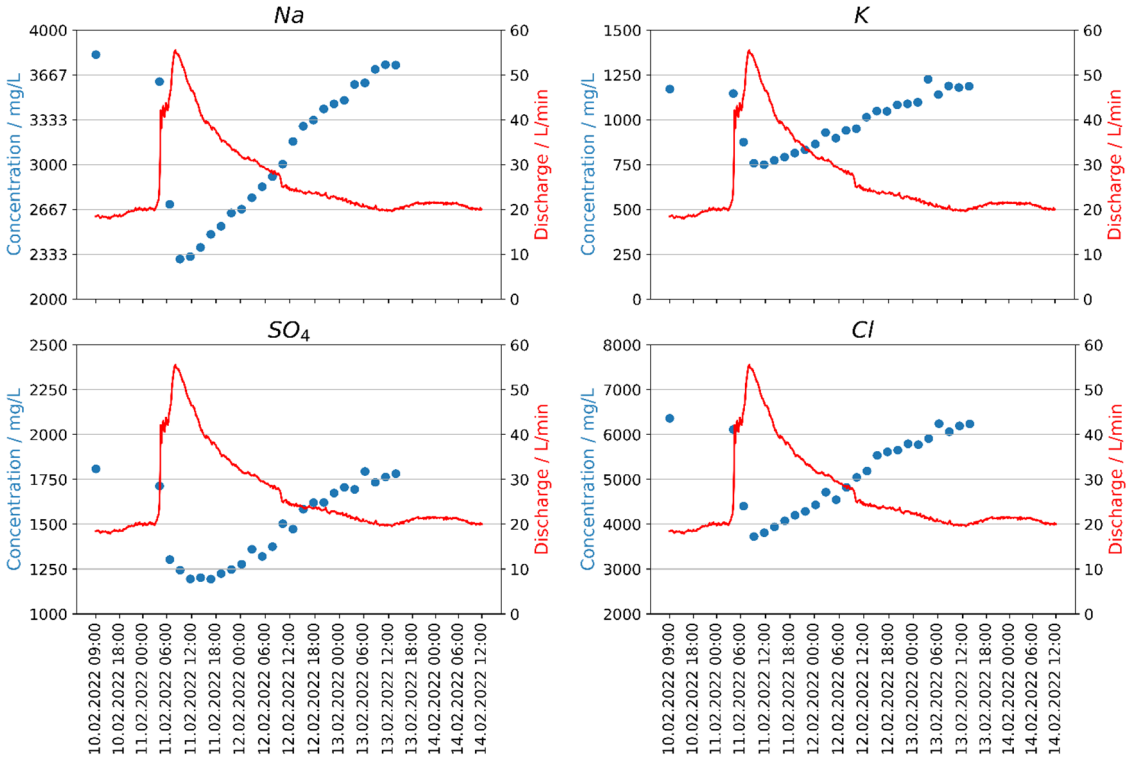

Fig. 7.2: Evolution of matrix elements concentration in the leachate during precipitation event.

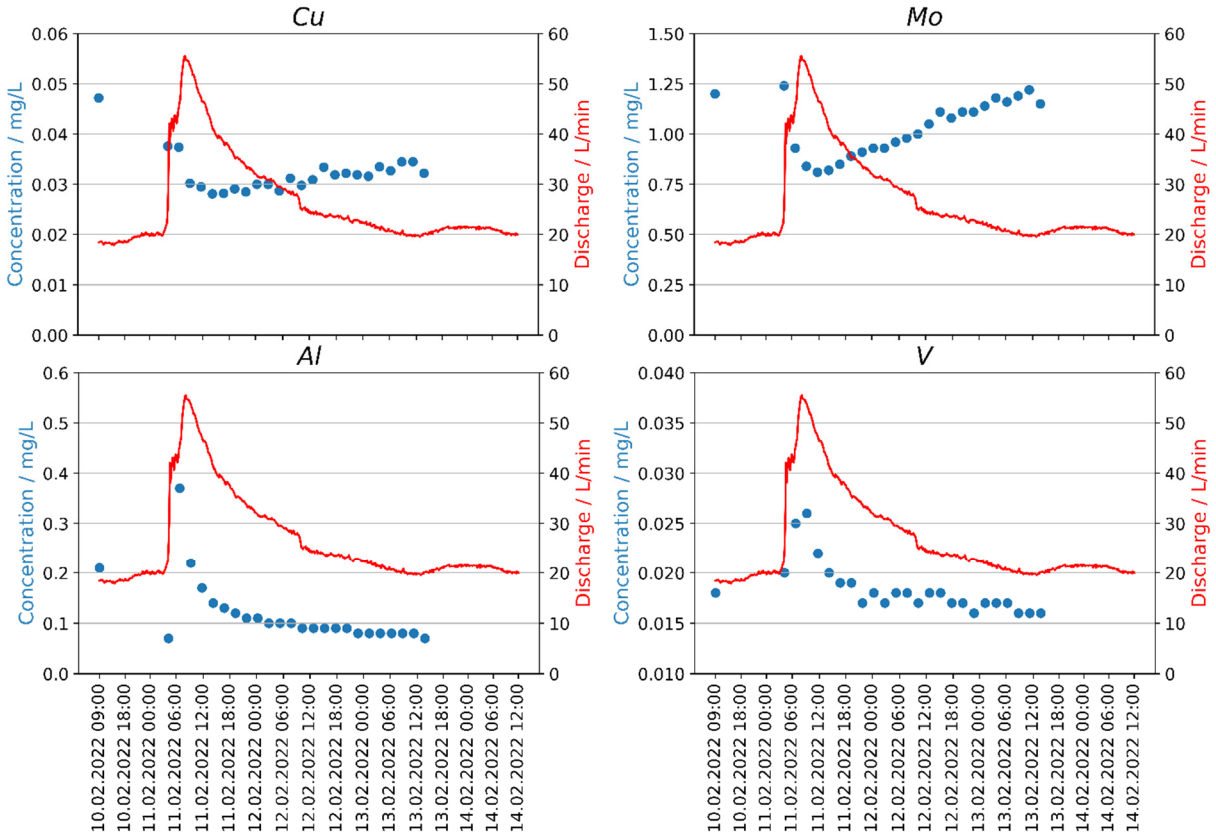

Fig. 7.3: Evolution of heavy metals concentration in discharged water during the precipitation event.

7.3 MSW fly ash: New Insights into ash-forming processes with thermodynamic modelling

Fly ash from municipal waste incineration contains significant amounts of heavy metals and is therefore deposited on landfills. MSWI fly ash consists of boiler and electrostatic precipitator ash and shows elevated concentrations of heavy metals (e.g. Zn, Cu, Cd, Pb). In the context of optimizing the heavy metal recovery during the acid leaching of MSWI fly ash, detailed knowledge about the geochemical properties and especially about the binding forms of the heavy metals is of great importance. In an earlier study (Wolffers et al. 2021), a detailed chemical and mineralogical characterisation of different MSWI ashes has already been performed. The study clearly shows that the detailed characterisation of the very fine-grained ashes and in particular, the heavy metal binding forms with low concentrations (Cu, Pb, Cd) are out of reach for conventional methods (XRD, SEM). Thus, more advanced high resolution characterisation techniques and modelling approaches are necessary to gain the knowledge about such binding forms. In this study, thermodynamic modelling is therefore used as a complementary approach to obtain information on the existing and thermodynamically stable heavy metal binding forms along the flue gas cooling path.

The thermodynamic calculations were performed with the Gibbs energy minimization (GEM) method using the GEM selector code package (Kulik et al. 2013, Wagner et al. 2012), (https://gems.web.psi.ch). In the equilibrium calculation in GEMS, the elemental composition of the system is distributed among the phases and their components such that the total Gibbs energy of the system is minimized at the given temperature and pressure. The IVTANTERMO thermodynamic database (Gurvich et al. 1982) was imported into the GEMS database and supplemented with molar volumes for the solid phases.

The flue gas composition could be estimated on the basis of annual mass balances and chemical analyses of the material flows arising from the flue gas stream (fly ash, quenching water, gas emissions downstream of the electrostatic precipitator). Four scenarios were defined with different O_2, HCl and SO_2 contents in the flue gas matrix (Tab. 7.1). In the input flue gas composition, the chemical composition of the fly ash was also included, consisting of O (282 g/kg), Ca (152 g/kg), Si (97 g/kg), Cl (96 g/kg), S (87 g/kg), Na (75 g/kg), K (58 g/kg), Zn (47 g/kg), Al (30 g/kg), Fe (17 g/kg), C (11 g/kg), F (8 g/kg), Pb (8 g/kg), Mg (4 g/kg), Cu (3.3 g/kg), Cd (0.3 g/kg).

In scenario A (reference scenario), the matrix phases $CaSO_4$ and the amorphous glass phase are predicted to be thermodynamically stable for the entire temperature range. In the higher temperature range > 750 °C,

Tab. 7.1: Composition of the flue gas matrix for the different scenarios

wt.%	Scenario A Reference Scenario	Scenario B High HCl	Scenario C High SO_2	Scenario D Low O_2
CO_2	11	11	11	11
H_2O	15	15	15	15
HCl	0.15	0.3	0.15	0.15
N_2	66	66	66	70
O_2	7.5	7.5	7.5	3.5

wollastonite, perovskite, sphene, ZnO and Ca-phosphate are predicted to be the dominant thermodynamically stable phases. At 750 °C, NaCl and KCl begin to form, followed by K_2SO_4, Zn_2SiO_4 at 675 °C, and cristobalite (SiO_2) at 625 °C. At 600 °C and above, quartz becomes the predominant SiO_2 phase. At 275 °C, Zn is preferentially incorporated into $ZnCl_2$. The matrix phases of scenario B and D are comparable to those of scenario A. However, in scenario B, cristobalite and SiO_2 exhibit higher stability than the Zn silicate Zn_2SiO_4 compared to scenario A. In scenario C, the matrix phases are instead dominated by sulfates, and K_2SO_4 and Na_2SO_4 are predicted to be dominant alkali phases. The amorphous glass, $CaSO_4$, K_2SO_4, and cristobalite form as early as 850 °C, followed by $ZnSO_4$ at 700 °C and Na_2SO_4 at 575 °C. Above 450 °C, the amorphous glass becomes less stable, and K-Al sulfate begins to form instead. For the phases containing heavy metals, predicted stability fields as a function of temperature are shown in Fig. 7.4. In the reference scenario, Zn is predicted to exist as ZnO at high temperatures up to 700°C. Thereafter, Zn_2SiO_4 becomes the most stable Zn phase, with small amounts of Fe_2ZnO_4 forming. At 275 °C, Zn is expected to exist as $ZnCl_2$. The predominant form of Cu is monoxide (CuO) in the higher temperature ranges, changing to $CuCl_2$ at temperatures < 250 °C. Lead and cadmium occur only as chlorides and precipitate below 425 °C. Other heavy metal phases are Cr_2O_3, Fe_2O_3, MnO_2, SnO_2, Fe_2NiO_4, and $NiSO_4$ to a lesser extent. Barium is mainly bound as $BaSO_4$ and titanium as TiO_2, $NiTiO_3$, $CaTiSiO_5$. The heavy metal binding forms of scenario D are identical to scenario A. In scenario B, it can be observed that the heavy metal-bearing silicates and oxides (e.g. Zn_2SiO_4, CuO) start to form at lower temperatures compared to the reference scenario, while

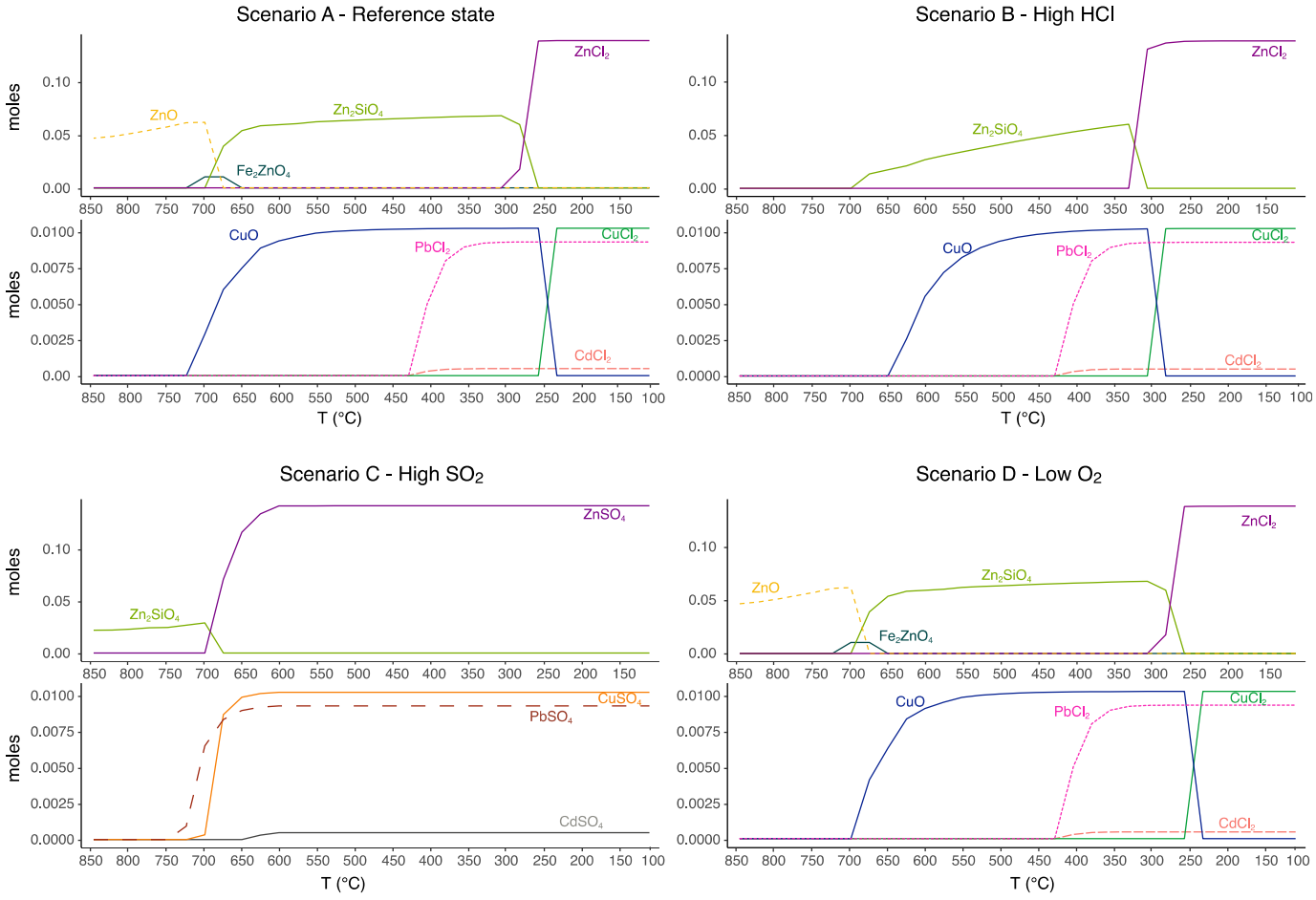

Fig. 7.4: Thermodynamically stable heavy metal binding phases for the different scenarios.

a shift towards earlier precipitation is observed for $ZnCl_2$. In scenario C with the high sulfur load, Zn, Pb, Cu, Cd are fixed predominantly as sulfates and at higher temperatures (600 - 750 °C).

The phase assemblage predicted for the reference scenario agree well with the phases observed in our previous study (Wolffers et al. 2021). Phases observed in the ash but not predicted to be thermodynamically stable under the given conditions include lime, calcite, (Ca) feldspars, and gehlenite. These phases are largely refractory minerals, so they are either travel in the flue gas as thermodynamically metastable compounds and accumulate in the ash without coming to equilibrium, or their formation is triggered by locally different chemical conditions, which is assumed for gehlenite formation (Traber et al. 2002). For the heavy metals, it is found that there are shifts at about 250 °C with respect to stable binding forms. The predicted transformation of CuO to $CuCl_2$ at decreasing temperatures is in agreement with the calculations of Verhulst et al. (1996). The calculated zinc phases of the boiler ashes (temperature range about 850 °C - 250 °C) were observed by scanning electron microscope in our previous study (Fig. 7.5). In the electrostatic precipitator ash, zinc was found mainly as K_2ZnCl_4. Thermodynamic calculations predict $ZnCl_2$ as the most stable zinc chloride, which is probably related to the quality of the existing thermodynamic data for K_2ZnCl_4. Variations in the S/Cl ratio of the flue gas were found to have greater effects on the equilibrium phase arrangements than variations in the O_2 content. Therefore, although the O_2 concentration of 3.5 vol% is low for flue gas conditions, there are no differences in the phase arrangements in scenario D compared to the reference scenario. The strong competition between S and Cl for the alkali metals Na and K has been also observed in previous studies (e.g. Jiao et al. 2011).

The thermodynamic calculations performed provide valuable insights into the ash formation processes during flue gas cooling, which can be summarized as follows: (i) Fluctuations in the S/Cl ratio of the flue gas have a stronger effect on the equilibrium phases than the fluctuations in the O_2 content. (ii) At a molar ratio of S/Cl < 1, Zn is predicted to be stable at high temperatures as ZnO, Fe_2ZnO_4, Zn_2SiO_4, and Cu as CuO. For Zn and Cu, a substantial change in heavy metal binding forms is predicted between 200 and 300 °C (depending on HCl concentration), leading to the formation of $ZnCl_2$ and $CuCl_2$. Cd and Pb are predicted to be stable as chlorides above 425 °C. (iii) The sulfates are the dominant solids at a S/Cl > 1 molar ratio in the flue gas. Under these conditions, the heavy metals begin to precipitate as sulfates at 600 - 750 °C and remain in the gas phase to a lesser extent. The shift of the heavy metals to sulfates with S/Cl > 1 is particularly relevant for heavy metal recovery, since the heavy metals tend to be less soluble as sulfates than chlorides.

7.4 Alternative Bed Materials for Fluidised Bed Incinerators Increase the Upcycling Potential for Biomass Bottom Ash as Cement Additive

As a leading expert in material characterisation, the FSSR contributes to an interdisciplinary project aiming at the research and development in the field of fluidised bed technology. In this project, twelve industrial residues were evaluated for their application as bed materials to replace the currently used quartz sand. Another requirement to the new bed material was that it contributes to an optimised quality of the resulting bottom ash to make it reusable in the cement production. This project touches on many aspects of sustainable development. A replacement of the primary quartz sand by a secondary industrial residue would not only limit expensive and unsustainable use of a primary resource. By finding a reuse application for the resulting bottom ashes, also valuable landfill site would be saved. To find innovative solutions, the project was conducted in collaboration with the plant designer (Bertsch-energy) and the cement industry (Holcim).

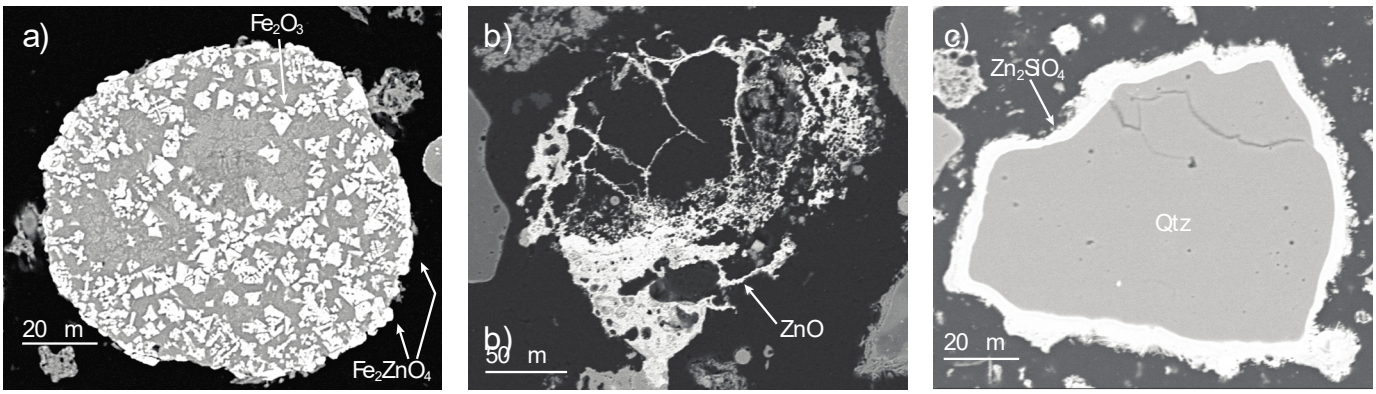

Fig. 7.5: Observed zinc phases in boiler ash by scanning electron microscope (backscattered electrons), from Wolffers et. al. 2021.

To gain a better understanding on the processes acting on the bed material, the first step was a thorough analysis of the reaction products between quartz sand and wood ash. During the incineration, an alkali-rich rim forms around the quartz. This reaction product increases the risk of slagging in the bed and therefore, the bottom ash is renewed at a constant rate. The resulting ashes are currently deposited on landfill sites. The formation of the reaction products was studied on the samples from three wood energy plants, all with different quartz sand renewal rates (Fig. 7.6). Rim formation around the original quartz sand (stage A) starts with in-diffusion of alkali elements, which form an initial rim 1. This alkali-silicate reaction product has a low melting point and ash particles accumulate on this sticky surface. This process leads to the formation of rim 2 (stage B). Advanced diffusion, often along fractures, leads to extension of rim 1, which now often contains holes (stage C). The final reaction product observed were large, idiomorphic crystals that form as inclusions in rim 1.

While previous studies only investigated the formation and chemistry of rim 1and rim 2, the formation of crystals has rarely been mentioned in existing literature. Considering that the ash chemistry can be described by the system SiO_2-CaO-K_2O, further investigations about the crystals formed may contribute to understand existing phases in this system. After the first phase diagram was published by Morey et al. in 1930, this only recently has again caught the attention of a group of researchers (Liu et al. 2021).

In a second step, the potential alternative bed materials were identified and tested. During the high-T treatment in the fluidised bed incinerator cement-reactive components in the bed material could potentially be activated. XRD heating-stage experiments were thus included in the test matrix designed to evaluate potential alternatives. Based on expected mineral transformations, bed material candidates were pre-selected for advanced experiments.

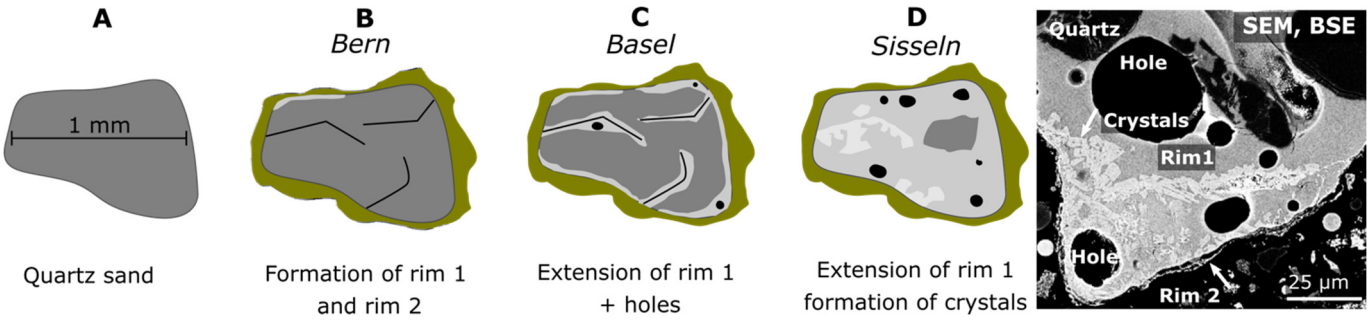

Fig. 7.6: Schematic sketch of the evolution of reaction products between quartz sand and wood ash. SEM-picture of the crystals forming in stage D on the right side.

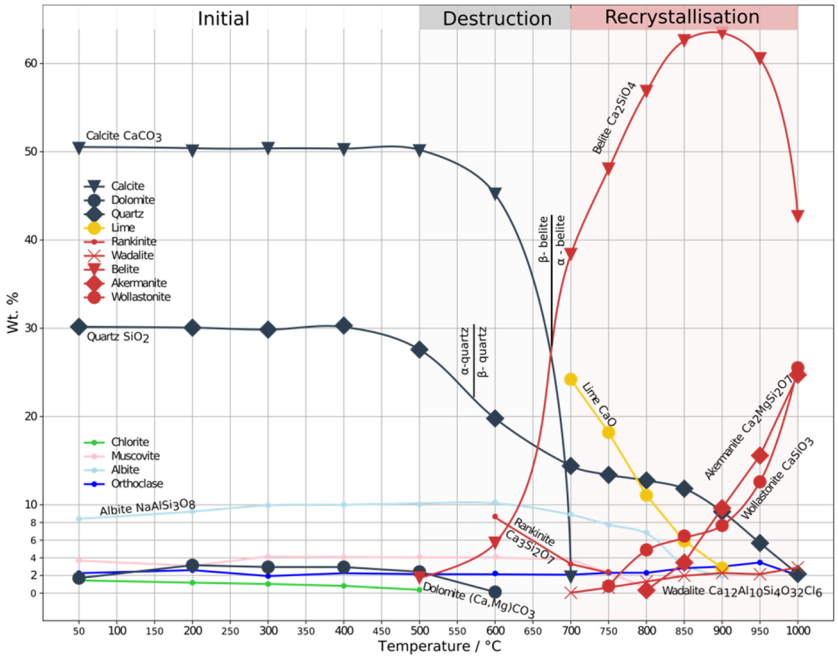

Fig. 7.7: Heating stage experiments with CDW-ff white: Semiquantitative evolution of the mineral paragenesis.

As an example, XRD heating-stage experiments of the construction and demolition waste fine-fraction (CDW-ff) showed that in the temperature range expected in the fluidised bed incinerator (700-800°C), calcite decarbonation to form lime takes place (Fig. 7.7). Also, belite formation was observed. Heating-stage experiments could thus be used to predict the quality of the bottom ash resulting from the use of an alternative bed material.

In cooperation with Bertsch-energy and the TU Vienna (BEST group), advanced experiments were conducted to investigate engineering parameters of the replacement materials. Using a bench-scale fluidised bed reactor designed for scientific purposes, it was possible to monitor the stability of the incineration process with a new bed material. During these experiments, ashes were generated. The quality of these ashes regarding the use as a cement additive was tested at the Holcim laboratories. The results were promising for two materials which allows for continuation of the project in terms of industry experiments within the next months. After careful evaluation of all tests and bench-scale experiments, a test run of one replacement material for quartz sand in an industrial incinerator is planned for summer 2023.

7.5 References

Bundesamt für Umwelt, BAFU (2016)
Verordnung über die Vermeidung und Entsorgung von Abfällen (VVEA).

Bundesamt für Umwelt, BAFU (2020)
Gewässerschutzverordnung (GSchV)

Bühler A., Schlumberger S. (2010)
Schwermetalle aus der Flugasche zurückgewinnen ‘Saure Flugaschenwäsche - FLUWA-Verfahren’ ein zukunftsweisendes Verfahren in der Abfallverbrennung.

Gurvich L.V., Veits I.V., Medvedev V.A. et. al. (1982)
Termodinamicheskie svoistva individual’nykh veshchestv. Thermodynamic Properties of Individual Compounds, Nauka, Moscow.

Liu H., Hildebrandt E., Krammer H., Kahlenberg V., Krüger H., Schottenberger H. (2021)
$K_4CaSi_6O_{15}$ —solving a 90-year-old riddle. Journal of the American Ceramic Society 104(12), 6678– 6695.

Kulik D.A., Wagner T., Dmytrieva S.V., Kosakowski G., Hingerl F.F., Chudnenko K.V., Berner U.R. (2013)
GEM-Selektor geochemical modeling package: revised algorithm and GEMS3K numerical kernel for coupled simulation codes. Comput. Geosci. 17, 1–24.

Morey G., Kracek F., Bowen N. (1930)
The ternary system K_2O-CaO-SiO_2. J. Soc. Glass. Technol. 14, 149–187.

Jiao F., Cheng Y., Zhang L., Yamada N., Sato A., Ninomiya Y. (2011)
Effects of HCl, SO2 and H2O in flue gas on the condensation behavior of Pb and Cd vapors in the cooling section of municipal solid waste incineration. Proc. Combust. Inst. 33, 2787–2793.

Johnson A., Kaeppeli M., Brandenberger S., Ulrich A., Baumann W. (1999)
Hydrological and geochemical factors affecting leachate composition in municipal solid waste incinerator bottom ash: Part II. The geochemistry of leachate from Landfill Lostorf, Switzerland, Journal of Contaminant Hydrology, 40, Issue 3, 239-259.

Verhulst D., Buekens A., Spencer P.J., Eriksson G., (1996)
Thermodynamic behavior of metal chlorides and sulfates under the conditions of incineration furnaces. Environ. Sci. Technol. 30, 50–56.

Wagner T., Kulik D.A., Hingerl F.F., Dmytrieva S.V., (2012)
GEM-Selektor geochemical modeling package: TSolMod library and data interface for multicomponent phase models. Can. Mineral. 50(5), 1173–1195.

Wolffers M., Eggenberger U., Schlumberger S., Churakov S.V. (2021)
Characterization of MSWI fly ashes along the flue gas cooling path and implications on heavy metal recovery through acid leaching. Waste Management 134, 231–240.

8 PUBLICATIONS

8.1 Peer reviewed research articles

Asaad A.[1], Hubert F.[1], Dazas B.[1], Razafitianamaharavo A.[2], Brunet J.[1], Glaus M.A., Savoye S.[3], Ferrage E.[1], Tertre E.[1] (2022)
A baseline study of mineralogical and morphological properties of different size fractions of illite du Puy. Applied Clay Science, 224, 106517.
[1] IC2MP, Equipe HydrASA, UMR 7285 CNRS/Université de Poitiers, 86073 Poitiers, France
[2] LIEC, UMR 7360 CNRS/Universit́e de Lorraine, BP 40, 54501 Vandoeuvre-ĺes-Nancy, France
[3] Université Paris-Saclay, CEA, DES-ISAS-Service d'Etude du Comportement des Radionucléides, F-91191 Gif-sur-Yvette, France

Cametti G., Nagashima M., Churakov S.V. (2022)
Role of the lone-pair electron localization in temperature-induced phase transitions in mimetite. Acta Crystallographica B, 78, 618-626.

Cametti G., Roos D., Prieur D., Scheinost A.C., Churakov S.V. (2022)
$Pb_x(OH)_y$ cluster formation and anomalous thermal behaviour in STI framework-type zeolites. Scientific Reports, 12, 15934.

Claret F.[1], Dauzeres A.[2], Jacques D.[3], Sellin P.[4], Cochepin B.[5], De Windt L.[6], Garibay-Rodriguez J.[7], Govaerts J.[3], Leupin O.[8], Mon Lopez A.[9], Montenegro L.[9], Montoya V.[3,7], Prasianakis N.I., Samper J.[9], Talandier J.[5] (2022)
Modelling of the long-term evolution and performance of engineered barrier system, EPJ Nuclear Sci. Technol. 8, 41.
[1] BRGM, 3 Avenue Claude Guillemin, 45060 Orleans, France
[2] IRSN, PRP-DGE/SRTG/LETIS, BP 17, 92262 Fontenay-aux-Roses Cedex, France
[3] SCK CEN, Belgian Nuclear Research Centre, Institute for Environment, Health and Safety, Mol 2400, Belgium
[4] SKB, Stockholm, Sweden
[5] Andra, 1/7, Rue Jean Monnet, Parc de la Croix-Blanche, 92298 Chatenay-Malabry Cedex, France
[6] MINES ParisTech, PSL University, 75272 Paris, France
[7] UFZ, Helmholtz Centre for Environmental Research–UFZ, Leipzig, Germany
[8] NAGRA, Nagra Hardstrasse 73, Postfach 280, 5430 Wettingen, Switzerland
[9] UDC, Centro de Investigaciones Cientıficas Avanzadas (CICA), ETS Ingenieros de Caminos, Canales y Puertos, Universidade da Coruna, A Coruna, Spain

Fleury M.[1], Gimmi T., Mazurek M.[2] (2022)
Porewater content, pore structure and water mobility in clays and shales from NMR methods. Clays Clay Miner. 70, 417–437.
[1] IFP Energies Nouvelles, Rueil-Malmaison, France
[2] RWI, Institute of Geological Sciences, University of Bern, 3012 Bern, Switzerland

He X.L.[1,2], Peng H.N., Zhang J.M.[2], Yuan H.[1] (2022)
Multiple Vapor Cavitation Bubble Interactions with A Thermal Lattice Boltzmann Method. Ocean Engineering, 266, 113058.
[1] Chongqing Southwest Research Institute for Water Transport Engineering, Chongqing Jiaotong University, Chongqing, China.
[2] State Key Laboratory of Hydraulics and Mountain River Engineering, Sichuan University, Chengdu, China.

Hidefumi I.[1], Nakarai K.[2], Kulik D.A. (2022)
Twenty-two-year investigation of strength development and surface deterioration of cement-treated clay in an in-situ field test. Cement and Concrete Composites, 134, 104783.
[1] Research and Development Laboratory, Japan Cement Association, 4-17-33, Toshima, Kita-ku, Tokyo, 114-0003, Japan
[2] Civil and Environmental Engineering Program, Graduate School of Advanced Science and Engineering, Hiroshima University, 1-4-1, Kagamiyama, Higashi-Hiroshima, 739-8527, Japan

Jäger T.[1], Mokos A., Prasianakis N.I., Leyer S.[1] (2022)
Pore-Level Multiphase Simulations of Realistic Distillation Membranes for Water Desalination. Membranes, 12(11), 1112.
[1] Department of Engineering, Faculty of Science, Technology and Medicine, University of Luxembourg, L-1359 Luxembourg, Luxembourg

Khatoonabadi M., Prasianakis N.I., Mantzaras J., (2022)
Lattice Boltzmann modeling and simulation of velocity and concentration slip effects on the catalytic reaction rate of strongly nonequimolar reactions in microflows. Physical Review E, 106(6), 065305.

Kulik D.A., Miron G.D., Lothenbach B.[1] (2022)
A structurally-consistent CASH+ sublattice solid solution model for fully hydrated C-S-H phases: Thermodynamic basis, methods, and Ca-Si-H2O core sub-model. Cem. Concr. Res. 151, 106585.
[1] Laboratory Concrete & Asphalt, Empa, Dubendorf, Switzerland

Liu X.[1], Tournassat C.[2], Grangeon S.[3], Kalinichev A.G.[4], Takahashi Y.[5], Marques Fernandes M. (2022)
Molecular-level understanding of metal ion retention in clay-rich materials. Nature Reviews Earth & Environment. 3, 461–476.
[1] State Key Laboratory for Mineral Deposits Research, School of Earth Sciences and Engineering, Nanjing University, Nanjing, China
[2] Institut des Sciences de la Terre d'Orléans, Université d'Orléans−CNRS−BRGM, Orléans, France
[3] BRGM, Orléans, France
[4] Laboratoire SUBATECH, Institut Mines-Télécom Atlantique, Nantes, France
[5] Department of Earth and Planetary Science, The University of Tokyo, Tokyo, Japan

Mahrous M., Curti E., Churakov S.V., Prasianakis N.I. (2022)
Pore-Scale Characterization, Spatial Autocorrelations, and Representative Elementary Volume Analysis of Indiana Limestones for Petrophysical Initialization of Core-Scale Reactive Transport Simulations, Journal of Petroleum Science and Engineering, 213, 110389.

Miron G.D., Kulik D.A., Lothenbach B.[1] (2022)
Porewater compositions of Portland cement with and without silica fume calculated using the fine-tuned CASH+NK solid solution model. Mater. Struct. 558(55), 1–13.
[1] Laboratory Concrete & Asphalt, Empa, Dubendorf, Switzerland

Miron G.D., Kulik D.A., Yan Y., Tits J., Lothenbach B.[1] (2022)
Extensions of CASH+ thermodynamic solid solution model for the uptake of alkali metals and alkaline earth metals in C-S-H. Cem. Concr. Res. 152, 106667.
[1] Laboratory Concrete & Asphalt, Empa, Dubendorf, Switzerland

Mokos A., Violeau D.[1], Sarret F.[2], De Leffe M.[2], Bercovitz Y.[3] (2022)
SPH modelling of the water nappe gravity fall over a dam. Journal of Hydraulic Research 60(4), 606-618.
[1] Electricité de France R&D, Chatou, France & Laboratoire d'Hydraulique Saint-Venant, École Nationale des Ponts et Chaussées, Paris, France
[2] Nextflow Software, Nantes, France
[3] Electricité de France R&D, Chatou, France

Owusu J.P., Karalis K., Prasianakis N.I., Churakov S.V. (2022)
Mobility of dissolved gases in smectites under saturated conditions: Effects of pore size, gas types, temperature, and surface interaction. The Journal of Physical Chemistry C, 126 (40), 17441-17455.

Tian Z.[1,2], Chee T.S.[3], Meng R.[1,2], Hao Y.[1,2], Zhou X.[4], Ma B., Zhu L.[5], Duan T.[5], Xiao C.[1,2] (2022)
Incipient Wetness Impregnation to Prepare Bismuth-Modified All-silica Beta Zeolite for Efficient Radioactive Iodine Capture. Environmental Functional Materials, 1(1), 92-104.
[1] College of Chemical and Biological Engineering, Zhejiang University, Hangzhou, China
[2] Institute of Zhejiang University-Quzhou, Quzhou, China
[3] Department of Nuclear and Quantum Engineering, Korea Advanced Institute of Science and Technology, Daejeon, South Korea
[4] Institut Franco-Chinois de L'Energie Nucléaire, Sun Yat-sen University, Guangzhou, China
[5] School of National Defence Science & Technology, Southwest University of Science and Technology, Mianyang, China

Voegelin A.[1], Wick S.[1], Pfenninger N.[1], Mangold S.[2], Baeyens B., Marques Fernandes M. (2022)
Thallium adsorption onto phyllosilicate minerals. Environmental Science: Processes & Impacts. 24, 1343–1359. |
[1] Eawag, Swiss Federal Institute of Aquatic Science and Technology, Dübendorf, Switzerland
[2] Karlsruhe Institute of Technology, Hermann-von-Helmholtz Platz 1, D-76344 Eggenstein-Leopoldshafen, Germany

Wang K.[1,2], Martinez A.F.[1], Simonelli L.[3], Madé B.[4], Hénocq P.[4], Ma B., Charlet L.[1] (2022)
Redox Interaction between Selenite and Mackinawite in Cement Pore Water. Environmental Science & Technology, 56(9), 5602-5610.
[1] University of Grenoble Alpes and CNRS, ISTerre, Grenoble, France
[2] Engineering Technology Centre of Decommissioning and Remediation, China Institute of Atomic Energy, Beijing, China
[3] BL22 − CLAESS, ALBA Synchrotron Light Source, Barcelona, Spain
[4] ANDRA, Chatenay-Malabry Cedex, France

Wang Y.R.[1], Peng H.N., He X.L.[1], Zhang J.M.[1] (2022)
Cavitation Bubbles with A Tunable-Surface-Tension Thermal Lattice Boltzmann Model. Physics of Fluids, 34, 102008.
[1] State Key Laboratory of Hydraulics and Mountain River Engineering, Sichuan University, Chengdu, China.

Wersin P. [1], Mazurek M. [1], Gimmi T. (2022)
Porewater chemistry of Opalinus Clay revisited: findings from 25 years of data collection at the Mont Terri Rock Laboratory, Applied Geochemistry 138, 105234.
[1] RWI, Institute of Geological Sciences, University of Bern, 3012 Bern, Switzerland

Yan Y.[1,2], Ma B., Miron G.D., Kulik D.A., Scrivener K.[2], Lothenbach B.[1,3,4] (2022)
Al uptake in calcium silicate hydrate and the effect of alkali hydroxide. Cement and Concrete Research, 162, 106957.
[1] Laboratory for Asphalt and Concrete, Empa, Dübendorf, Switzerland
[2] STI IMX LMC, MXG 230, Station 12, EPFL, Lausanne, Switzerland
[3] Institute of Geological Sciences, University of Bern, Bern, Switzerland
[4] Department of Structural Engineering, Norwegian University of Science and Technology, Trondheim, Norway

Yang Z.[1], Ning Y. [1], He C. [1], Yumei Li[2], Yang S.[1], Yang B.[1], Kang J.[1], Dähn R., Li Y.[1] (2022)
Identification of the Chromate Sorption Mechanism Conversions in a Quartz–Montmorillonite–Ferrihydrite System, ACS Earth and Space Chemistry, 6(1), 90-99.
[1] School of Environmental Studies, China University of Geosciences, No. 68, Jincheng Street, Wuhan East Lake High-Tech Development Zone, Wuhan 430074, P. R. China;
[2] CCDC Shale Gas Exploration and Development Department, CNPC Chuanqing Drilling Engineering Company Limited, No. 6, Mengzhuiwan Street, Chenghua District, Chengdu 610051, P. R. China

Zhang Y.[1], He M.[1], Wang L.[2], Yan J.[2], Ma B., Zhu X.[3], Ok Y.S.[4], Mechtcherine V.[5], Tsang D.C.[1,2,6] (2022)
Biochar as construction materials for achieving carbon neutrality. Biochar, 4(1), 1-25.

[1] Department of Civil and Environmental Engineering, The Hong Kong Polytechnic University, Hong Kong, China
[2] State Key Laboratory of Clean Energy Utilization, Zhejiang University, Hangzhou, China
[3] School of Civil Engineering, University of Leeds, Leeds, UK
[4] Korea Biochar Research Center, APRU Sustainable Waste Management Program & Division of Environmental Science and Ecological Engineering, Korea University, Seoul, Korea
[5] Institute of Construction Materials, Technische Universität Dresden, Dresden, Germany
[6] Research Centre for Resources Engineering towards Carbon Neutrality, The Hong Kong Polytechnic University, Hong Kong, China

Zhang Y.[1], Wan Z. [1], Wang L.[2], Guo B.[3], Ma B., Chen L.[1], Tsang D.C.[1,2] (2022)
Designing Magnesium Phosphate Cement for Stabilization/Solidification of Zn-Rich Electroplating Sludge. Environmental Science & Technology, 56(13), 9398-9407.

[1] Department of Civil and Environmental Engineering, The Hong Kong Polytechnic University, Hong Kong, China
[2] State Key Laboratory of Clean Energy Utilization, Zhejiang University, Hangzhou, China
[3] Department of Earth Resources Engineering, Kyushu University, Fukuoka, Japan

8.2 Technical reports

Gimmi T., Aschwanden L.[1], Camesi L.[1], Gaucher E.C.[1], Jenni A.[1], Kiczka M.[1], Mäder U.[1], Mazurek M.[1], Rufer D.[1], Waber H.N.[1], Wersin P.[1], Zwahlen C.[1], Traber D.[2] (2022)
TBO Bözberg-2-1: Data report Dossier VIII. Rock properties, porewater characterisation and natural tracer profiles. Nagra Arbeitsbericht NAB 21-22.

[1] RWI, Institute of Geological Sciences, University of Bern, 3012 Bern, Switzerland
[2] Nagra, Hardstrasse 73, 5430 Wettingen, Switzerland

Marques Fernandes M., Baeyens B. (2022)
Determination of the Cation Exchange Capacities and Exchangeable Cations of Deep Drilling Core Samples from the Siting Regions Jura Ost, Nördlich Lägern and Zürich Nordost. Nagra Arbeitsbericht NAB 21-01.

Prasianakis N.I., Kosakowski G., Gimmi T., Miron G.D., Pfingsten W., Churakov S.V. (2022)
Cement-clay interactions: synthesis of transport across the cement-clay interface. Nagra Arbeitsbericht NAB 22-34.

Wersin P.[1], Aschwanden L.[1], Camesi L.[1], Gaucher E.C.[1], Gimmi T., Jenni A.[1], Kiczka M.[1], Mäder U.[1], Mazurek M.[1], Rufer D.[1], Waber H.N.[1], Zwahlen C.[1], Traber D.[2] (2022)
TBO Bözberg-1-1: Data report Dossier VIII. Rock properties, porewater characterisation and natural tracer profiles. Nagra Arbeitsbericht NAB 21-21.

[1] RWI, Institute of Geological Sciences, University of Bern, 3012 Bern, Switzerland
[2] Nagra, Hardstrasse 73, 5430 Wettingen, Switzerland

8.3 Conferences/workshops/presentations

Cametti G., Nagashima M., Churakov S.V. (2022)
Lone -pair electron localization in temperature induced phase transitions in mimetite. International Mineralogical Conference (IMA) 2022, Lyon, 18-22th July 2022. Oral contribution.

Cametti G., Roos D., Churakov S.V., Scheinost A.C., Prieur D. (2022)
A combined experimental and theoretical approach to interpret the anomalous thermal behavior of Pb-exchanged zeolite (STI). 33rd European Crystallography Meeting, 23-27th August 2022, Versailles, France. Oral contribution.

Claret F., Pepin G., Cances C., Kolditz O., Prasianakis N.I., Baksay A., Lukin D. (2022)
Development and improvement of Numerical methods and Tools for modelling coupled processes (poster). 8th International conference on clays in natural and engineered barriers for radioactive waste confinement, 13-16 June 2022, Nancy, France.

Claret F., Pepin G., Cances C., Kolditz O., Prasianakis N.I., Baksay A., Lukin D. (2022)
Supporting implementation and optimisation by developing and improving numerical methods and tools for modelling coupled processes: IGD-TP's international symposium on the role of optimisation in geological disposal programmes for radioactive waste (poster), 20-22 September 2022, Zürich, Switzerland.

Dähn R., Marques Fernandes M., Baeyens B. (2022)
Zn uptake by illite and argillaceous rocks. 8th International meeting "Clays in Natural and Engineered Barriers for Radioactive Waste Confinement", Nancy, France, 8-11 June 2022.

Dähn R. (2022)
A micro-XAS and XRD study of the crystalline alkali-silica reaction products. 16th International Conference on Alkali-Aggregate Reaction in Concrete – ICAAR 2020-2022, 31.5.-2.6.2022, Lisbon, Portugal.

Dörfler P., Eggenberger U. , Wolffers M. (2022)
Alternative Bettmaterialien für Wirbelschichtöfen - Potenzial zur Wiederverwendung als Zementzuschlagstoff, Recy-Depotecah Leoben, 2022.

Gimmi T., Churakov S.V. (2022)
Modelling water retention and diffusion in unsaturated clays: Connecting atomistic and pore scale simulations. 8th International meeting "Clays in Natural and Engineered Barriers for Radioactive Waste Confinement", Nancy, France, 8-11 June 2022.

Gimmi T., Mazurek M., Emmerich K. and the CLAYWAT team (2022)
NEA Clay Club project CLAYWAT: Interaction of pore water and mineral surfaces in clays and shales. 8th International meeting "Clays in Natural and Engineered Barriers for Radioactive Waste Confinement", Nancy, France, 8-11 June 2022.

He X., Liu Y., Peng H., Zhang J., Yuan H. (2022) The inception, growth, and collapse of near-wall vapor cavitation bubble with a thermal lattice Boltzmann method, 31st International Conference on Discrete Simulation of Fluid Dynamics in conjunction with the 10th Chinese National Conference of Lattice Boltzmann Method and Applications, 22-26 Aug 2022, Suzhou, China.

Hoving A.L., Qian Y, Marques Fernandes M., Griffioen J., Behrends T., Scheinost A.C. (2022) Redox-active iron in different types of clay minerals – mediated electrochemical characterization and reactivity towards Se^{IV}. 8th International meeting "Clays in Natural and Engineered Barriers for Radioactive Waste Confinement", Nancy, France, 8-11 June 2022.

Katheras A.S., Karalis K., Krack M., Scheinost A.C., Churakov S.V. (2022)
Ab initio modelling of magnetite surfaces for Pu retention. ATAS-AnXAS Joint Workshop, Grenoble, France, 17-21 October 2022.

Klinkenberg M., Marques Fernandes M., Baeyens B., Bosbach D., Brandt F. (2022)
Retention of ^{226}Ra by clay minerals: an adsorption study. 8th International meeting "Clays in Natural and Engineered Barriers for Radioactive Waste Confinement", Nancy, France, 8-11 June 2022.

Kosakowski G., Wieland E. (2022)
Assessing the impact of chemical processes on the long-term evolution of waste packages by geochemical modelling. NUWCEM 2022 - International Symposiium on Cement-Based Materials for Nuclear Wastes, 4-6 May 2022, Avignon, France.

Kosakowski G., Hax Damiani L., Vinsot A. (2022) Numerical modeling of reactive gas transport in the framework of the Mont Terri HT experiment. 8th International conference on clays in natural and engineered barriers for radioactive waste confinement. 13-16 June 2022, Nancy, France.

Krejci Ph., Gimmi T., Van Loon L.R. (2022)
Modeling cation transport in clays: Combining diffuse layer and Stern layer diffusion. 8th International meeting "Clays in Natural and Engineered Barriers for Radioactive Waste Confinement", Nancy, France, 8-11 June 2022.

Luraschi P., Gimmi T. (2022)
Long-term evolution of mineralogy and porosity at cement-clay interfaces. 8th International meeting "Clays in Natural and Engineered Barriers for Radioactive Waste Confinement", Nancy, France, 8-11 June 2022.

Ma B., Lothenbach B. (2022)
Structural incorporation pathways of FeIII into zeolite frameworks in cement-relevant environments. 4th International Symposium on Cement-Based Materials for Nuclear Wastes (NUWCEM2022), 4-6 May 2022, Avignon, France.

Mahrous M., Curti E., Churakov S.V., Prasianakis N.I. (2022)
Crystal Growth in Porous Media: A Pore-Scale Perspective. Gordon Research Conference on Flow and Transport in Permeable Media, 17-22 July 2022, Les Diablerets, VD, Switzerland.

Mahrous M., Poonoosamy J., Curti E., Churakov S.V., Prasianakis N.I.(2022)
On the Challenges of Pore Scale Models to Capture Minerals Precipitation and Dissolution in microfluidic setups: A Combined Computational-Lab-on-a-Chip Approach. The 14th Annual Meeting of the International Society for Porous Media (Interpore), Abu Dhabi, UAE.

Mahrous M., Curti E., Churakov S.V., Prasianakis N.I. (2022)
Digital Rock Physics as a Tool for Upscaling Cores Petrophyiscal Properties from Pore Scale to Continuum Scale, The 14th Annual Meeting of the International Society for Porous Media (Interpore), Abu Dhabi, United Arab Emirates, 20 May – 2 June 2022.

Marques Fernandes M., Miron G.D., Kulik D.A., Serno S., Wüst R., Baeyens B. (2022)
Development of sorption data bases for long-term safety assessments based on mechanistic adsorption models. 8th International meeting "Clays in Natural and Engineered Barriers for Radioactive Waste Confinement", Nancy, France, 8-11 June 2022.

Marques Fernandes M., Serno S, Wüst R., Baeyens B. (2022)
Determination of cation exchange capacity and exchangeable cations on deep drilling core samples by the caesium displacement method. 8th International meeting "Clays in Natural and Engineered Barriers for Radioactive Waste Confinement", Nancy, France, 8-11 June 2022.

Mokos A., Karalis K., Patel R.A., Churakov S.V., Prasianakis N.I. (2022)
Nano- and micro-scale simulations of boiling at heterogeneous surfaces. International Conference on Numerical Methods in Multiphase Flows, 28-30 September 2022 Venice, Italy.

Mokos A., Patel R.A., Peng H., Karalis K., Churakov S.V., Prasianakis N.I. (2022)
Simulations of boiling flow on the heterogeneous surface of a nuclear reactor fuel assembly system. International Conference for Mesoscopic Methods in Engineering and Science, June 27th-July 1st 2022 La Rochelle, France.

Owusu J., Prasianakis N.I., Churakov S.V., Karalis K. (2022)
Partitioning and diffusion of gaseous molecules in partially saturated clay rocks from molecular dynamics simulations, 8th International conference on clays in natural and engineered barriers for radioactive waste confinement, 13-16 June 2022, Nancy, France.

Prasianakis N.I., Laloy E., Jacques D., Claret F., Meeussen H., Miron D., Kulik D., Churakov S.V., Idiart A., Samper J., Mon A., Montenegro L., Sochala P., Tournassat Ch., Claret F. (2022)
Machine Learning Benchmark for geochemistry and reactive transport modelling with application to cementitious and uranium relevant systems, 8th International conference on clays in natural and engineered barriers for radioactive waste confinement, 13-16 June 2022, Nancy, France.

Prasianakis N.I., Gimmi T., Churakov S.V. (2022) Multiscale modelling of gas transport in clays, at the limits of very low saturation, 8th International conference on clays in natural and engineered barriers for radioactive waste confinement, 13-16 June 2022, Nancy, France.

Prasianakis N.I., Pfingsten W., Haller R., Curti E., Marques M., Baeyens B., Kulik D.A., Churakov S.V. (2022)
Reactive transport of radionuclides in compacted clays: advanced geochemical modelling, machine learning, uncertainty of parameters and sensitivity analysis, 8th International conference on clays in natural and engineered barriers for radioactive waste confinement, 13-16 June 2022, Nancy, France.

Poonoosamy J., Prasianakis N.I., Loenartz M., Yang Y., Deissmann G., Bosbach D. (2022)
A lab on a chip concept for rationalizing hydro-geochemical processes at the pore scale, American Chemical Society (ACS) Spring 2022 National Meeting & Exposition, 20-24 March 2022.

Qian Y., Scheinost A.C., Grangeon S., Hoving A., Greneche J.M., Churakov S.V., Marques M. (2022) Retention of redox-sensitive Tc(VII) on Fe(II)/Fe(III) bearing clay minerals. 10th Euratom Conference on Reactor Safety & 10th Euratom Conference Radioactive Waste Management, Lyon, France, 30 May – 3 June 2022.

Qian Y., Scheinost A.C., Grangeon S., Hoving A., Greneche J.M., Churakov S.V., Marques M. (2022) Retention of redox-sensitive Tc(VII) and Se(IV) on Fe(II)/Fe(III) bearing clay minerals. 8th International Conference on Clays in Natural and Engineered Barriers for Radioactive Waste Confinement, Nancy, France, 13-16 June 2022.

Qian Y., Scheinost A.C., Grangeon S., Hoving A., Greneche J.M., Churakov S.V., Marques M. (2022) Retention of Tc and Se on Fe-bearing clay minerals. 5th International Workshop on Advanced Techniques in Actinide Spectroscopy & 9th Workshop on Speciation, Techniques and Facilities for Radioactive Materials at Synchrotron Light Sources, Grenoble, France, 17-21 October 2022.

Peng H., Mokos A., Rajyaguru A., Curti E., Grolimund D., Churakov S.V., Prasianakis N.I. (2022)
Geochemical digital twin: Mesoscopic modeling and Machine Learning as the key enabling technology. 18th International Conference for Mesoscopic Methods in Engineering and Science, June 27th-July 1st 2022, La Rochelle, France.

Wersin P., Mazurek M., Pekala M., Gimmi T. (2022) Porewater chemistry of Opalinus Clay revisited: Findings from 25 years of data collection at the Mont Terri Rock Laboratory. 8th International meeting "Clays in Natural and Engineered Barriers for Radioactive Waste Confinement", Nancy, France, 8-11 June 2022.

Wolffers M., Kulik D.A., Miron G.D., Eggenberger U., Churakov S.V. (2022)
Genese von KVA-Flugaschen: Neue Einblicke mittels thermodynamischer Modellierung, Recy-Depotech Leoben, 2022

Zerva D., Glaus M.A., Churakov S.V. (2022)
Diffusion and retention of surface complexing radionuclides in different ionic forms of compacted illite. Euradwaste ’22 conference, 30 May – 3 June, Lyon, France.

Zerva D., Glaus M.A., Churakov S.V. (2022)
Diffusion and retention of surface complexing radionuclides in different ionic forms of compacted illite. 8th international clay conference, 13-16 June, Nancy, France.

8.4 Invited Talks

Gimmi T.
Diffusion as a dominant transport process in Opalinus Clay — from the details to the large picture. Scientific Symposium 25th anniversary Mont Terri Project, 13 Sept. 2022, Porrentruy, Switzerland.

Prasianakis N.I.
Multiscale multiphysics digital twins: machine learning as the key enabling technology, (Keynote talk) Machine Learning and Artificial Intelligence in Georesource Workshop, German Research Centre for Geosciences (GFZ), Potsdam, Germany (19.01.2022)

8.5 Teaching

Cametti G.
Bachelor course: Einführung Röntgenbeugung
Institut für Geologie, Universität Bern, Fall Semester.

Cametti G.
Master course: Natural Zeolites
Institut für Geologie, Universität Bern, Fall Semester.

Churakov S.V.
Bachelor course: Kristallographie I+II, Institut für Geologie, Universität Bern, Spring and Fall Semester.

Churakov S.V.
Bachelor course: Kristalloptik. Institut für Geologie, Universität Bern, Fall Semester.

Gimmi T.
Master course: Fluids in the Crust. Institut für Geologie, Universität Bern. Fall semester 2022.

Eggenberger U., Wolffers M., Gfeller F.
Master Course: X-Ray Powder Diffraction, Institut für Geologie, Universität Bern. Spring semester 2022.

Eichler R., Burgherr P., Hummel W., Kämpfer T., Kober T., Streit M., Zhang X
Master Course: Nuclear Energy Systems, ETH Zurich. Spring semester.

Plötze L.M., Hummel W.
Master Course: Landfilling, Contaminated Sites and Radioactive Waste Repositories, ETH Zurich. Fall semester.

Weibel G., Wolffers M.
Master Excursion: From Waste to Resources and the Challenges in Between, Spring semester 2022

Weibel G., Wolffers M.
Master Course: Geochemical Analysis of Rocks, Institut für Geologie, Universität Bern. Fall semester 2022.

8.6 PhD thesis defences

March 2022: Mirjam Wolffers
Thermodynamic model of flue gas cooling path and implications on heavy metal recovery from MSWI fly ash.

December 2022: René Jens Schliemann
Towards understanding the dissolution mechanism of clay minerals – An ab initio simulations study.

8.7 Other

Churakov S.V. (2022)
Examinateur at PhD thesis defence, K. Damodaran, Etude des mécanismes contrôlant la dissolution des verres alumino-borosilicatés et développement d'un nouveau modèle Monte Carlo, 9. December 2022, CEA Marcoule, France.

Kosakowski G. (2022)
Examinateur at PhD thesis defence, K. Ferjaoui, Nanoscale modelling of ionic transport in the porous C-S-H network, 26. August 2022, EPF Lausanne, Lausanne, Switzerland.

Pfingsten W. (2022)
Grading Board member at PhD thesis defence of Zhi Zou, Capacitive Mixing for Extracting Concentration Gradient Energy, 3 November 2022, KTH, Stockholm, Sweden.

Prasianakis N.I. (2022)
Examinateur PhD thesis defence, F. Marson, Directional lattice Boltzmann boundary conditions, University of Geneva, 31st January 2022.

Paul Scherrer Institut :: Forschungsstrasse 111 :: 5232 Villigen PSI :: Switzerland :: Tel. +41 56 310 21 11 :: www.psi.ch